

ELEMENTAL ANALYSIS OF MATERIALS INCLUDING SILICON (100) AND
(111) CRYSTALS WITH SINGLE AND DOUBLE PULSED LIBS

A THESIS SUBMITTED TO
THE GRADUATE SCHOOL OF NATURAL AND APPLIED SCIENCES
OF
MIDDLE EAST TECHNICAL UNIVERSITY

BY

ELİF YURDANUR TAŞEL

IN PARTIAL FULFILLMENT OF THE REQUIREMENTS
FOR
THE DEGREE OF DOCTOR OF PHILOSOPHY
IN
PHYSICS

MAY 2012

Approval of the thesis:

**ELEMENTAL ANALYSIS OF MATERIALS INCLUDING SILICON (100)
AND (111) CRYSTALS WITH SINGLE AND DOUBLE PULSED LIBS**

submitted by **ELİF YURDANUR TAŞEL** in partial fulfillment of the requirements for the degree of **Doctor of Philosophy in Physics Department, Middle East Technical University** by,

Prof. Dr. Canan Özgen _____
Dean, Graduate School of **Natural and Applied Sciences**

Prof. Dr. Mehmet Zeyrek _____
Head of Department, **Physics**

Prof. Dr. Sinan Bilikmen _____
Supervisor, **Physics Dept., METU**

Examining Committee Members:

Prof. Dr. Arif Demir _____
Physics Dept., Kocaeli University

Prof. Dr. Sinan Bilikmen _____
Physics Dept., METU

Prof. Dr. İbrahim Günal _____
Physics Dept., METU

Assoc. Prof. Dr. Elif Kaçar _____
Physics Dept., Kocaeli University

Assist. Prof. Dr. Barış Bayram _____
Electrical and Electronics Engineering Dept., METU

Date: _____

I hereby declare that all information in this document has been obtained and presented in accordance with academic rules and ethical conduct. I also declare that, as required by these rules and conduct, I have fully cited and referenced all material and results that are not original to this work.

Name, Last name : Elif YURDANUR TAŞEL

Signature :

ABSTRACT

ELEMENTAL ANALYSIS OF MATERIALS INCLUDING SILICON (100) AND (111) CRYSTALS WITH SINGLE AND DOUBLE PULSED LIBS

YURDANUR TAŞEL, Elif

PhD., Department of Physics

Supervisor: Prof. Dr. Sinan BİLİKMEN

May 2012, 111 pages

Laser Induced Breakdown Spectroscopy (LIBS) which is used to determine the elemental content of various samples, inspects the emission spectroscopy of samples of interest for searching certain elements or identifying the unknown content.

In this study, spectroscopic analyses of various kinds of metals, namely, Cu, Fe, Mo, Ti, W, some compounds such as CuBe, ZnSe, ZnS, GaSe, some semimetals like Si, Ge and even gases were investigated by means of a compact-commercial portable LIBS system and an independently constructed experimental set-up consisting of a single pulse system and various kinds of double pulse configurations using Nd:YAG lasers.

The contributions of this thesis to the LIBS community can be classified into two main groups- which are experimental and code development. One of the

experimental contributions was the investigation of the different crystal surfaces of silicon in which dangling bond density were taken into account for a more precise comparison of atomic emissions. The second experimental contribution was the polarization experiments by which polarization dependency, to some extent, was demonstrated. The third and final one was the orthogonal double pulse configuration with a 45° incidence angle for both lasers in opposite directions by which it was shown that the positioning becomes straightforward yielding the desired reproducible results. The second major contribution was to develop a basic code for analyzing the experimental data more accurately.

In conclusion, by means of the different experimental approaches, factors relating to the enhancement in intensity were investigated and as a result of developing the code, flexibility in upgrading the constraints of element searching was obtained and the updating of the database was accomplished.

Keywords: Laser Induced Breakdown Spectroscopy, Laser Induced Plasma Spectroscopy LIBS, Crystal Surface, Polarization

ÖZ

TEK VE ÇİFT DARBELİ LİBS İLE SİLİKON (100) VE (111) KRİSTALLERİ DAHİL MALZEMELERİN ELEMENT ANALİZİ

YURDANUR TAŞEL, Elif

Doktora, Fizik Bölümü

Tez Yöneticisi: Prof. Dr. Sinan BİLİKMEN

Mayıs 2012, 111 sayfa

Lazerle İrkitilmiş (İndüklenmiş) Bozunum Spektroskopisi (LİBS) çeşitli örneklerin element içeriklerini tespit etmek için kullanılan bir tekniktir. Söz konusu LİBS tekniği, örneklerin yayılım spektroskopilerini inceleyerek, içeriklerinde belirli bir element arama veya bilinmeyen içerik tespiti gerçekleştirir.

Bu çalışmada, taşınabilir-ticari LİBS sistemi ve bu sistemden bağımsız olarak kurulan Nd:YAG lazerlerinin kullanıldığı tek darbe ve çeşitli çift darbe konfigürasyonlarından oluşan laboratuvar deney düzenekleri ile Cu, Fe, Mo, Ti, W gibi bazı metal; Si, Ge gibi yarı metal; CuBe, ZnSe, ZnS, GaSe gibi bileşikler ile gaz dahil pek çok malzemenin spektroskopik analizi gerçekleştirilmiştir.

Bu tezin LİBS dünyasına katkıları, biri alışılmamış deney yaklaşımlarının uygulanması ve diğeri geliştirilen bilgisayar kodu olmak üzere iki ana grupta toplanabilir. Deneysel katkılarından birisi, Silisyumun farklı kristal yüzeylerinin

incelenmesidir. Bu aşamada, kristallerin atomik yayılım karşılaştırmalarının yapılması istenildiğinde daha hassas olunması amacıyla atomların bağ yapmayan yüzey yoğunluklarının dikkate alınmasının gerekliliği savı dile getirilmiştir. İkinci katkı, polarizasyon etkisinin araştırıldığı deneylerle oluşan, lazerle etkileşen plazmanın belirli bir düzeyde polarizasyondan etkilendiği yönündeki sonuçlardan gelmektedir. Üçüncü olarak da, birbirine dik ve normal düzleme 45° açı ile ancak ters yönlerden gelen çift darbe deney konfigürasyonudur. İki lazer darbesinin örnek üzerinde aynı noktaya odaklanması diğer konfigürasyonlara oranla kolaydır. Böylelikle, konum ayarlama sorunları basite indirgenmiş ve dolayısıyla dilenilen tekrarlanabilir sonuçlara ulaşmada yarar sağladığı tespit edilmiştir. Diğer katkı ise, deney verilerinin analizinde hassasiyet kazandıran bilgisayar kodunun geliştirilmesidir.

Sonuç olarak, farklı deney düzeneği yaklaşımları ile ışınım şiddetinin artışı konusundaki etkenler incelemiş ve geliştirilen kod ile gerekli durumlarda arama kısıtlamalarının değiştirilip geliştirilebilmesi ve veritabanının güncellenmesi özellikleri kazanılmıştır.

Anahtar Kelimeler: Lazerle İrkitilmiş Bozunum Spektroskopisi, Lazerle İndüklenmiş Plazma Spektroskopisi, LIBS, Kristal Yüzeyi, Polarizasyon

To my lovely parents and precious husband...

ACKNOWLEDGEMENTS

I would like to express my gratitude to my supervisor Prof. Dr. Sinan Bilikmen for his guidance, support, understanding and encouragement throughout the work. It has always been pleasure working with him.

I would like to thank my thesis supervising committee members, Prof. Dr. İbrahim Günal and Assist. Prof. Dr. Barış Bayram, who gave helpful recommendations and inspired me during this study. I would also like to thank to Assoc. Prof. Dr. Elif Kaçar for the peace she gave me about her last check offer for the thesis.

I would like to thank my colleagues, Dr. İnanç Kanık, Dr. Vedat Tanrıverdi and Dr. Emel Kilit for their support, criticism and advice on the thesis. I cannot pass without recalling secretaries of our department, especially I need to thank to Gülşen Özdemir Parlak and Zeynep Eke, for their kind help.

I would like to express appreciation to my colleague Dr. Halil Berberoğlu for his support and efforts especially in the endless experiment days. I also owe my gratitude to my friend Mehmet Ali Erol for his support in the code developing studies rather than that for his being there all the time for strengthening my motivation when I needed.

My deepest gratitude goes to my mother, Ayla Yurdanur and father, Önder Yurdanur for them being themselves. I cannot be me without their love, support, sensibility and patience.

For the last, but as always not the least, besides his support, patience and great effort on this thesis, I would like to thank to my love, Erdinç Taşel, for being the best husband ever.

TABLE OF CONTENTS

ABSTRACT.....	iv
ÖZ.....	vi
ACKNOWLEDGEMENTS.....	ix
TABLE OF CONTENTS.....	xi
LIST OF TABLES.....	xiv
LIST OF FIGURES.....	xv
LIST OF SYMBOLS AND ABBREVIATIONS.....	xx
CHAPTERS	
1. INTRODUCTION.....	1
1.1 Development History and Application Areas of LIBS.....	1
1.2 LIBS in Turkey.....	12
1.3 Research Objectives and Scope.....	13
2. LASER INDUCED BREAKDOWN.....	16
2.1 Breakdown in Gases.....	16
2.2 Breakdown in Solids.....	17
2.3 Characteristic Line versus Continuum Emissions.....	21
2.4 Double Pulse LIBS.....	25
3. EMISSION SPECTROSCOPY.....	31
3.1 Line Broadenings – Electron Density and Temperature Calculation	31
3.1.1 Natural Line Broadening.....	32

3.1.2 Doppler Broadening	32
3.1.3 Zeeman Broadening.....	33
3.1.4 Pressure Broadening.....	34
3.1.5 The Boltzmann Equation	34
3.2 Qualitative Emission Analysis.....	36
3.3 Quantitative Emission Analysis	37
4. FUNDAMENTAL LIBS COMPONENTS	40
4.1 Lasers.....	40
4.2 Detectors and Spectrometers.....	42
4.3 Targets	43
4.4 Optics	44
5. EXPERIMENTAL APPROACHES	46
5.1 Portable LIBS System	46
5.2 Double Pulse Experiments	48
5.3 Different Crystal Surface Experiments.....	56
5.4 Polarization Experiments.....	60
5.5 Air Spectroscopy Experiments	62
6. EXPERIMENTAL RESULTS	65
6.1 Single Pulse versus Double Pulse Experiments.....	65
6.2 Different Crystal Surface	71
6.3 Polarization Experiments.....	73
6.4 Air Spectroscopy Experiments	83
7. ELEMENT IDENTIFICATION VIA SOFTWARE	85
7.1 Software of the Portable LIBS System	86

7.2 The New Code and the Database	90
8. CONCLUSIONS	94
REFERENCES	97
APPENDIX.....	105
A. GROTRIAN DIAGRAMS	105
CURRICULUM VITAE	110

LIST OF TABLES

TABLES

Table 1 Some selected milestones of LIBS development.....	3
Table 2 FWHM calculations for the graphs in Figure 42 (a) and (b).....	78
Table 3 FWHM calculations for the graphs in Figure 43 (a) and (b).....	80
Table 4 FWHM Calculations for the graphs in Figure 44 (a) and (b).....	81

LIST OF FIGURES

FIGURES

Figure 1. Digital photo of a spontaneous emission images of a breakdown induced by 532 nm laser radiation. (a) 2, (b) 4, (c) 6, (d) 14, (e) 16, (f) 20, (g) 26, (h) 36 nsec after breakdown	2
Figure 2. The spectrum of RDX residue on aluminum between 720 to 780 nm in air (dotted line), in argon (solid line)	6
Figure 3. (a) Double pulse spectrum with time delay of 2 μ sec, (b) single pulse spectrum of bulk RDX, (c) enlarged C and N lines with double (dotted line) and single pulse (solid line)	7
Figure 4. Double pulse experimental apparatus of Hohreiter et. al	9
Figure 5. Single versus double pulse LIBS spectra showing atomic emission lines of interest, Si I at 288.16 nm and Mg I at 285.21 nm [12].	9
Figure 6. SEM picture of ablation of human dental enamel with 400 μ J, 700 fs Ti:Sapphire laser at 800 nm, 1.6 mJ, 50 ns Er:YAG laser at 2940 nm.....	10
Figure 7. Copper spectrum of single fs pulse (solid curve) and a fs ablative pulse combined with a ns air spark pulse (dashed curve).....	11
Figure 8. Timing of a LIBS process: (a) plasma ignition, (b) broadband emission due to Bremsstrahlung and free-bound transitions, (c) line emission due to bound-bound transitions.....	19
Figure 9. Schematic elements of expanding plasma.....	20
Figure 10. Electron transitions in an atom or ion.....	23
Figure 11. A schematic view of temporal history of a LIBS plasma formation, t_d is the time delay between laser pulse and start of detection, t_b is the integration time for the detector	25

Figure 12. A schematic view of temporal history of a LIBS plasma formation, Δt is the time delay between first laser pulse and second laser pulse, t_d is the time delay between second laser pulse and start of detection, t_b is the integration time for the detector	26
Figure 13. Plasma image of (a) single pulse, (b) double pulse with a time delay of 2.5 μ sec; spectra of (c) 50 single pulses, (d) 50 double pulses with a time delay of 2.5 μ sec; SEM view of ablation crater of (e) 50 single pulses, (f) 50 double pulses with a time delay of 2.5 μ sec.....	27
Figure 14. Copper plasma formation with changing of delay times as indicated in each image	28
Figure 15. Experimental setup configurations proposed by Pasquini et al...	30
Figure 16. An example of calibration curve.....	38
Figure 17. Two different Nd:YAG lasers, One at 1064 nm (Ekspla NL 301) and the other is the second harmonic, i.e. at 532 nm (Big Sky)	41
Figure 18 A CCD array detector (Ocean Optics, HR2000)	43
Figure 19 ZnSe target with different sized craters on it due to different spot sizes of the focusing laser.....	44
Figure 20 A converging lens and fiber optic cable for collecting the spectral emission.....	45
Figure 21. Picture of the StellarNet PORTA-LIBS 2000 composed of batteries for the spectrometers and the laser, plasma chamber, spectrometers and fiber optic cables	47
Figure 22. Newport beam profiler result of 532 nm-laser, (a) 3-D illustration of the beam, (b) vertical beam profile of them fitted to a Gaussian curve and (c) horizontal beam profile of them fitted to a Gaussian curve	49
Figure 23. Picture from LIBS Lab with some components	50
Figure 24. Q-switch out and PIN diode signals of 532 nm-laser shown in oscilloscope screen.....	51
Figure 25. Pulse timings of the laser shown in oscilloscope screen.....	52

Figure 26. Orthogonal configuration of double pulsed LIBS setup, either the laser of Fokus Engineering is sent first to generate plasma of the target first or the laser of Big Sky is sent to produce an air spark	53
Figure 27. 45 Degree Configuration of Double Pulse Experiment.....	54
Figure 28. Close up picture of 45 degree configuration experimental setup	55
Figure 29. Unit cell structure of face centered cubic lattice illustration.....	57
Figure 30. (100) and (111) crystal surfaces with corresponding Miller indices	57
Figure 31. 3-D illustration of Si (100) and Si (111), respectively	58
Figure 32. Schematic representation of packing of the fcc (111) and (100) respectively.....	59
Figure 33. Illustration of atoms corresponding to (a) (111) and (b) (100) surfaces of fcc.....	60
Figure 34. (a) Picture of Si (100) (b) SEM (Scanning Electron Microscope) picture of 180 μm diameter crater of Si (100) taken at METU Central Laboratory.....	61
Figure 35. Polarization experimental setup.....	63
Figure 36. Experiment on ZnSe by using single pulses of 532 nm and 1064 nm laser and double pulse configurations with a time delay of approximately 2 μsec between the two lasers, the minus sign indicates that 532 nm-laser shoots first	68
Figure 37. Experiment on Si (100) by using single pulses of 532 nm and 1064 nm laser and a double pulse configuration with different time delays of the lasers	69
Figure 38. 45 degree configuration double pulse experiment on Cu with 100-accumulation recording with an integration time of 100ms	70
Figure 39. Single pulse spectral results for Si (100) and Si (111) by using PORTA-LIBS System of StellarNet Inc. (x being the corresponding wavelength in nm and y being the relative intensity in arbitrary unit)	72

Figure 40. Double pulse spectral results for Si (100) and Si (111) with a time delay of approximately 1 μ sec between lasers	73
Figure 41. Polarization Angle vs Intensity graph of Si II ions for both Si (100) and Si (111)	74
Figure 42. (a) Si (100) vs (b) Si (111) by using a polarizer at 120-degree angle (x being the corresponding wavelength in nm and y being the relative intensity in arbitrary unit).....	79
Figure 43. (a) Si (100) vs (b) Si (111) by using a polarizer at 180-degree angle (x being the corresponding wavelength in nm and y being the relative intensity in arbitrary unit).....	80
Figure 44. (a) Si (100) by using a polarizer at 180-degree angle vs (b) Si (100) without a polarizer (x being the corresponding wavelength in nm and y being the relative intensity in arbitrary unit).....	82
Figure 45. Air plasma vs air plasma under Nitrogen gas flow (x being the corresponding wavelength in nm and y being the relative intensity in arbitrary unit).....	84
Figure 46. The experimental results obtained by commercial PORTA-LIBS to identify 99.95 % Mo element, search tolerance 0.20 nm, search threshold 15 %.....	87
Figure 47. The experimental results obtained by commercial PORTA-LIBS to identify (a) 99.99% Fe element, and (b) high purity CuBe compound, (st stands for search tolerance in nm, and sthresh for search threshold in percentage).....	88
Figure 48. Library of the software with customer addition.....	89
Figure 49. The experimental results obtained by commercial PORTA-LIBS to identify CuBe with additional library	90
Figure 50. High purity Cu element is investigated with an element precision of 15.....	91
Figure 51. Results of new code.....	93

Figure 52. Grotrian Diagram for 385.6 nm Si emission line	106
Figure 53. Grotrian Diagram for 385.6 nm Si emission line	107
Figure 54. Grotrian Diagram for 504.1 nm Si emission line	108
Figure 55. Grotrian Diagram for 634.7 nm Si emission line	109

LIST OF SYMBOLS AND ABBREVIATIONS

Å	: Angstrom
ARL	: Army Research Laboratory
CCD	: Charged Coupled Devices
CID	: Charge Injection Device
eV	: Electron Volt
fs	: Femtosecond
FWHM	: Full Width at Half Maximum
Hz	: Hertz
ICCD	: Intensified CCD
InGaAs	: Indium Gallium Arsenide
IPDA	: Intensified PDA
K	: Kelvin
LASS	: Laser Spark Spectroscopy
LIBS	: Laser Induced Breakdown Spectroscopy
LIPS	: Laser Induced Plasma Spectroscopy
LSS	: Laser Spark Spectroscopy
LTE	: Local Thermal Equilibrium
mJ	: Milli Joule

Nd:YAG	: Neodymium-Doped Yttrium Aluminum Garnet
nm	: Nanometer
ns	: Nanosecond
PD	: Photodiode
PDA	: Photodiode Array
PMT	: Photomultiplier Tube
ppm	: Parts per million
ps	: Picoseconds
SEM	: Scanning Electron Microscope
TUBITAK	:The Scientific and Technological Research Council of Turkey
UV	: Ultra-violet
V	: Volt
W	: Watt
μ sec, μ s	: microsecond

CHAPTER 1

INTRODUCTION

Brief history of LIBS will be mentioned with pointing out the application areas of it. LIBS studies in Turkey including the place of this study will be discussed. The objectives and the scopes will then be emphasized.

1.1 Development History and Application Areas of LIBS

Laser Induced Breakdown Spectroscopy (LIBS) which is a technique to determine the elemental composition of various samples by means of atomic emission spectroscopy is sometimes called as Laser Induced Plasma Spectroscopy (LIPS) or Laser Spark Spectroscopy (LASS or LSS). As the name of the technique emphasizes, a laser is used to generate breakdown or in other words, plasma of a material of interest and this plasma is investigated via spectroscopic detection system for “fingerprint” analysis of the material.

Breakdown or plasma formation occurs due to the energy transfer from laser to the material. A tiny amount of material is usually ablated and the atoms, ions and electrons originating from this ablation start interacting with each other and also with the rest of the incoming laser beam and sometimes with a second laser beam. Such a plume consisting of the atom, ion and electron components is called a breakdown or plasma. Occurrence, expanding during

survival and cooling lasts about a hundred of μsec for this breakdown formation. First few nsec-expansion of the breakdown to the incident laser direction is pictured by Il'in et al. [1] as seen in Figure 1. In Figure 1 (a) a pre-pulse is sent and (e) a second pulse is sent and by this, interaction of laser beam with previously formed plasma is observed.

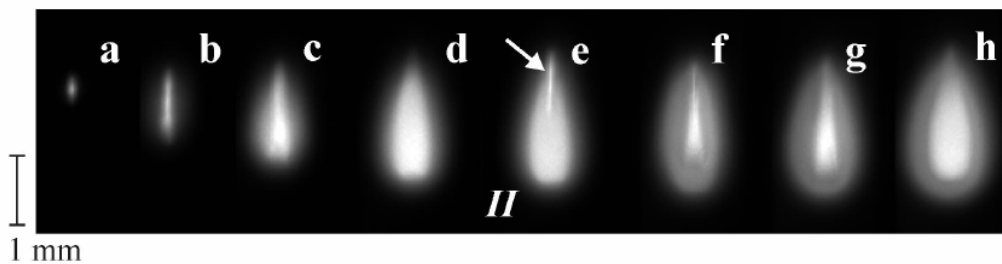


Figure 1. Digital photo of a spontaneous emission images of a breakdown induced by 532 nm laser radiation. (a) 2, (b) 4, (c) 6, (d) 14, (e) 16, (f) 20, (g) 26, (h) 36 nsec after breakdown [1]

LIBS is an attractive elemental analysis technique due to some of its outstanding features. For instance, it enables to deal with any kind of samples, including metals, semi-metals, non-metals, as well as any other states, liquids, gases and aerosols. Non-invasive property and needing of a little or no sample preparation are some of the other charming benefits of LIBS over other forms of atomic spectroscopy. A promising capability of the technique is its appropriate nature for remote sensing or standoff applications for developing necessities of today's world. The most resplendent advantage can be named as the real time multi-element analysis ability of LIBS.

L. Radziemski and D. Cremers, in their book [2], listed the significant milestones for the development of LIBS. Some of the selected milestones are listed in Table 1 in order to provide an opinion about the coverage and history of the development. The overview of milestones for the development of LIBS actually gives quite a good idea about the literature review. Some deeper

literature information concerning the scope of the thesis will be included for picturing the evolution of LIBS.

Table 1 Some selected milestones of LIBS development as listed in [2]

1963	First analytical use of a laser-plasma on surfaces, the birth of LIBS
1963	Laser plasmas in liquids were initially investigated
1971	Biological materials investigated
1984	Analysis of liquid samples and hazardous aerosols demonstrated
1992	Portable LIBS unit for monitoring surface contaminants developed
1992	Stand-off LIBS for space applications demonstrated
1999	Pulses from different lasers used to enhance LIBS performance
2009	LIBS approved for 2009 Mars mission

The birth of LIBS goes back nearly to the invention of the ruby laser in 1960. The first publication is reported in 1962 by F. Brech and L. Cross about their observation of emission spectrum from a metal target using a ruby laser [3], [4]. To move a step forward from the scientific curiosity to daily applications cannot find opportunity until the time-gated CCD (Charged Coupled Devices) detectors become available [4]. LIBS takes its today's aspect by the work of L. Radziemski and D. Cremers in 1980's and the acronym LIBS is first stated by their study group [4]. In 1990's, daily applications bring environmental contamination monitoring into the stage [3]. From then on, portable systems mostly including fiber optic cables are built and used for different purposes in fields.

In the work of Cremers et al [5], some spectra of rock samples have been collected from distances up to 24 m. The plasma is induced by focusing a 150-500 mJ Nd:YAG laser at 10 Hz repetition rate with fiber optic cables followed by a lens. It is then collected by means of fiber optic cables and

recorded by a CCD detector. They reported that they listed the elements in rock samples with an accuracy changing between 1 to 24%.

Other than rock, soil is of interest for remote detection, Theriault et al. [6] studied heavy metal contamination in soils using a fiber optic LIBS system. A 10 Hz Nd:YAG laser with a pulse width of 20 ns is used together with a 60 m long fiber cable for plasma generation. The resulting power density was 3 GW/cm² and collected by a time gated photodiode array detector with 100 shot accumulation. The work concentrated in detecting Pb contamination in sea sand and in soil by focusing on 405.7 nm emission line of it. As a result, they demonstrated that the detection limits for Pb on sand and soil were in low ppm range.

In addition to the direct analysis to environmental contamination, LIBS can be used for risk analysis that concerns environment indirectly, as in the case of the risk analysis in UK's Hunterston "B" and Hinkley Point "B" Advanced Gas-Cooled Reactor nuclear power station [4]. In Whitehouse's publication [4], it is stated that they found out that the superheater steam tube bifurcation were cracking and they needed to know whether the components up to 528 pieces could hold or be under risk of failure before the station life. The unfortunate situation was that these 528 pieces were not identified among 2112 of them. By means of a 75 m-fiber optic coupled to the LIBS system they succeed to inspect the cracking components remotely per less than 3 minutes with an accuracy of 25%. Similarly, in the same publication [4], it is also denoted that by means of remote LIBS system, in Thermal Oxide Reprocessing nuclear plant, characterization of high-level radioactive waste behind biological shield of a 1 m thick lead-glass window was achieved.

One of the other useful standoff applications is, no doubt, the ones related to the chemical and biological threats and explosives. The facility of LIBS for real-time standoff detection makes it an ideal candidate for hazardous material detection. Standoff spectrum collection is not enough for explosive detection; it is in need of to be classified as explosives and non-explosives [7].

In a study of U.S. Army Research Laboratory (ARL), it is mentioned that, even though LIBS is a very powerful candidate for explosive detection at standoff distances in real-time, atmospheric contributions complicates the discrimination of explosives from other organic materials [8]. Carbon, hydrogen, nitrogen and oxygen are the main elements of military explosives. A common method to discriminate explosives from non-explosives is to investigate the relative amount of nitrogen and oxygen to the amount of carbon and hydrogen. However, due to the contribution of atmospheric nitrogen and oxygen, this discrimination becomes very complex. In Figure 2, the experimental result from an explosive (RDX) in air is shown. In order to minimize the contribution from O and N, the experiment is repeated in argon atmosphere in laboratory conditions.

In argon medium, the real O and N content leads to identify the explosives, however, argon atmosphere can only be supplied in laboratory conditions. Therefore, for standoff field application, in the work of De Lucia et al. [8], they claimed that the usage of double pulse LIBS could minimize this complexity in discrimination originating from atmospheric contributions. They performed double pulse LIBS to demonstrate the improvement in explosive-based signal. The double pulse system of ARL consists of two Nd:YAG lasers, a digital delay/pulse generator (Stanford Digital Delay/Pulse Generator) for creating a time delay between the lasers, some optics for focusing the laser

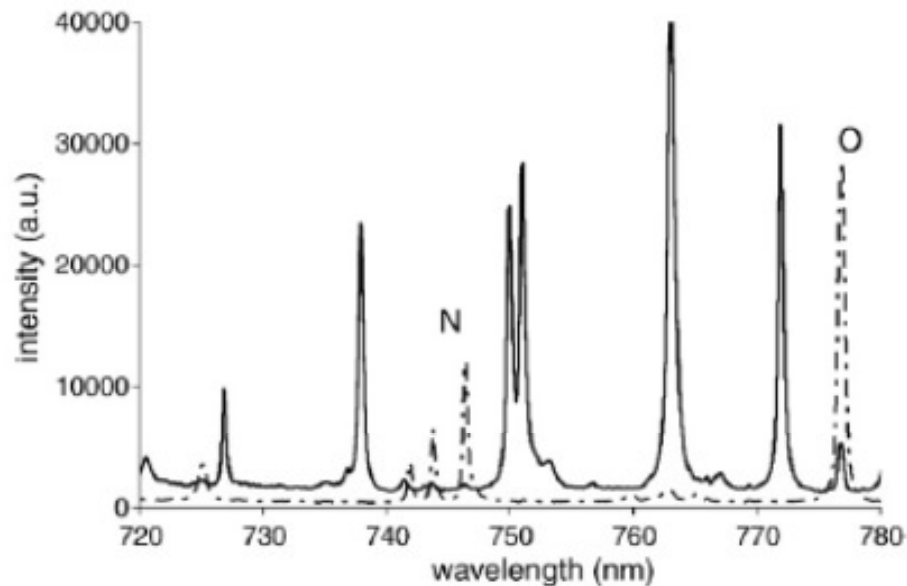


Figure 2. The spectrum of RDX residue on aluminum between 720 to 780 nm in air (dotted line), in argon (solid line) [8]

beams and a fiber optic cable attached to Echelle spectrometer with an ICCD for collecting the spectrum. The comparable result, graphs for single and double pulse experiments are shown in Figure 3. As the figure indicates, a decrease is observed in the O to C emission ratio from single to double pulse LIBS. They concluded that by means of double pulse not elimination, but an effective minimization of interference due to atmospheric O and N lines is possible.

In the work of Gottfried et al [9], the same study group at ARL reported that they have distinguished five different chemical and biological warfare agents despite their similar stoichiometric¹ formulas in real time at the field using standoff LIBS. They used an Nd:YAG laser of 5 ns pulse width, having about 275 mJ energy per pulse and providing two collinear pulses. The laser shots were focused with a 3 μ s interval to create plasma on surfaces at standoff

¹ relative quantities of reactants and products in chemical reactions

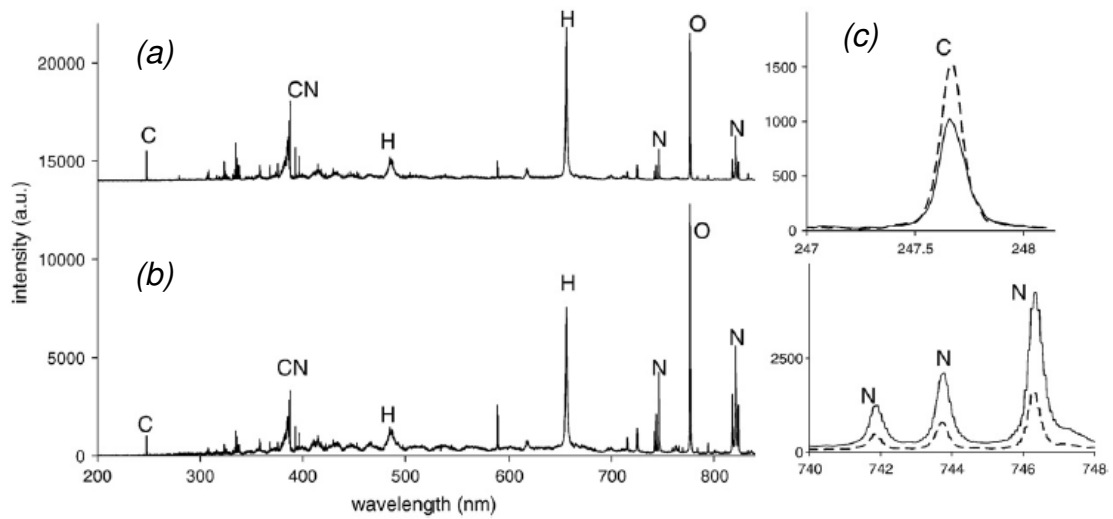


Figure 3. (a) Double pulse spectrum with time delay of 2 μ sec, (b) single pulse spectrum of bulk RDX, (c) enlarged C and N lines with double (dotted line) and single pulse (solid line) [8]

distances; even they had successful experiences for 50 m at field and 100 m indoor, these experiments were performed at 20 m. The emission spectrum from the plasma 20 m away was collected by a 14-inches telescope and sent to a CCD by means of fiber bundle and recorded after a gate delay of 2 μ s with a 100 μ s integration time. The analysis is performed with a constructed linear correction library. They define the linear correlation as “simple measure of strength of the relationship between two variables”. By means of this correlation library, they had removed the single spectrum library and had chance to correlate spectrum with the remaining library members.

With the above examples and more other studies, the advantages of rapid multi element analysis, with no sample preparation and remote sensing ability in harsh, hazardous and extreme environments are mentioned. However, as discussed above, LIBS emission signals from the material of interest still needs to be improved. Such improvements are needed in liquid and solid targets too, this time not because of the atmospheric gases but due to the continuum emission contributions to the spectrum. The continuum emission is the radiation that occurs due to the free electron transitions and

therefore they do not carry characteristic information about the target (detailed explanation can be found in Section 2.3).

Double pulse LIBS originated more than 25 years ago in a research of Cremers et al., with coaxial laser shots to aqueous solutions [10]. A newer example is performed by a compact and portable system for material analysis concerning art and archaeological applications [11]. The system was composed of a laser head, a spectrometer-detector (Ocean Optics HR2000+) and a control box that triggers the system. They observed enhancement in the intensities of the characteristic lines and improvement in signal to noise ratios. Their other conclusions were noticeable, they emphasized on the degree of enhancement which differs from element to element and moreover from emission line to emission line within an element. Besides these; they observed that plasma generated with double LIBS lasted longer than single pulse induced plasma [11].

Other than collinear double pulse configuration, orthogonal laser shots are possible. For instance, in the experimental setup of Hohreiter and Hahn [12], first an air spark was produced ~1 mm above the target and the second laser directed to the target was sent as seen in Figure 4. Two Nd:YAG lasers were used, one of which operating at 1064 nm with an energy of 200 mJ and the other at 532 nm with an energy of 100 mJ. They observed both increase in continuum emission and characteristic emission. The characteristic emission showed 2 to 9 times increase in intensity in the cases of double-pulse experiment with respect to single laser pulse operation, as seen in the graph of Figure 5.

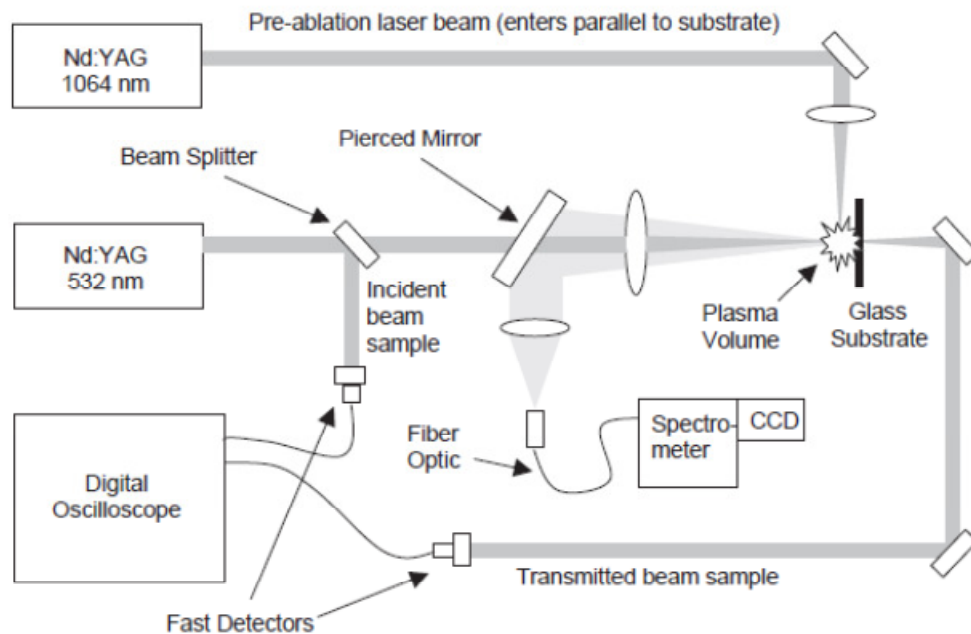


Figure 4. Double pulse experimental apparatus of Hohreiter et. al [12]

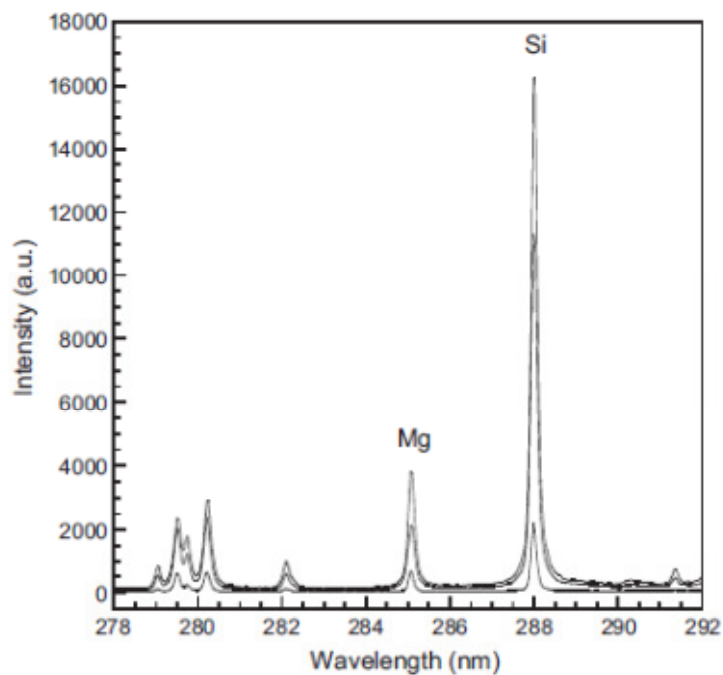


Figure 5. Single versus double pulse LIBS spectra showing atomic emission lines of interest, Si I at 288.16 nm and Mg I at 285.21 nm [12].

Moreover, by the improvement in laser technology while dealing with double pulse, researchers started to combine nanosecond pulsed lasers with femtosecond (fs) or picoseconds (ps) pulsed ultra fast lasers. Characteristics and influences of such lasers differ from ns lasers, as expected. In the work of Mayorov [13], femtosecond laser shots are compared with nanosecond shots as seen in Figure 6. They observed that the ablation crater due to ns laser was larger showing a significant amount of laser pulse energy was converted into mechanical energy of shock wave. The conical form of the ns ablation crater indicated energy deposition was not precise, however cylindrical crater in fs ablation crater showed the opposite [13].

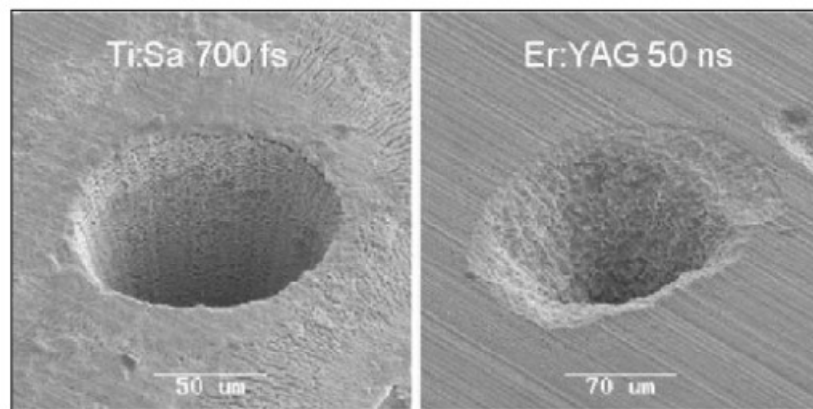


Figure 6. SEM picture of ablation of human dental enamel with 400 μ J, 700 fs Ti:Sapphire laser at 800 nm, 1.6 mJ, 50 ns Er:YAG laser at 2940 nm [13].

Scaffidi et al. [14], combined ns and fs laser pulses in an orthogonal double pulse configuration (more information can be found in Section 2.4). They reported improvement in signal to noise ratio for copper and aluminum targets when combining fs pulse with ns as shown in Figure 7. They also compared the combined laser pulsed spectrum with single fs pulsed LIBS and reported 30 times enhancement.

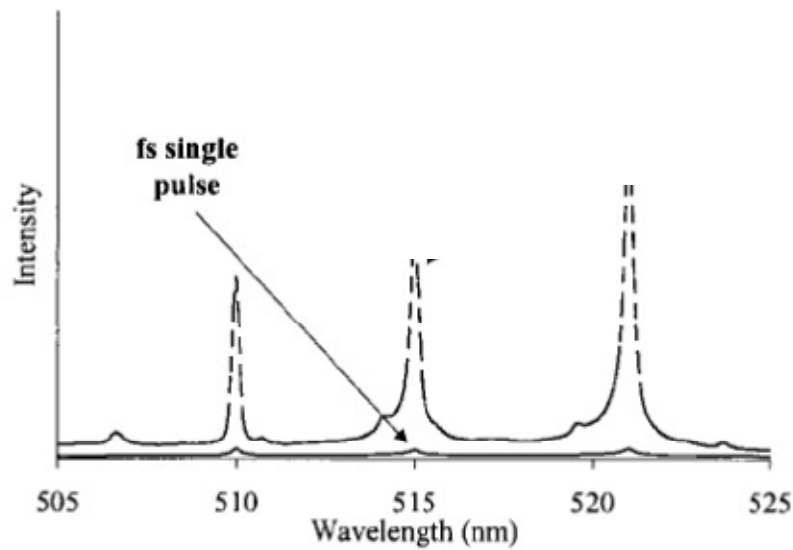


Figure 7. Copper spectrum of single fs pulse (solid curve) and a fs ablative pulse combined with a ns air spark pulse (dashed curve) [14]

Usage of double pulse LIBS [11, 15-17] with different configurations [12, 16, 18] are investigated by many other groups. As some of them discussed above, this versatile LIBS technique can be used in various fields of application like biomedicine, defense, industry, archeology, forensic, nuclear industry and so on. Remote sensing in determination of concentrations [4-6, 9], even at open fields [20, 21] have already been mentioned. Studies of soil composition [22, 23], aerosol detection [24], corrosion in nuclear reactors [4], environmental contamination [6, 21, 25], are some other successful application areas. Recently LIBS has been popularly used in civil engineering [26], military application and security [20], art and archaeological applications [11]. Detection of explosives [7, 27], landmines [28, 29], biological weapons [30, 31] and heavy metals [6, 32, 33] are some other areas that LIBS can succeed.

1.2 LIBS in Turkey

LIBS researches and applications in our country can be treated as “new” when compared with the world. As far as investigated, three universities, Izmir Institute of Technology, Kocaeli University and Middle East Technical University are dealing with LIBS, approximately starting from 2006 up to now.

In Chemistry Department of Izmir Institute of Technology, Assoc. Prof. Dr. Şerife YALÇIN and her group are using LIBS technique for mostly investigating aqueous solutions. She also gives a lecture concerning the fundamentals of LIBS and supervises thesis on the subject [34]. This institute hosted an international symposium called 6th Euro-Mediterranean Symposium on Laser-Induced Breakdown Spectroscopy in September 2011.

In Physics Department and Laser Technologies Research and Application Center [35] of Kocaeli University, Prof. Dr. Arif DEMİR, Assoc. Prof. Dr. Elif KAÇAR and their group work on LIBS both experimentally and theoretically for modeling issues. The group has developed a spectrometer [35] with a 1.8 nm resolution covering 300-800 nm wavelength interval. Such a spectrometer appropriate for LIBS is unique in that it is the first developed spectrometer by Turkish researchers.

At METU, LIBS laboratory in the Physics Department, Prof. Dr. Sinan BİLİKMEN and his group are dealing with LIBS. Experimental activities are ongoing since 2010. The laboratory now consists of a portable system, an electronically controlled-double pulse system, a vacuum chamber for gas and aerosol studies. This PhD thesis is a product of such experimental facilities.

1.3 Research Objectives and Scope

In this experimental study, laser induced breakdown spectroscopy is investigated by using different kinds of elements and compounds either in solid or gaseous form. Some experiments including portable system or constructed laboratory set-up for single and double pulse experiments on various samples are performed which have also been realized by different study groups who published similar findings with this current study. However, some other experiments that are covered in this thesis are performed for the first time. Those experiments are remarked as *“the first time”*, since they have not been come to across throughout the wide literature research in the subject. Besides the experimental studies, the results are analyzed and tried to relate to physical basis. Moreover, during this analysis of the results, a new updatable code is developed for elemental identification purposes.

One of the so-called first-time experiments includes the orthogonal double pulse configuration with 45 degrees of incidence angle for both of the laser beams in opposite directions. The second is the investigation about the behavior of different crystal surfaces of the same element, namely Si (100) and Si (111). Another experimental series are performed in relation to polarization behavior of the laser induced plasma of Silicon under a nsec laser pulse influence.

The objectives of the study involve constituting a LIBS laboratory which is very rare in Turkey and supplying an improvement for the identification applications of LIBS by

- evaluating different experimental set-ups,
- investigating contribution of crystal property,

- approaching enhancement status in a different way considering polarization effects,
- developing an inspection code with updatable properties and database.

After having quite sufficient idea about LIBS and general information of scope of the present study, the coverage of the rest of the chapters can be mentioned briefly.

In Chapter 2, physical background of the laser induced plasma mechanism is stated for both solids and gases. By means of the explanation of mechanism, the emission lines of the spectrum that are of interest are emphasized among the others. Then, one way of enhancing the emission lines of interest, the double pulse configuration, is mentioned with some examples in the literature.

In Chapter 3, line broadenings that are significant in emission spectroscopy of LIBS are explained. Their part in calculation of electron density and temperature is mentioned and some simple ways for such calculations are stated. The qualitative and quantitative analysis, their purposes, drawbacks and ways for improvements are explained.

In Chapter 4, the fundamental components including the lasers, detectors and spectrometers, optics and the target itself are stated. The requirements and roles of the commonly used components for a working LIBS system are briefly mentioned.

In Chapter 5 and 6, some of the experiments that are covered during the study are explained including the experimental setups and the analysis of the results with identifications and probable physical reasoning.

In Chapter 7, element identification by software is mentioned. The drawbacks of the software of the current portable system and usage of a database without verification are stated. A way for creating and updating database is proposed and the developed code for more accurate identification is explained.

Finally, findings, contributions and potential future works are summarized in the conclusion chapter.

CHAPTER 2

LASER INDUCED BREAKDOWN

The devices and the operation of LIBS is relatively simple, however the underlying physics and the technique are complicated. Therefore, after many years of experience, still quantitative even qualitative measurements are difficult to handle. The complexity is arising from the difficulty in understanding and controlling the breakdown or the plasma induced by a laser.

2.1 Breakdown in Gases

In order to create breakdown in gases, free electrons are needed to be present in the laser beam area. If there are no electrons naturally then a few photons of the laser produce some. That is how the multiphoton process occurs. This is formulated in [2];



where M and M^+ represent an atom and corresponding ion, respectively, e^- is the electron, m is the number of photons and $h\nu$ is the photon energy.

These free electrons are accelerated by the electric field during collisions. These electrons generate further electrons and ions [2], that is;



The process of electron generation continues during the laser pulse and leads ionization which is an indication of breakdown in gas. This process can be followed by the three-body collisions, like electron-photon-atom or due the increase in ions, electron-photon-ion collisions. These collisions also yield new electron generations [2]. Since there is no surface limiting, after the breakdown, plasma expands in all directions.

2.2 Breakdown in Solids

The interaction of a laser beam with a solid surface is a complicated process depending on many different characteristics of the laser and the solid target [36]. For a laser beam of high enough energy to induce plasma, the laser pulse helps to heat, melt and vaporize the sample. Some of the laser energy continues to penetrate to the sample, some heats the evaporated material and some are absorbed by the plume and may lead ionization [2].

The formation process and the expansion of plasma depend on many factors. The laser characteristics that affect the plasma are namely, pulse width, wavelength, intensity, spot size, spatial and temporal fluctuations [36, 37]. Optical, thermal and chemical properties of the sample, the pressure and composition of the ambient gas are the other factors that have effects on the plasma indeed.

For an easier look to plasma formation process, a time domain division is proposed by Kompitsas et al. [37] as shown in Figure 8. The first domain (a) of the three consists of heating and evaporation of the sample. For consistency with explanation of breakdown in gases, the process can be formulated as follows;

Evaporation:



(M: an atom, s: solid state, g: gas state, hv : a photon with a specific energy)

The first seed electrons are generated, either due to multiphoton ionization or thermal emission of the sample.

Evaporation & Ionization:



where e^- is the electron.

These electrons further absorb photons of the same laser beam and transfer their energy to the ions and atoms by means of collisions. This leads more ions to be produced, while a shock wave is observed because of the fast heating of the plume reaching high temperatures [37].

The second domain (b) of Figure 8 is responsible for the continuum emission, in other words, the broadband emission originating from the electron-ion or electron-atom recombination or Bremsstrahlung (the radiation emitted by a charged particle during the collision [38]) of free electrons [37].

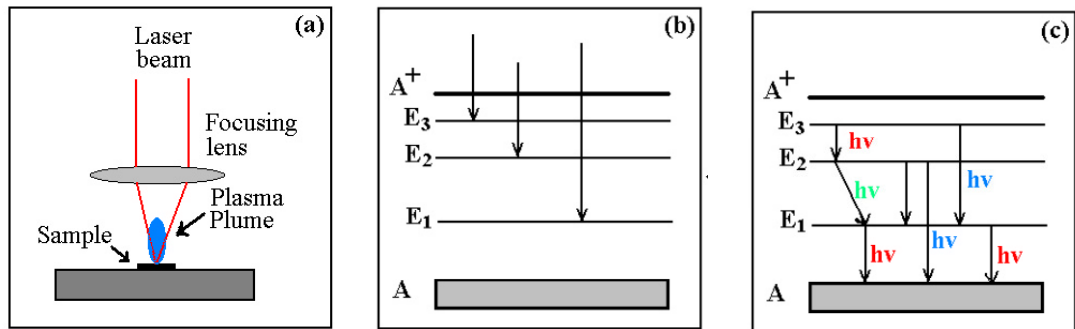
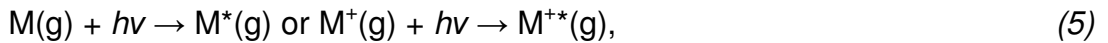


Figure 8. Timing of a LIBS process: (a) plasma ignition, (b) broadband emission due to Bremsstrahlung and free-bound transitions, (c) line emission due to bound-bound transitions [37]

The third time domain (c) of Figure 8 is responsible of characteristic emission. An atom or an ion by absorbing a photon that is equal to the difference between two energy levels or gaining an energy due to some other process like collision, becomes excited, as visualized like;

Excitation by photons (*: excited state):



This excitation does not last long, so the ion or the atom emits the characteristic energy to get to the stable state as before. These characteristic emissions are the ones that are taken into account in LIBS technique.

In order to investigate the plasma expansion, the waves that are generated posterior to first interaction of laser-matter are needed to be considered. Since the vaporization and ionization are created by the earlier part of the laser pulse, the rest of its energy can be absorbed by the created plasma plume. When a laser pulse of sufficient energy interacts with matter, significant hot plasma is induced. This plasma exerts high pressure on the surrounding material and leads generation of a shock wave [38]. The energy absorption in the expanding plasma happens in three different mechanisms

(for further reading [2, 36]). In every mechanism a plasma front, an absorption zone and a shock wave are created as illustrated in Figure 9. Shock waves are created in a medium when a sudden impact comes to the stage [38]. At higher irradiances these zones are merged. After these zones, the plasma loses energy and decays by recombination, radiation and conduction [2].

According to Singh et al. [36], the plasma expands normal to the sample and according to Cremers et al. [2] it expands towards the laser beam. In the case of normal incidence of laser beam, both approaches emphasize the same direction which is also illustrated in Figure 9. However, as a remark, in the case of an incline in the target with respect to the laser, according to an investigation [36], the path length of the radiation in the plasma is shortened.

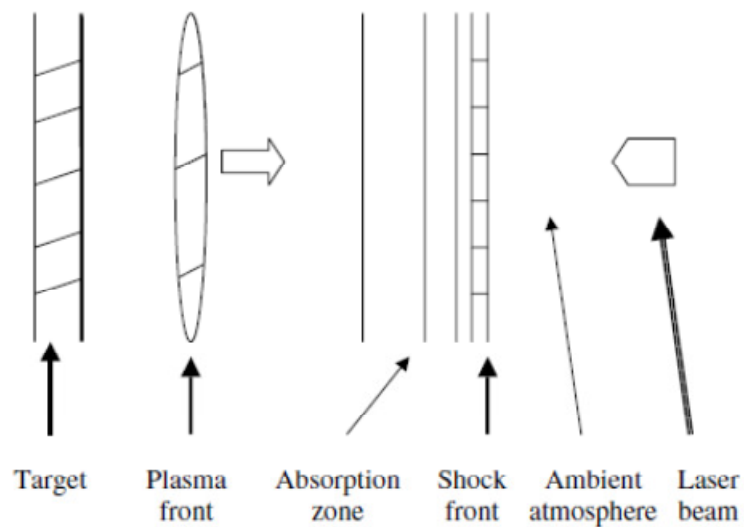


Figure 9. Schematic elements of expanding plasma [2]

2.3 Characteristic Line versus Continuum Emissions

Laser interaction with plasma results in different electron transitions, namely free-free, bound-free and bound-bound transitions as illustrated in Figure 10.

The continuum radiation is emitted as a result of free-free and free-bound transition in the plasma. Free-free transitions are because of the collision between free electrons and ions within the plasma. When a photon of energy $h\nu$ is emitted during this interaction, process is called Bremsstrahlung emission; if inverse happens, which is photon absorption is experienced, then it is called the inverse Bremsstrahlung [38]. These can be illustrated below, M^+ being an ion in an arbitrary ionization stage [38];

B (Bremsstrahlung);



IB (Inverse Bremsstrahlung);



In laser-induced plasmas, the continuum radiation is fed with Bremsstrahlung emission. In laser produced plasmas, the energetic electrons have long free paths and therefore can interact with cold matter. In this case, Bremsstrahlung spectrum is modified because electrons with different energies are slowed down by cold matter due to the interaction with them [36].

In free-bound transition, if a photon of energy $h\nu$ is emitted due to the electron capture of an ion, then the process is called the radiative recombination. If the inverse, absorption of a photon is experienced with a

release of a bound electron, this is called the ionization or more famously the photoelectric effect. These can be illustrated as follows, M^+ being either an atom or an ion and M^{++} being an ion in different and arbitrary ionization stage than M^+ ;

RR (radiative recombination);



PE (photoelectric effect);



In a laser induced plasma, a free electron with a kinetic energy is captured by an ion leading a photon emission, or in other words a radiative recombination. This emitted photon has energy equal to the sum of the kinetic energy of the electron and the ionization energy of the ion; therefore the spectra show discontinuities [36] and therefore feeds the continuum radiation.

Finally, the bound-bound transitions are responsible of the spectral or in other words characteristic line emissions. For an excitation of electron from a lower electronic state to higher one, a photon is absorption is needed. This process is called the line absorption. For the inverse situation, when an electron “drops” from a higher electronic state to a lower state within an atom or ion, a photon is emitted with energy, $h\nu$, equal to the amount of energy difference of the two states. This process is called the line emission. Since the energy differences of electronic states of elements are characteristic properties of them, the emitted photons carry information about the energy difference of the electronic states of the corresponding element.

LE (line emission);



LA (line absorption);

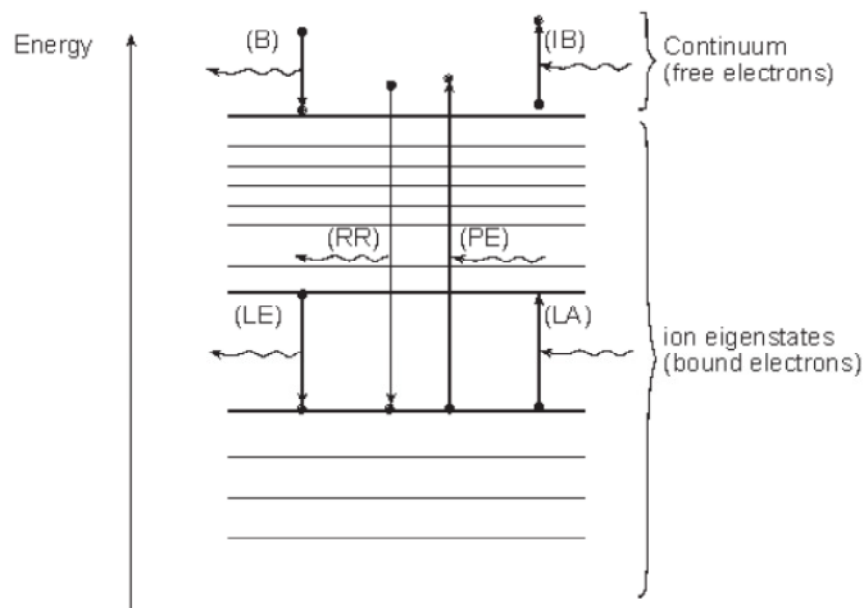


Figure 10. Electron transitions in an atom or ion [38]

This line emission is the one that is detected in LIBS experiments in order to have information about the donor sample. Therefore it is also called the characteristic line emission. As indicated in name, these emissions are differing from the continuum emissions. The difference is also reflected by their shapes. These line emissions are discrete and more or less resemble to lines at least when compared to continuum emission. Actually, they are not precisely line-shaped and the reason why they are not purely line-shaped can be explained with two bases. First, there exist many possible configurations of line emissions especially for high atomic number atoms and

these possible transitions are so close to each other that they interfere and destroy a narrow line-shape. Second, the line broadenings effects induce an effective energy band and therefore a broadened line shapes are faced [38]. Actually these line shapes and some possible shifts can be used for diagnostic purposes for the principal broadening mechanism and line widths could give clue about plasma temperature and electron density [2] (Section 3.1).

On the other hand, in laser induced plasma, the emissions during the early formation of the plasma are corresponding to intense continuum emission rather than characteristic line emission. These emission lines have been observed close to the target surface [36]. When the plasma expands from the target, it gets cool and the characteristic emission starts to dominate. During this expansion, since the hotter region is close to the target, the characteristic emissions from highly ionized atoms are observed near to the target. However, the emissions corresponding to neutral atoms are observed in the plume away from the target [36]. Therefore the characteristic emissions from the multiply ionized atoms that occur at the time of plasma formation are superimposed intensely on continuum. The singly ionized and neutral atoms are observed nearly 500 ns after the formation of the plasma [36]. Fortunately, the decay rates of continuum and characteristic emissions are different. Due to Bremsstrahlung from hot plasma, continuum emission decays faster. That generates the necessity of recording characteristic emission lines after a certain time delay in order to reduce the continuum emission, in other words, to reduce the noise in the spectrum. Such a time evaluation is illustrated in Figure 11, indicating in the early stages, continuum emission, or the noise is higher, where after a certain time delay, the characteristic emission lines are dominating.

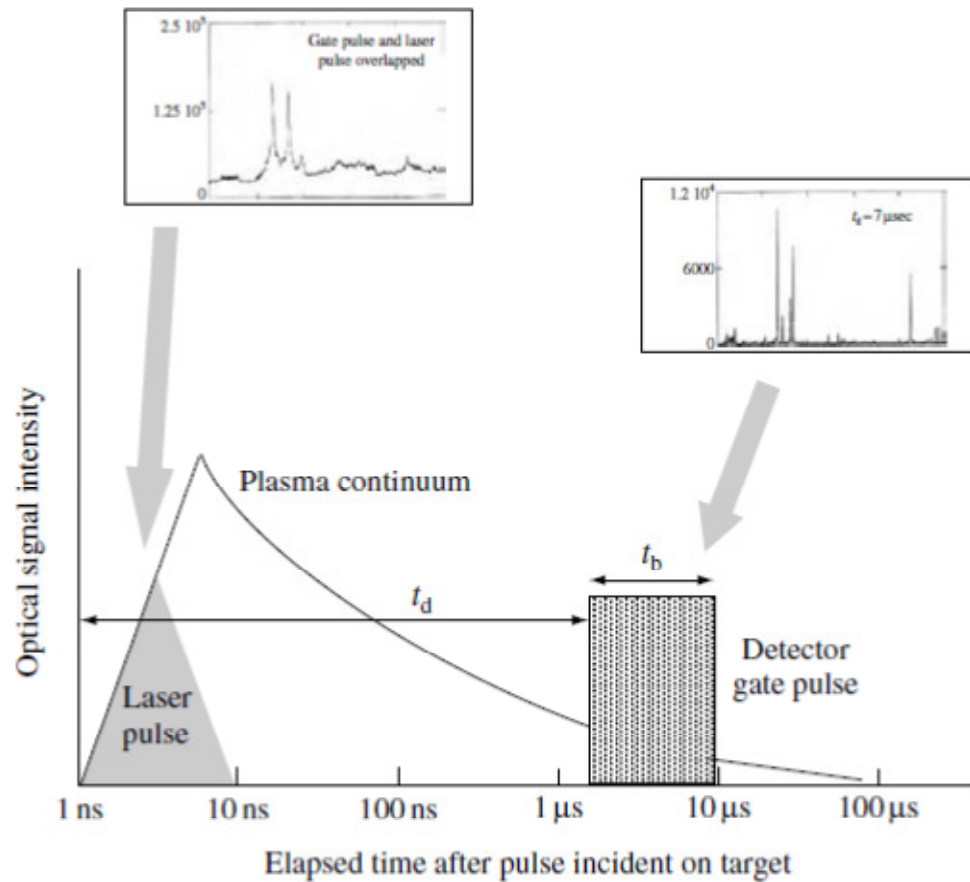


Figure 11. A schematic view of temporal history of a LIBS plasma formation, t_d is the time delay between laser pulse and start of detection, t_b is the integration time for the detector [2]

2.4 Double Pulse LIBS

In order to have enhancement in the characteristic emission lines or to reduce the continuum emission, researchers search for methods. One of which improved the signal to noise ratio or enhance the characteristic emission line is using double-pulses in LIBS experiments. The expected idea is simple, the first pulse is used for the material ablation just as in the case of an ordinary single pulse LIBS, after a while the consequent pulse is sent to serve heat to the surviving plasma for optimum condition for emission. Time schedule of this process is illustrated in Figure 12.

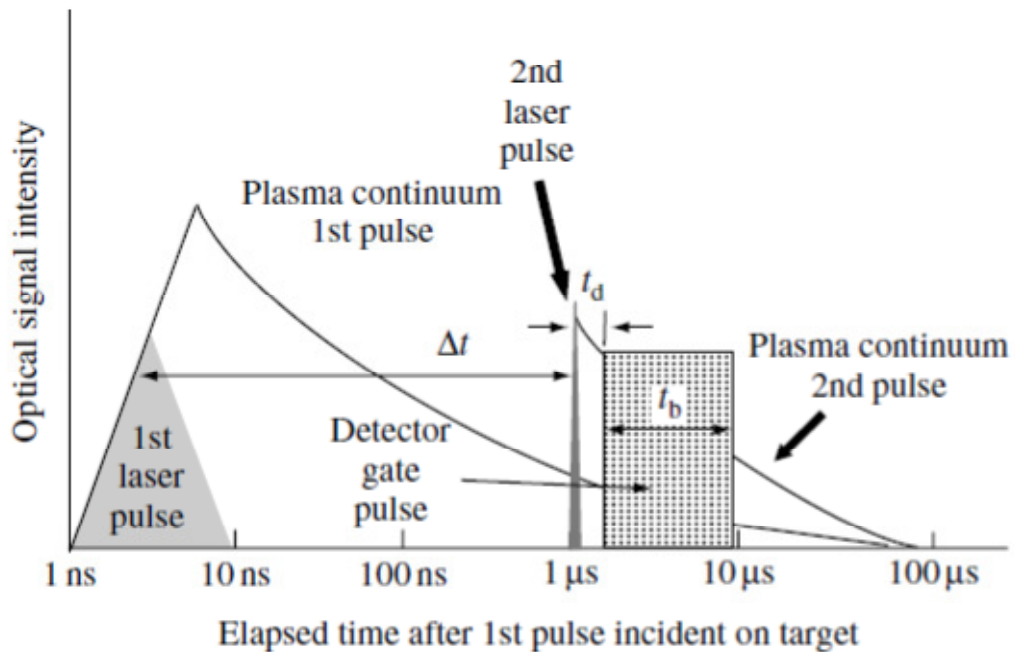


Figure 12. A schematic view of temporal history of a LIBS plasma formation, Δt is the time delay between first laser pulse and second laser pulse, t_d is the time delay between second laser pulse and start of detection, t_b is the integration time for the detector [2]

The idea concerning double pulse LIBS depends on the need of signal to noise ratio improvement, or the improvement in characteristic emission to continuum emission. The formation and the expansion of plasma, the gain in signal to noise ratio and ablation crater created after two pulses are different in double pulse experiments compared to single pulse experiments. Such differences sourcing from the presence of the second pulse are visualized in Figure 13 about a study with copper target [39]. The time delay of the two pulses is 2.5 μsec and in both single and double pulses accumulation of 50 pulses are preferred.

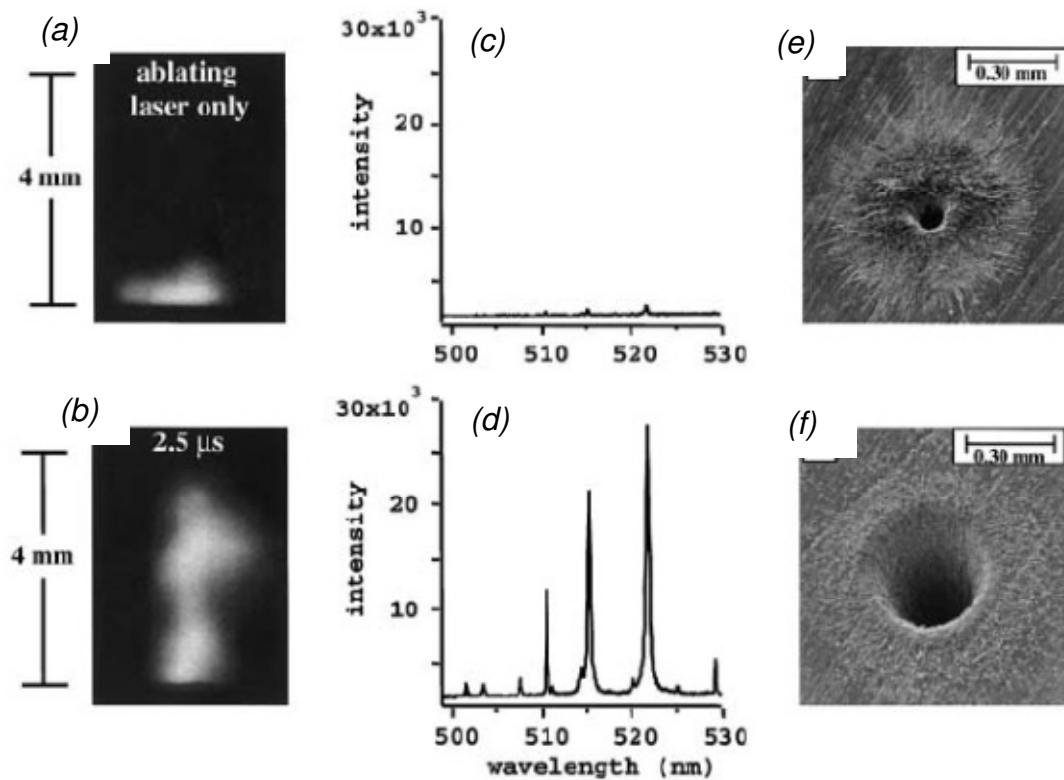


Figure 13. Plasma image of (a) single pulse, (b) double pulse with a time delay of 2.5 μ sec; spectra of (c) 50 single pulses, (d) 50 double pulses with a time delay of 2.5 μ sec; SEM view of ablation crater of (e) 50 single pulses, (f) 50 double pulses with a time delay of 2.5 μ sec [39]

The time delay between two consecutive pulses is important for degree of enhancement. With experimental conditions, the behavior of the plasma expansion and the optimum time delay could change. An example of the plasma expansion in the presence of second pulse is shown in Figure 14. It is clear from this figure that, the overall shape and size of the plasma generated have been changed with different time delays between two pulses. Therefore, the ideal timing for an improved signal to noise ratio is one of the important issues for double pulse experiments.

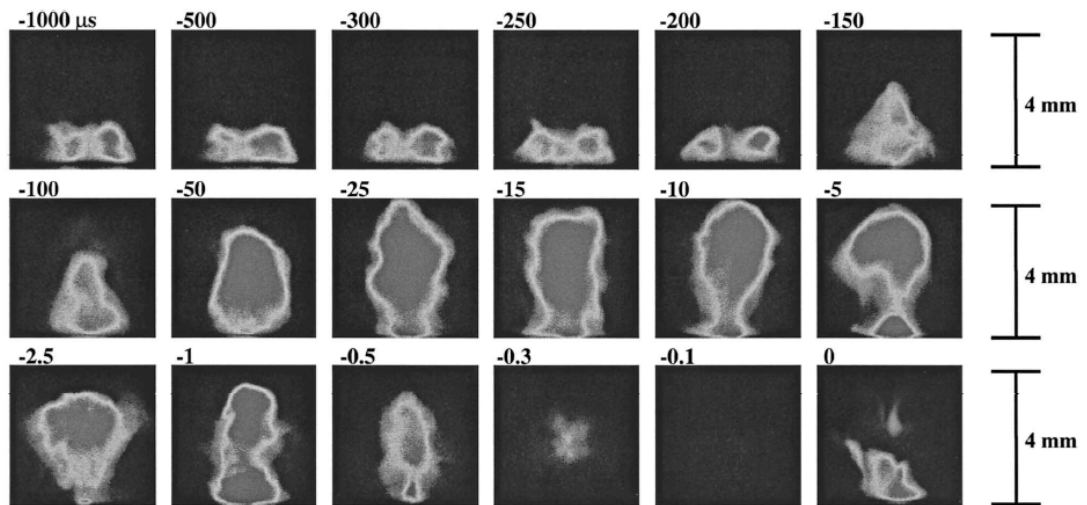


Figure 14. Copper plasma formation with changing of delay times as indicated in each image [17]

For double pulse experiments, several kinds of configurations of pulses have been tried. They are summarized in [2] as,

- (1) “Multiple pulses within the same flashlamp pulse,
- (2) Collinear beams to the target,
- (3) Orthogonal beams
 - a. Pulse normal to the target shoots, before the laser parallel is lased (reheating),
 - b. Pulse normal to the target shoots, after the laser parallel is lased to produce an air spark (pre-ablation).”

Any of the above configurations results in achievement about enhancement in emission line intensities as stated by many research groups [11,12, 15-17, 40]. In collinear double pulse, the reason of an enhancement occurring in characteristic emission lines can be explained by the combination of improved ablation, increased electron density and temperature [10]. For the orthogonal configurations, the improvement can be explained by the laser-plasma interaction or the pre-heating process which yields reduction of

atmospheric pressure and density [10] and gives extra energy to bound electrons.

For instance, in the work of Corsi et al. [16], processes of laser ablation and plasma formation obtained with single and double pulse LIBS are investigated. The lasers were Nd:YAG lasers of 1064 nm each having an energy about 200 mJ in 8ns pulse width and they are settled perpendicularly. The spectrum was recorded by Echelle type spectrometer coupled with an ICCD. In order to reduce the spectral fluctuations, they tried a series of 100 single and double pulse experiments and they reported that by means of double pulse an enhancement is observed in characteristic emission line signal. They also stressed on that “the most effective increase in the signal” was observed with a time delay of 2 μm between consecutive pulses [16]. That kind of a time delay is also supported by Singh and Thakur in their book [36], they emphasize that the maximum enhancement is seen with time delays of 2-3 μm which serves an optimum expansion of pre-plasma that will help the second laser to be absorbed more effectively.

Besides the common pulse configurations mentioned above, Pasquini et al. proposed a different configuration. As seen in Figure 15, there have been different configurations one of which contains two collinear pulses (a), the other two orthogonally positioned, as mentioned above in (b) first laser hits the target and generates plasma and in (c) first laser focuses just above the sample and produces air spark. However, the last one is quite different than the earlier approaches; the laser beams are still orthogonal to each other, but both of them hit the target. The hitting is not the normal incidence as the case of collinear laser shots, this time with an angle of 45 degrees.

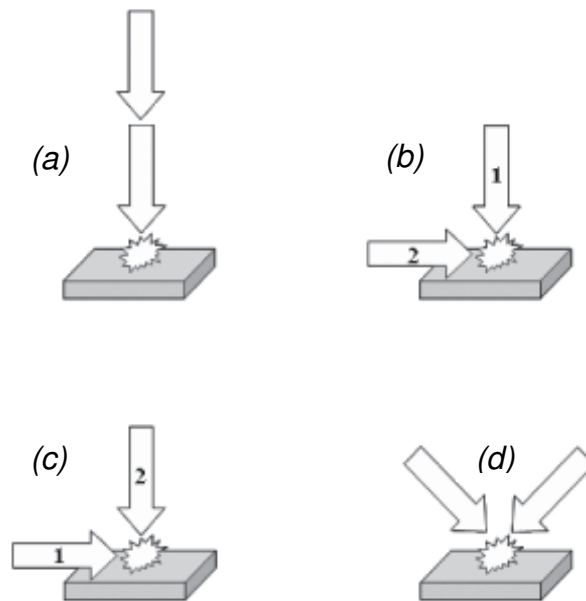


Figure 15. Experimental setup configurations proposed by Pasquini et al [18]

Such a configuration arises a professional curiosity and within the literature search during this study no coincidence to the configuration is found. Therefore, that configuration (Figure 15 (d)) and the other orthogonal configurations ((b) and (c)) are experienced and discussed in Chapters 5 and 6 about the experimental approaches and the results.

CHAPTER 3

EMISSION SPECTROSCOPY

There are some methods to calculate the electron density and electron temperature of plasma. Emission spectrum has significant information concerning them. Evaluating the line broadening mechanisms of the emissions lines or comparing the intensities of them are some of the methods for such calculations. In this chapter, some useful calculations for electron density and temperature and the basics of the qualitative and quantitative LIBS analysis are mentioned.

3.1 Line Broadenings – Electron Density and Temperature Calculation

The characteristic line emissions from the plasma, as stated above, does not have an ideal line appearance, however a broadened shape keeping valuable information about the plasma. The spectral line as well as its profile can be interpreted in order to gain information about the electron density and temperature which are also explained in the famous books of the field [2, 36, 41-43].

The underlying mechanisms of line broadenings are also explained exhaustively in the books Greim [42, 43] and Eliezer [38]. Many different line broadenings are faced in plasma emissions. They are the natural line

broadening, the Doppler broadening, the Zeeman broadening and the pressure or Stark broadening.

3.1.1 Natural Line Broadening

Electrons that are excited during the plasma formation and expansion go back to their initial states in order to obtain equilibrium. The energy they gain and the life time they stay in excited state are not sharp, but have widths; these are ΔE and Δt , respectively. According to Heisenberg uncertainty principle, the product of the two cannot be less than the Planck constant [44]. However, according to Cremers and Radziemski [2], this broadening due to uncertainty is not wide enough to be detected with spectrometer resolutions that are used in LIBS experiments. Nevertheless, it can be considered for extremely highly ionized ions like Fe^{+25} [36] which are unlikely to be present in LIBS conditions or since its shape is Lorentzian, it can only make contribution to the wings of the line [44].

3.1.2 Doppler Broadening

The Doppler broadening is named due to the Doppler Effect. It occurs because of thermal or directed motion of the emitting ions. In case of Maxwellian distributions, these broadenings have Gaussian profiles given by,

$$\Delta\lambda_D = \lambda \sqrt{\frac{2kT_e}{Mc^2}} \quad (12)$$

where $\Delta\lambda_D$ is the full width at half maximum (FWHM) of the corresponding peak due to the Doppler broadening, λ is the central wavelength of the line,

kT_e is the thermal energy of emitting ions or atoms, M is the mass of them, c is the speed of light.

Equation (12) can be rearranged [43] by using the rest mass of ions or atoms, Mc^2 , in terms of proton rest mass energy times (938 MeV) the atomic weight, A , that is;

$$kT_e \approx 4.7 \times 10^8 \left(\frac{\Delta\lambda_D}{\lambda} \right)^2 A \quad [\text{eV}] \quad (13)$$

Therefore the temperature of the plasma can be calculated from the Doppler broadening, $\Delta\lambda_D$, however, before calculation, it is necessary to be sure that the most significant broadening mechanism is the Doppler broadening.

According to Singh et al. [36] and Griem [43], Doppler broadening is the dominant mechanism at low electron densities. Thus, Doppler broadening starts to dominate when plasma expands and cools and therefore electron density is decreased [36]. Mostly, LIBS plasmas are at high electron densities when the necessary information is collected which is the survival time of the plasma before it starts cooling.

3.1.3 Zeeman Broadening

Magnetic field affects the energy of the bound electrons leading a splitting of the emission lines. This effect is not only seen due to an external magnetic field, but is effective also in the presence of flowing current that generates magnetic field. However, other than fusion or discharge plasma, this broadening is not strong enough to characterize the broadening [45]. In LIBS plasmas, external or induced magnetic fields are not practically expected.

3.1.4 Pressure Broadening

In dense plasmas, in other words, in high electron density plasmas, natural and Doppler broadenings are negligible, since radiating ions and atoms interact with surroundings effectively [43]. During the early stages of plasma formation in LIBS experiments electron densities are about $10^{15} - 10^{18} \text{ cm}^{-3}$, therefore for a considerable period, pressure broadening is the dominant broadening mechanism [36]. Because the electric fields are involved, it is called Stark broadening. The width of the Stark-broadened line depends mainly on the electron density [36]. This dependence and the corresponding coefficients are calculated and tabulated by Griem [42]. The simpler version that can be used for comparison purposes is;

$$N_e = C (N_e, T_e) \Delta\lambda_S^{3/2} \quad (14)$$

where $\Delta\lambda_S$ is the FWHM of the corresponding peak due to the Stark broadening, N_e is the electron density, T_e is the electron temperature and parameter C depends weakly on N_e and T_e , which is mostly treated as a constant.

3.1.5 The Boltzmann Equation

There is another approach to determine plasma temperature by optical emission spectroscopy. That is based on the relative intensities of two lines from the same element and ionization stage under the assumption that the Boltzmann equation which describes the population densities of excited energy levels as a function of temperature is valid to relate upper energy level population densities. The emission intensity is commonly defined as [2];

$$I = \frac{hcN_0gA}{4\pi\lambda Z} \exp \frac{-E}{kT_e} \quad (15)$$

where h is the Planck's constant, c is the speed of light, N_0 is the total population, g is the statistical weight of the upper level, A is the transition probability (Einstein coefficient), λ is the transition wavelength, Z is the partition function usually taken as the statistical weight of the ground state and k is the Boltzmann constant. Then E being the energy level and subscript 1 and 2 referring to the different emission lines, the temperature can be determined from two emission lines belonging to the same ionization stage by so-called Boltzmann two-line method as;

$$\ln \frac{I_2}{I_1} = -\frac{1}{kT_e} (E_2 - E_1) \quad (16)$$

In the study of Aragon and Aguilera [46], it is emphasized that the temperature resulting from the Boltzmann two-line method is used in several works and they stressed on this calculated temperature is sometimes called as the excitation temperature, which is the temperature determined in plasmas not in thermal equilibrium [45]. However, they claimed that in the case of local thermal equilibrium, the temperature should be equal to electron kinetic energy. As is known, in thermal equilibrium, the parameters like temperature and pressure are not changing but constant within the system. In local thermal equilibrium (LTE) situation, these parameters are varying in space and time nevertheless these changes are happening so slowly that it is fair to ignore their change within some neighborhood. Some constraints have been defined to evaluate a medium in LTE. These can be mentioned referring to [2], where for LTE, temperature is suggested to be 1 eV (~ 11000 K) and under atmospheric pressure, an electron density to be 10^7cm^{-3} . According to Cremers and Radziemski [2], LIBS plasma produced by an

irradiance of $>10^8\text{W/cm}^2$ at atmospheric pressure which ensures the LTE situation. Consequently, LTE situation enables usage of the Boltzmann two-line method.

3.2 Qualitative Emission Analysis

The qualitative analysis of a sample can be used for one of the purposes typed below [36]:

- (1) Search for definite elements or molecules
- (2) Identification of unknown elements

Searching for definite elements is quite easier since expectation narrows the range of inspection. Finding persistent lines of the definite element can confirm the presence of it. However, there may have strong lines of other elements closely adjacent to the one that is defined. Else, there are some elements which have emission lines more likely to appear so they can shadow the lines of desired element. For instance, the lines with ionization potentials of 6 eV or less are more likely to be observed than that of 10 eV or more [2]. That means, while searching for definite elements, strong or more probable emission line of other element may hinder to find them.

Even identification of unknown requires more effort. Some expectations can be developed for easier inspection for unknowns. For example, if a persistent line of an element is observed than the other persistent line corresponding to the same ionization stage should appear too. Another expectation can be about the emission line intensities of elements for certain compounds. For

instance, while inspecting RDX², the oxygen to carbon, the nitrogen to carbon, the nitrogen to hydrogen or oxygen to hydrogen ratios can be defined prior to analysis. These pre-defined ratios could help to distinguish RDX from other organic materials. One other way of being certain about existence of an element is determining at least three emission lines of the same element for without doubt to identify an element.

The homogeneity and the surface conditions are very effective factors while identification is the aim. For a non-homogeneous sample or a sample with corrosion on the surface, the emission spectrums cannot be realistic. In order to minimize such effects some methods have been developed. By scanning, in other words, sending laser beam to different sector of the sample, non-homogeneous samples can be analyzed or by using more than one single shot but a series of laser shots, the corrosion effects can be eliminated since penetration depth gets larger due to ablation at the surface with every shot.

As a result, due to these difficulties, searching for an element or a ratio of elements yields much more accurate results rather than identification applications. Therefore, sorting materials, soil investigations, finding biological or chemical treats or explosives are the few prosperity examples for successful qualitative applications.

3.3 Quantitative Emission Analysis

Quantitative analysis does not only include the elemental identification or searching for a definite element but also the determination of elemental concentration. In order to have information about the concentration, relative line intensities need to be taken into account. The observed intensities

² An explosive, chemical name cyclotrimethylene-trinitramine

should be compared with some known standards. For such a comparison, some standard samples and accordingly some calibration curves are prepared. The standards obviously should be prepared under the same experimental conditions with the samples. There are many factors affecting quantitative analysis like the sample itself or the laser and detector fluctuations. For instance, lasers should be chosen within more stable laser types and kept under constant temperature in order to ensure the shot to shot coherency or detectors should be calibrated and should be used in their linear response regions or even aligning and focusing of optics should be kept constant from sample to sample in order to eliminate different potential causes like aberration or different size of the focusing spot. An example of a calibration curve is displayed in Figure 16.

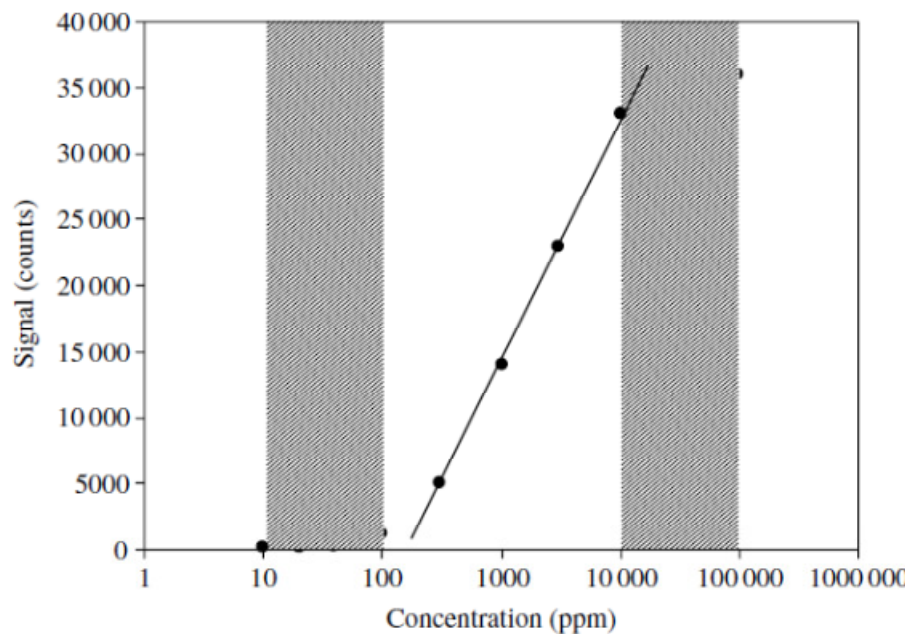


Figure 16. An example of calibration curve [2]

Similar calibration curves for certain purposes can be constituted by means of standards for definite experimental conditions. Since quantitative analysis

is out of scope for this study further reading can be found elsewhere [2, 36, 41].

CHAPTER 4

FUNDAMENTAL LIBS COMPONENTS

LIBS system consists of a laser, a focusing system, a wavelength selection device, a detection system, a time-delay system, and a signal-processing system with a spectral database and of course the material of interest. The laser, detectors and spectrometers, the target and the optics are briefly discussed below. The other components are actually not sine qua non, in other words, are not the essential ones for a simple experimental setup, however they have been included in the Chapters 5 and 7.

4.1 Lasers

As the name implies in order to induce plasma, a laser with sufficient power is needed in LIBS technique. This power should be on the order of 5 MW [2] and can become pulsed by Q-switching. Therefore the peak power per unit area, the irradiance, should be $\geq 10^8$ W/cm² [36] in order to beat the threshold value for plasma formation of the material. Shot-to-shot laser stability is a necessity for LIBS measurement, especially in quantitative analysis. The beam quality of the laser can also be counted for its reliability.

Majority of the LIBS measurements are performed using an Nd:YAG (Neodymium-doped yttrium aluminum garnet) laser. The preference depends on the reliability, compactness and usefulness of these lasers. Moreover,

besides the fundamental lasing wavelength in near infrared region, by harmonic generation, a green, a blue or an UV region laser can be obtained through a single laser (*Figure 17*). For such an Nd:YAG laser, the Q-switched pulses are about 5-20 ns in width which are sufficient for LIBS applications.



Figure 17. Two different Nd:YAG lasers, One at 1064 nm (Ekspla NL 301) and the other is the second harmonic, i.e. at 532 nm (Big Sky)

Some other lasers, namely, excimer, CO₂ or microchip lasers are also in use [2]. Furthermore, with increase in popularity of double pulse LIBS, a combination of a nanosecond pulse and a femtosecond pulse like from a Ti:Sapphire laser or a fiber laser take their place in literature [14], some researchers also perform experiments by only using femtosecond [47-49], even picosecond pulses [39, 50]. It is concluded that, duration of characteristic emission lines and plasma decay rates are much faster in femto and picosecond experiments, therefore gated detection is a must for their cases [36].

4.2 Detectors and Spectrometers

While operating a LIBS experiment, a wavelength selection device and a detection system are needed. The expectations from such devices are the high spectral resolution (<1 nm) and coverage of the desired wavelength range (at least 200-800 nm).

The signal from the plasma can be detected simply by using photodiodes (PD), photomultiplier tubes (PMT) or photodiode arrays (PDA). In PD and PMT, the signal intensity is detected and this should be spectrally selected by another device like monochromator. PMT and PD have advantages of high sensitivity, fast response and low noise, however, since they are huge and several channels of interest cannot be measured simultaneously.

More commonly, charge transfer devices like charged-coupled devices (CCD) and charge injection devices (CID) are in use. PDA, CID and CCD (Figure 18) are solid state light-integrated devices that make them slower, since they collect light for a period of time and the read-out comes after. However, if they are equipped with a microchannel plate which amplifies the incoming light, they can make the process quicker [41]. Such a technology is called the intensified CCD or intensified PDA that are ICCD or IPDA. They provide time-resolved information [2]. As expected, such a technology need more financial support so deciding on CCD and PDA sometimes comes to stage instead of them. Since PDAs consists of one-dimensional arrays of photodiodes they can provide only one-dimensional spatial intensity information; however, CCDs consisting of two-dimensional arrays can provide intensity information for two-dimensions [41].

In recent years, CDD and PDA are in use usually by coupling with a spectrometer like Czerny-Turner or Echelle spectrometers for resolving the light more efficiently.

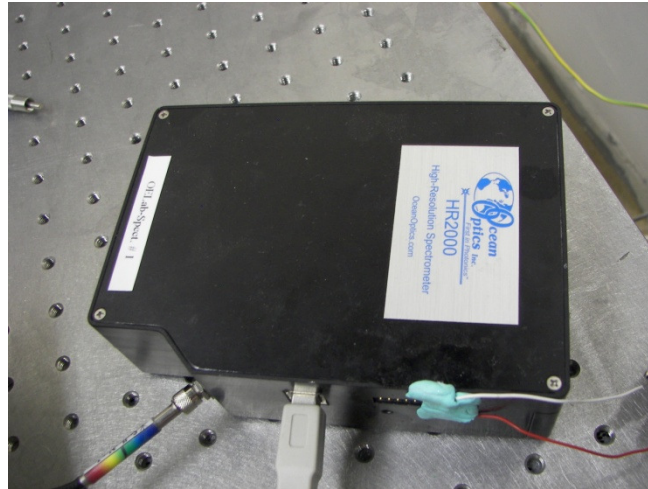


Figure 18 A CCD array detector (Ocean Optics, HR2000)

4.3 Targets

The physical, mechanical and thermal properties of the target affect the size and shape of the crater that is created by focusing of the laser. The reflectivity of the target decides the interaction with the laser. The reflectivity, density, specific heat and boiling and melting temperatures have an important influence in the threshold value for plasma formation of a material and the crater created (Figure 19), obviously [36].

Some elements have more probable transition lines than others, which make them easily be found in a compound, however, also make them to shadow the others. For instance, metals have low ionization potentials which make them easy to be observed, however this makes a need of more effort for other elements within spectrally close neighborhood to be identified.



Figure 19 ZnSe target with different sized craters on it due to different spot sizes of the focusing laser

Even no sample preparation is needed in LIBS experiments; surface roughness and the homogeneity of the materials are also effective while identification analyses are of interest.

Moreover, the physics beyond the technique quite changes with different physical states of the material. Although it is applicable to all solid, liquid, gas states and aerosol, the findings, under the same experimental conditions, change accordingly.

Therefore, the properties of the target should be taken into account while working with LIBS.

4.4 Optics

The laser is focused on or above the target of interest. For focusing the laser a converging lens is needed, it can be a spherical one, with corresponding aberrations or a cylindrical or parabolic lens for special purposes. The laser can also be needed to be directed to the focusing area, in which case some mirrors can be in use. However, for any optics in use with direct laser beam has to be coated properly. That means coating should take wavelength and power of the laser into account for both long life time of the optics and

elimination of the contribution from lens or coating elements to the sample of interest.

Another possible usage of some kinds of optics is in collecting signals from the plasma. Another converging lens or a fiber optic cable (Figure 20), or a coupled version of the two can be constructed before the detection system. For the lasers having wavelength within the spectral interest range, some kind of a wavelength selection optical filter has to be included for not to saturate the detection system and/or not to shadow characteristic emission lines.

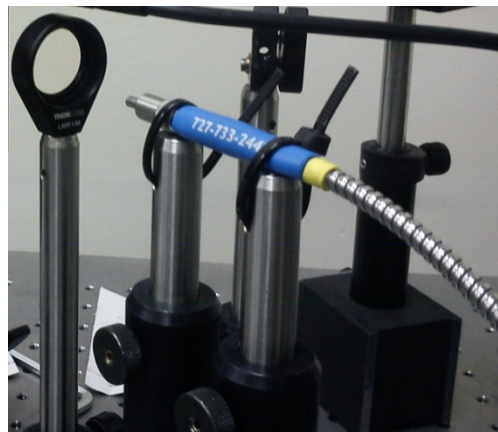


Figure 20 A converging lens and fiber optic cable for collecting the spectral emission

CHAPTER 5

EXPERIMENTAL APPROACHES

In this chapter, the different experimental approaches including the commercial portable LIBS system, the constructed double-pulse LIBS, the polarization and the air spectroscopy experimental setups that had been used throughout the study are discussed in detail.

5.1 Portable LIBS System

For the portable LIBS experiments of this study, briefcase size PORTA-LIBS-2000 (StellarNet Inc.) has been used. The system is composed of a high peak power pulsed-Nd:YAG laser and high resolution EPP2000 spectrometers. The pulse width of the laser is 6 ns and the power is 30 mJ operating at 1064 nm. The spectrometer has 4-channels which cover 200-1100 nm with a resolution of 0.2 nm and detector type of 2048 pixel CCD array. Samples are hold in a plasma chamber of 2 x 2 x 3 inches box in which there are 4 openings; one is for the incoming laser beam and the rest are for the fibers connected to the spectrometer. Within the PORTA-LIBS 2000 (Figure 21), two fiber cables are outgoing from the plasma chamber, one directly reaches to the one of the detectors corresponding to a specific channel, and the other is split into three more fibers connected to the other detectors. The system is also connected to a battery and a computer. Although there are many devices and cables around, the system can be

moved to field and can work without electricity for a while. It can be treated as the truly portable low cost analyzer that can be used for real-time qualitative measurements of trace elements.

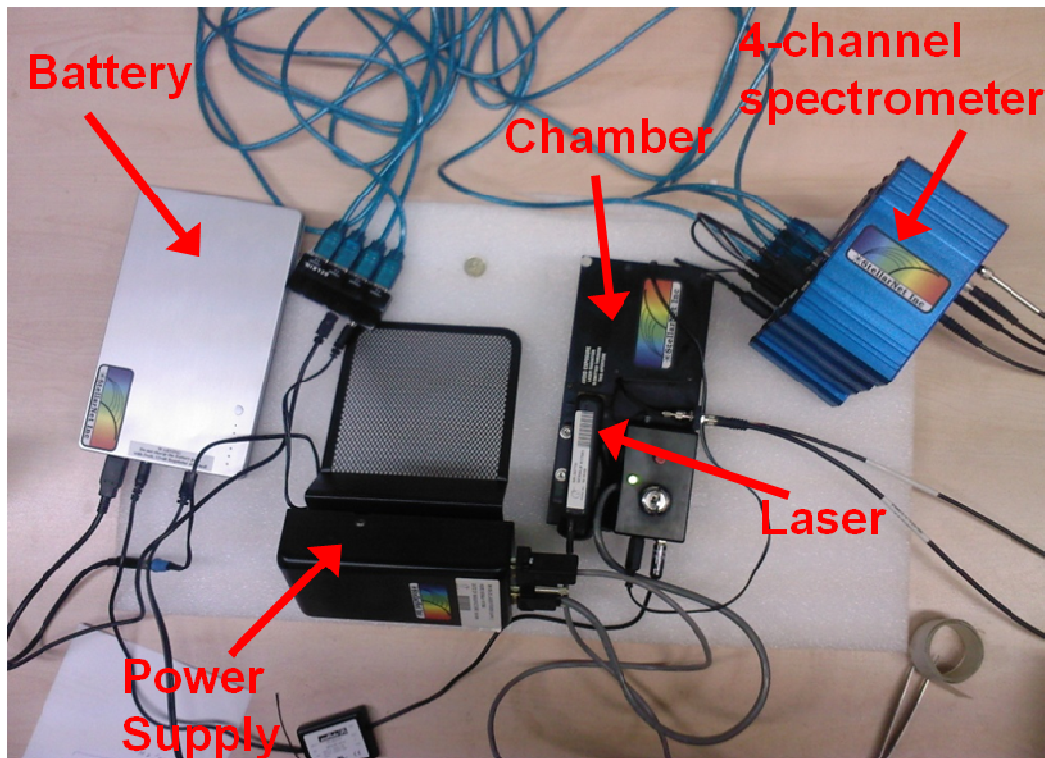


Figure 21. Picture of the StellarNet PORTA-LIBS 2000 composed of batteries for the spectrometers and the laser, plasma chamber, spectrometers and fiber optic cables

Since the basic principle of a LIBS system is to direct a laser shot to the sample and then detect the emissions sourced from that shot and look for the elemental emission spectra through a database, the system has software to perform UV (ultraviolet) - VIS (visible) - NIR (near infrared) spectral analysis of unknown samples which will be discussed in the Section 7.1.

5.2 Double Pulse Experiments

As mentioned in Section 2.4, usage of double pulse in LIBS applications lead enhancement in intensities of the characteristic emission lines which helps to identify the sample content. However, the portable LIBS system has only one laser that is focused to a closed chamber and this only laser cannot generate two consecutive pulses. Therefore, for double pulse investigations, a new experimental setup over an optic table is designed.

Single pulse experiments are performed prior to double pulse experiments for comparison concerns and they are realized just omitting one of the lasers in the system during the operation. Therefore, the detailed explanation of the double pulsed experimental setup will cover the experimental setup for the single pulse-experiments.

In the double pulsed experiments, two Q-switched Nd:YAG lasers with sufficient shot-to-shot stability and high beam quality are used. One of the lasers (Big Sky-Quantel) which have around 25 mJ of energy operates at 532 nm with a repetition rate of 1-100 Hz and a pulse width of 6 ns. The beam profile of the 532 nm-laser is investigated and the result can be stated as Gaussian as seen in Figure 22 which make it appropriate for LIBS applications. The other laser is developed by a regional firm called Focus Engineering, the IR-100; it operates at 1064 nm with the repetition rate of 1-100 Hz and pulse width of 20 ns with an energy about 45 - 60 mJ (Figure 23).

All the data are recorded either by 4-channel spectrometers (EPP2000) of the aforementioned portable system with a high resolution about 0.2 nm or by the HR 2000 spectrometer of Ocean Optics covering the same wavelength range (200-1100 nm) with a CCD array and having sensitivity about 1 nm.

The output emissions are collected by a fiber optic cable and transferred to either of the spectrometers. A notch filter blocking the 532 nm-laser line is often used in order not to shadow the meaningful information around the laser line. It is placed just before the fiber optic cable that is connected to the spectrometer.

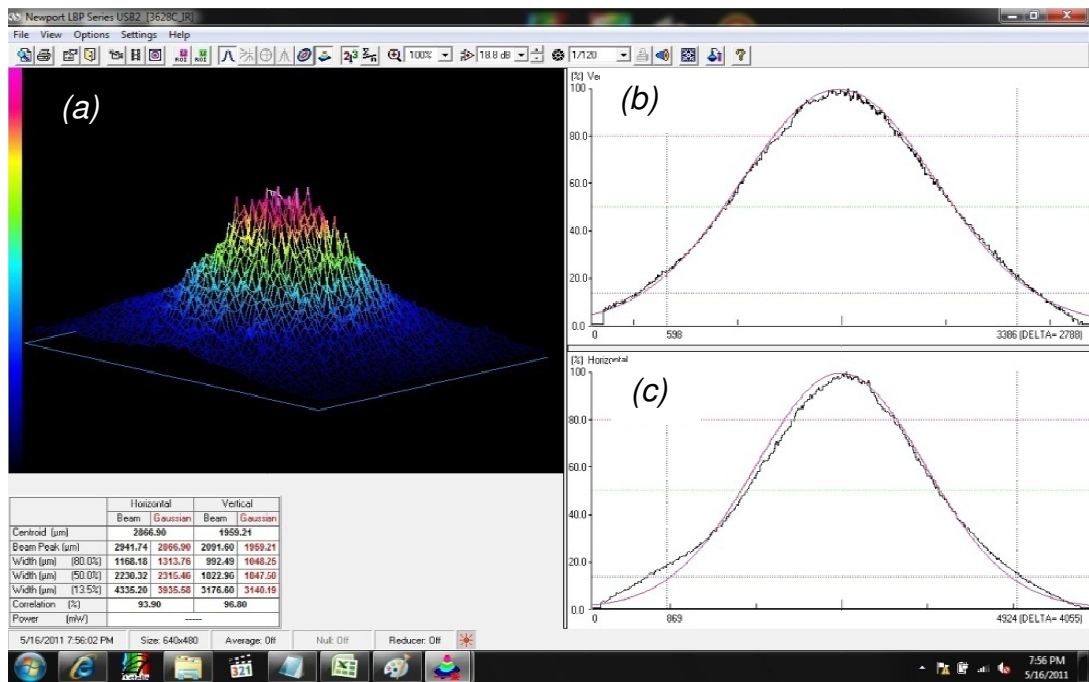


Figure 22. Newport beam profiler result of 532 nm-laser, (a) 3-D illustration of the beam, (b) vertical beam profile of them fitted to a Gaussian curve and (c) horizontal beam profile of them fitted to a Gaussian curve

For both single and double pulse experiments, a pulse generator (Stanford Digital Delay/Pulse Generator) is used in order to trigger the spectrometer to prepare it to start recording at a sufficient time after the pulse(s) being sent. In order to amplify the voltage output of this Stanford pulse generator from 4 V to 5 V which is a need to feed the spectrometer, one of the Agilent 33220a or Thandar TG 105 pulse generators are also used. The Stanford Digital Delay/Pulse Generator is also used in the case of double pulse experiments, at which there should be a certain time delay between the two consecutive

pulses of the lasers. So, in short, the Stanford pulse generator has two roles, one is to trigger the second laser to send the second pulse after a certain time delay; the other is to trigger the spectrometer after a different time delay after the last laser shot is sent.

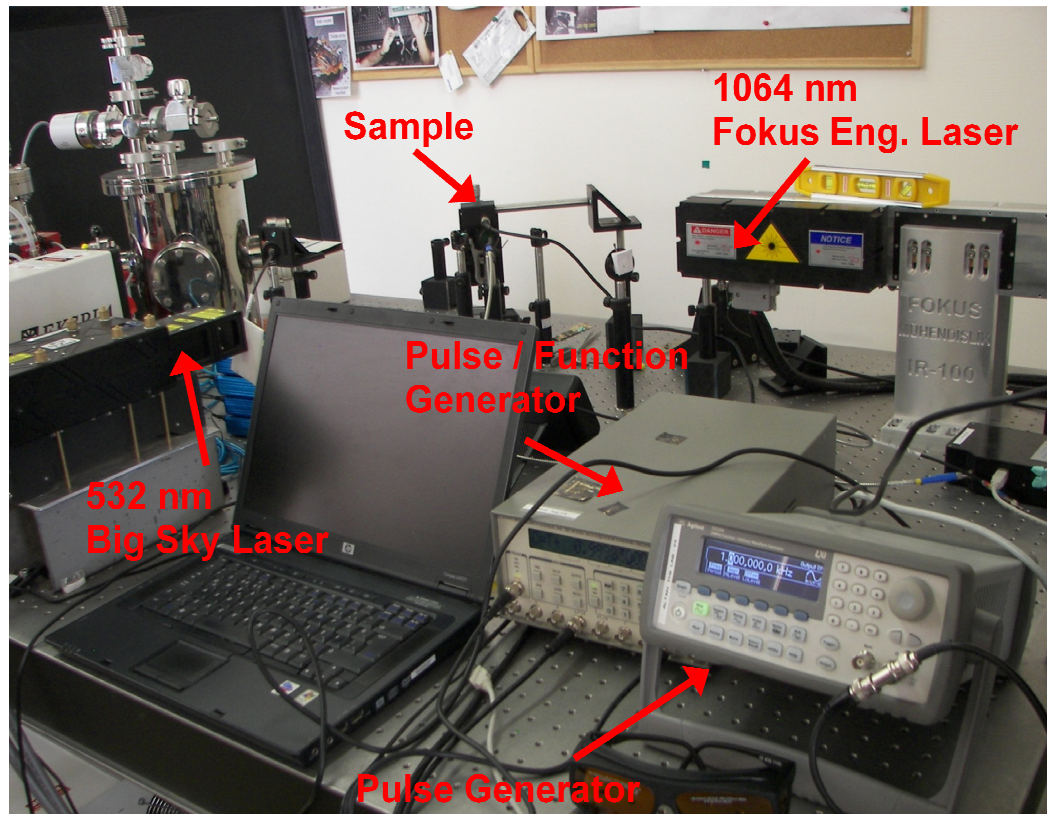


Figure 23. Picture from LIBS Lab with some components

There are few key concepts while dealing with double pulse LIBS, one is the timing. In order obtain desired results; timing should be taken into account carefully. Therefore, although the time delay is generated by a function generator, the given time delay between the laser pulses is double-checked to ensure there is no time loss in cables. This double checking is performed with a sensitive digital oscilloscope (LeCroy 6100A) through PIN diodes which are fast-response monitors for light. To make the time-delay check

procedure clear and show the time keeping is accurate enough, it is necessary to explain the usage of the PIN diodes together with the oscilloscope. The first check is performed for the laser shot of the 532 nm-laser. The Q-switch BNC-out of the 532 nm-laser is connected to the high resolution-oscilloscope. A Si PIN diode (ET-2000, Electro-Optic Technologies, Inc.) is placed close to the point where the laser shot is focused and the BNC cable from the diode is also connected to the oscilloscope. Then the laser is operated and the signal of laser beam from the PIN diode and the Q-switched out signals are displayed simultaneously on the oscilloscope as pictured in Figure 24. The comparison of the two signals showed that the rising edge of the Q-switch out signal is occurring precisely at the same time with the laser shot. This leads to use the rising edge of the Q-switch out signal for shot time of the 532 nm-laser in all of the experiments.

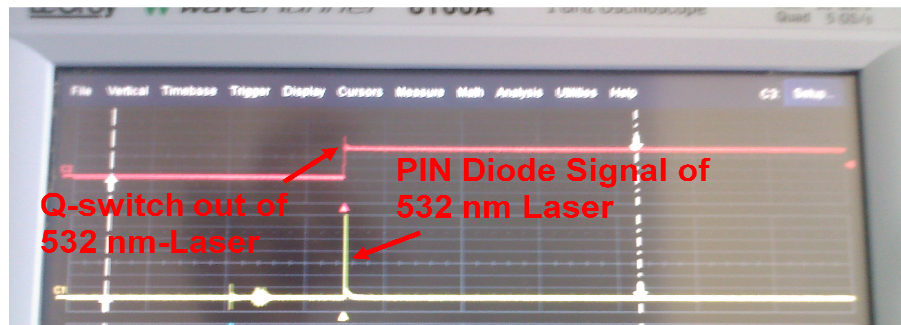


Figure 24. Q-switch out and PIN diode signals of 532 nm-laser shown in oscilloscope screen

For shot time of the other laser, PIN diode signal is always taken into account in the experiments. Even though the Si PIN diode showed the same timing, due to its more sensitivity to the lasing wavelength, the InGaAs PIN diode (EOT 3000, Electro-Optic Technologies, Inc.) is used for the 1064 nm-laser. Ultimately, the time delay is actually provided by the pulse/function generator, but since the electronic transfer could add extra delay, the time between two

adjacent pulses from the two lasers (Figure 25) is also checked by the digital oscilloscope of read out sensitivity of 0.001 μm .



Figure 25. Pulse timings of the laser shown in oscilloscope screen

For the collinear configuration proposal, Figure 15 (a), the easiest way is to use a single laser and control its two adjacent pulses. Although both of the lasers that are used in these LIBS experiments can be tuned to any frequency desired, since to stop lasing exactly after sending two shots is an issue in short response times. Moreover, such configuration is examined plenty of times by other study groups [11, 15, 16]. Therefore, the (b), (c) and (d) configurations of Figure 15 are experienced. In the first configuration, (b), the first laser hits the target, the second one is sent orthogonally to focus just above the target where the plasma is occurred due to the first laser shot. The second configuration, (c), has the same orthogonal structure; however, this

time the laser orthogonal to the normal of the target is first sent and focused just above the target, where plasma will occur after the second laser lying at the normal to the target hits the sample (Figure 26). Although the last configuration, (d), is proposed by a work group [18], it has not been encountered in the literature during this study. It also contains an orthogonal laser settlement; however in this case, none of the lasers hits the target at normal incidence angle. One of the laser hits the target with an angle 45 degrees to the normal and the other laser also hits the target with the same magnitude of angle but from the opposite side as seen in Figure 27.

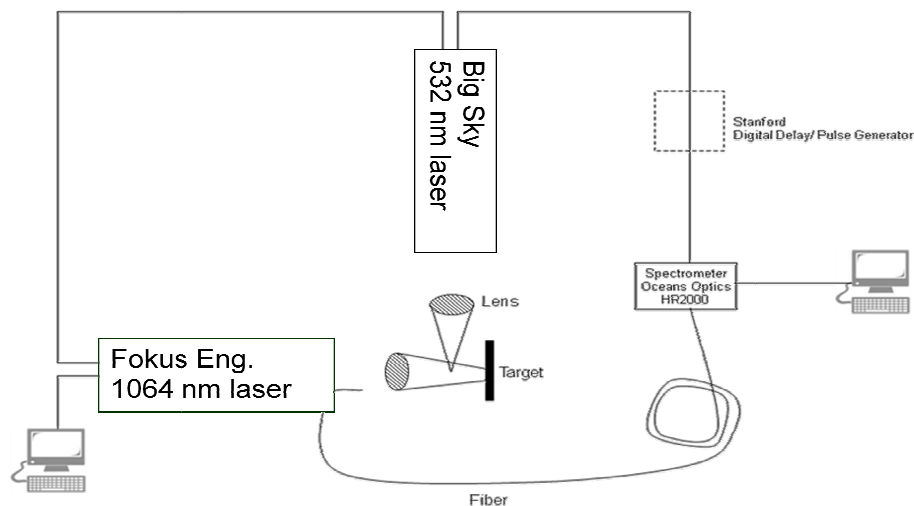


Figure 26. Orthogonal configuration of double pulsed LIBS setup, either the laser of Fokus Engineering is sent first to generate plasma of the target first or the laser of Big Sky is sent to produce an air spark

For the (b) and (c) proposed configurations, the experimental setup shown in Figure 26 is designed. The 1064 nm-laser and the 532 nm-laser are set perpendicular to each other. The target is placed so that the 1064 nm-laser is in its normal direction and the 532 nm-laser beam is parallel to and 1 mm above from the surface of the target. Anti-reflection coated lenses are fixed so that, one focuses a little beyond the target surface, the other 1 mm above the sample in the local where the other lens is focused through.

One of the key concepts of double pulse LIBS, the timing, was mentioned before; the second but not the least one is the positioning. Focusing two lasers to desired and related points in order to have optimal plasma is not an easy step to take. Precisely, fine alignment is very difficult without a plasma monitoring device. Instead of using such a plasma monitor, a two-dimensional translational stage is used for alignment, however still finding the beam waist of the 532 nm-laser and focusing it on the place where center of the plasma is or will be occurred is a problem. Using the benefits of the optic table and micrometer sensitive translational stage, and with many time-trials the necessary positioning can be achieved to some extent.

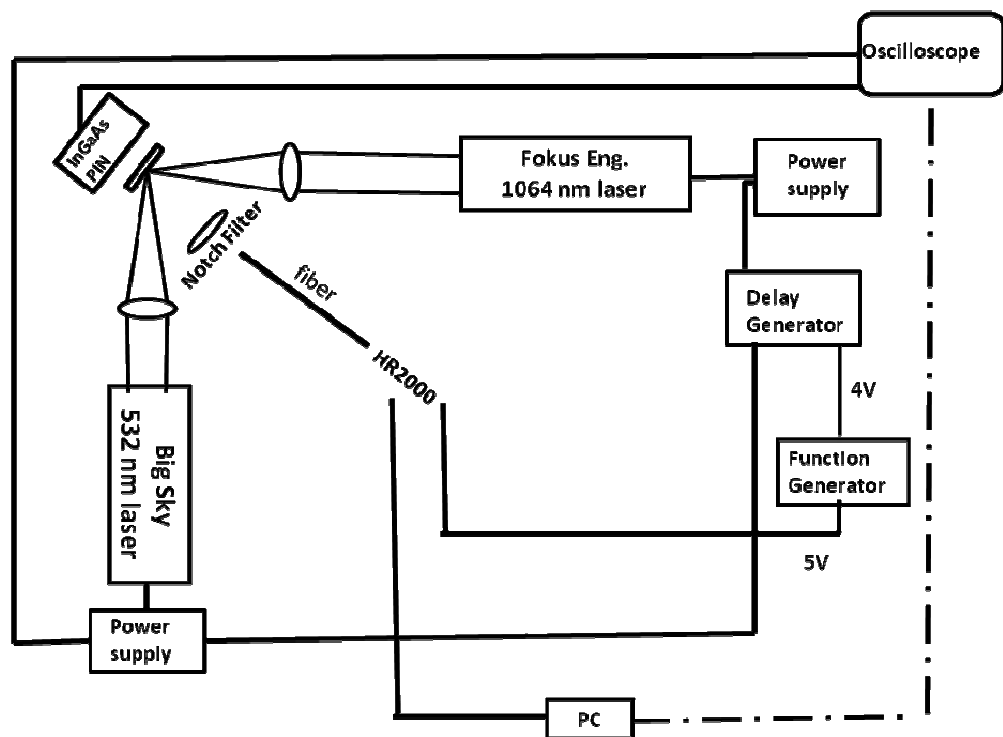


Figure 27. 45 Degree Configuration of Double Pulse Experiment

In the case of configuration (d) of Figure 15, these positioning difficulties are easier to handle. In this configuration, the two shots are aimed to hit the target at the same point although they are originating from lasers that are

perpendicular to each other (Figure 27). Since naked eye can see distinctly the spots of the lasers on sample, the positioning is not as difficult as in the previous configurations. The two lasers are directed and by using converging lenses focused to the sample with an angle of 45 degrees to the normal from either side of the sample (Figure 28). Once the two spots are focused on the same point at the target surface, the positioning issue is almost entirely solved. Therefore, for reliable comparison needs, especially like in different crystal surfaces of the same element experiments as in Section 5.3, this configuration can be treated as more favorable. Furthermore, by hitting the target with both lasers, ablation is increased so the interaction in the plasma is improved.

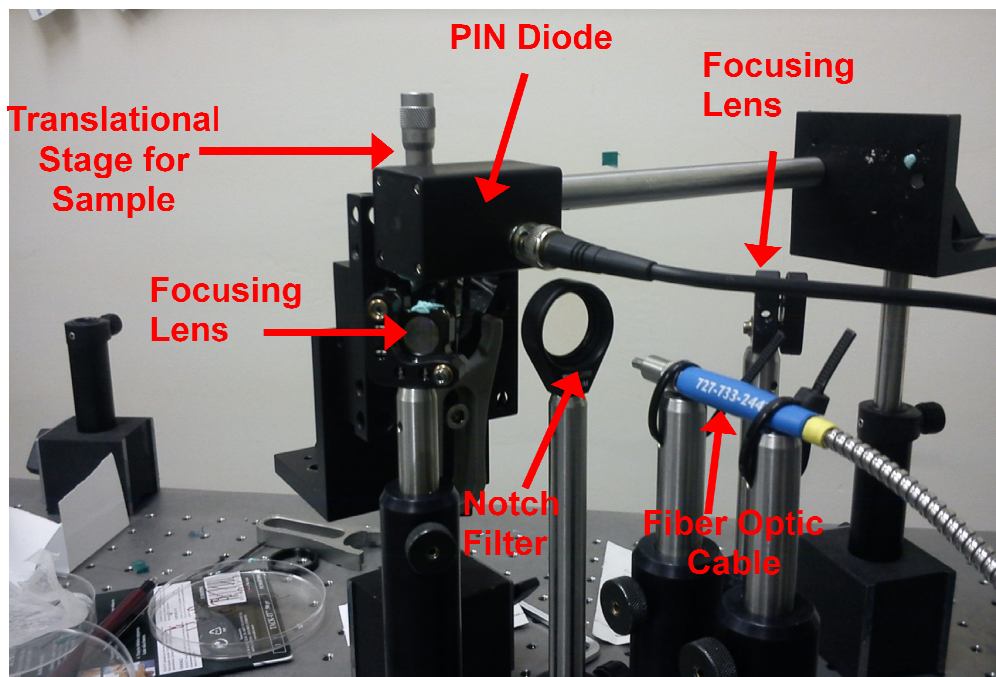


Figure 28. Close up picture of 45 degree configuration experimental setup

5.3 Different Crystal Surface Experiments

Various kinds of samples are investigated in literature and also in this thesis. Some similar behaviors for similar groups have been observed. However, LIBS has never been applied to an element with different crystal surface as far as it has been investigated through this study. Hence, such an investigation of different crystal surface of an element under LIBS inspection is attempted to cover in this study.

Crystals are extraordinary structures that are composed of periodic array of atoms. In solid state physics, crystal structures are defined as a kind of a logical summation of *basis* and *lattice*. A lattice is an infinite array of points in space and arranged in a way that every point has the same surroundings [51]. The smallest arrangement that repeat itself is called a unit cell. The length of a unit cell is the lattice parameter, a , which is constant for an element. There are different types of lattices. Their geometries can be cubic, tetragonal, orthorhombic, rhombohedral, hexagonal, monoclinic and triclinic. The structures are also classified according to the locations of atom in the mentioned geometries. For instance, for a cubic geometry if the atoms are placed only on the corners of the cube, the structure is called the simple cubic structure, Polonium has such a structure. For structures more complex than a simple cube, the direction to survey the structure differs. This direction refers to the orientation or surface of a lattice that is faced. In the case of the experiments performed in this study, only Silicon element, with two different crystal directions are dealt and they are going to be discussed deeper below. For more information about other elements and drawings to illustrate the definitions, solid state books [51, 52] will be efficient.

Silicon has the diamond cubic structure consists of two interpenetrating face-centered cubic lattices. Face-centered cubic (fcc) structure means the atoms are placed on the corners and the center of the every edge of the cube as illustrated in Figure 29. In the Silicon element experiments, the two different crystal surfaces investigated are called as (100) and (111), they are the index numbers (Miller indices) indicating the orientations as illustrated in Figure 30. For simpler visualizing, in Figure 31 the Si surfaces are presented as they are arranged in the crystal.

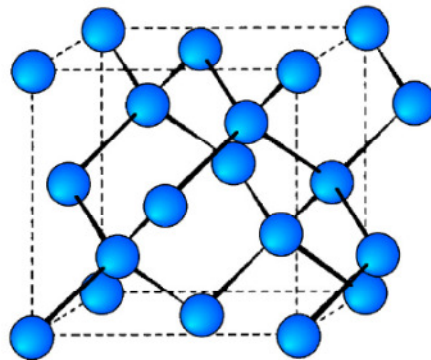


Figure 29. Unit cell structure of face centered cubic lattice illustration [53]

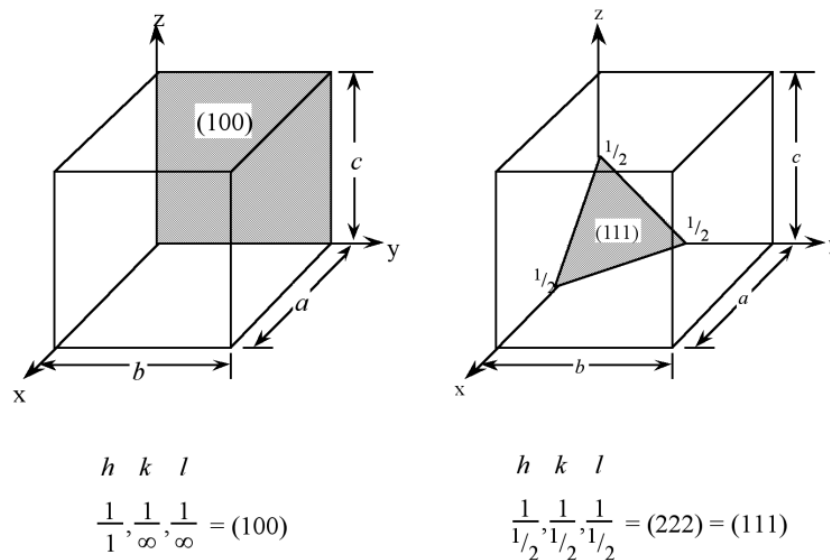


Figure 30. (100) and (111) crystal surfaces with corresponding Miller indices [53]

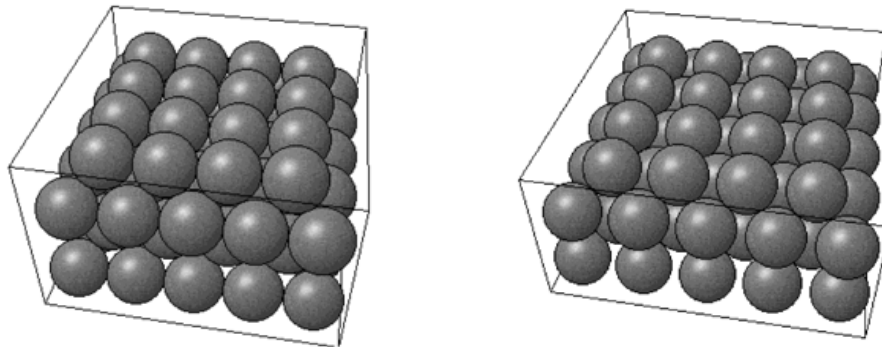


Figure 31. 3-D illustration of Si (100) and Si (111), respectively [54]

The surfaces in a crystal can be differentiated in a number of ways, one of which is evaluating their atom and bond densities. The atom density of a surface may be defined as the number of atoms in a unit area. The hexagonal packing for Si (111) and square packing for Si (100) and the orientation of both Si surfaces are visualized in Figure 32. Determination of planar area of Si (111) needs simple geometric calculation. The hexagon consists of 6 equilateral triangles of edge length $a/\sqrt{2}$; a being the lattice parameter for Si, 5.43 Å. So the area calculated for Si (111) is 38.3019 Å^2 . For Si (100) case, calculation is much easier, a square of edge length, a , so the area for Si (100) is 29.4849 Å^2 . Si (111) has three Si atoms in one of its hexagons. It can be counted as; the one atom in the center counts 1 and one third of the six corner atoms count 2 more. That is 3 atoms in a planar area of 38.3019 Å^2 . So the planar density is the ratio of them, 0.0783 Å^{-2} . Si (100) has two Si atoms in one of its squares, as one in the center counts 1, and one fourth of the four atoms counts 1 more. That is 2 atoms are in a planar area of 29.4849 Å^2 . So the planar density is the ratio of them, 0.0678 Å^{-2} . These planar densities in atoms/cm² unit are also calculated by Banerjee, [55] in his thesis. The ratio of the planar densities is (100):(111) = 1:1.1543 and it is constant for similar structured crystals [56].

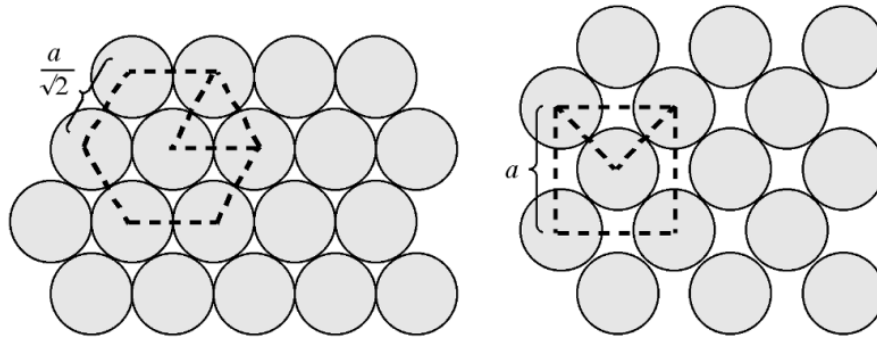


Figure 32. Schematic representation of packing of the fcc (111) and (100) respectively [56]

For bond density calculations, *coordination number* which is determined by the structure of the material should be mentioned. For instance, all atoms within a bulk of Si are in a tetrahedral four-coordinate environment [56]. However, for different surfaces, it is seen that these four bonds are not necessarily occupied. The missing bonds are called the *dangling bonds* [56]. In Si (111) surface three of four coordination numbers are bonded. In Figure 33 (a), the atom at the surface colored in blue is bonded just to the three red colored atoms. That leaves one dangling bond. On the other hand, Si (100) has two bonded atoms as seen in Figure 33 (b). The blue colored atom is bonded to the two red colored atoms, leaving two dangling bonds [55, 56]. So the ratio of dangling bonds for (100):(111) = 2:1. By using the planar density ratios, dangling bond density ratios can also be calculated; that is, (100):(111) = 1:0.577 [56].

The reason why growth of Si (111) planes is slower than that of Si (100) is connected to the dangling bonds as stated by Barron [56]. Furthermore, according to Banerjee [55], Si (100) surface having two dangling bonds is “highly reactive and unstable”.

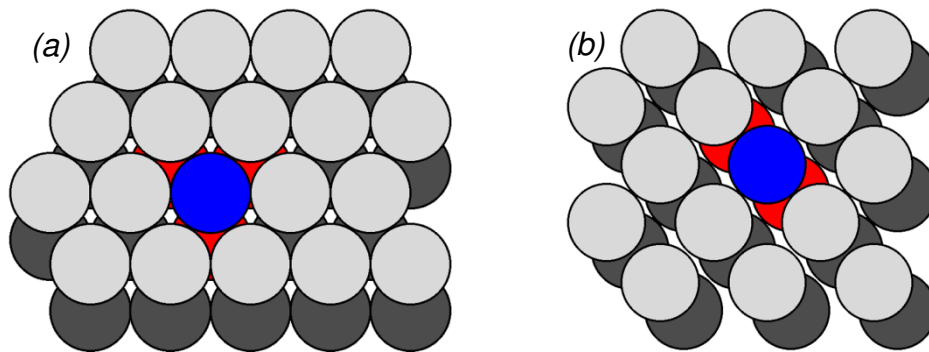


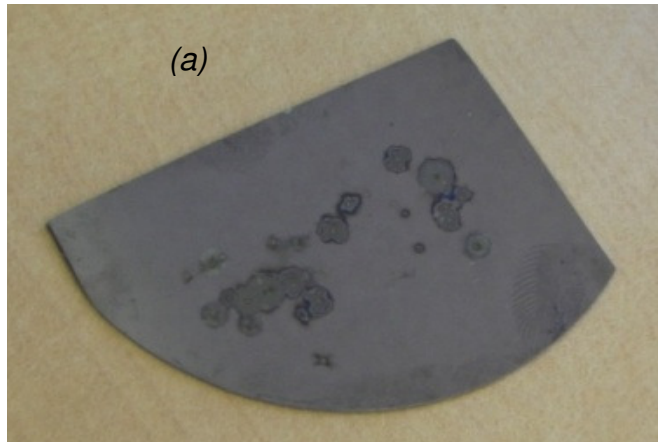
Figure 33. Illustration of atoms corresponding to (a) (111) and (b) (100) surfaces of fcc [56]

For investigating the differences, if there exist; both single pulse and double pulse LIBS experiments are performed on the above mentioned surfaces. Due to its nature, Silicon can be amorphized when facing a laser hit. The sample and the SEM image of it after LIBS experiments are pictured in Figure 34. As seen by naked eye or via SEM, the surface is deformed after laser application.

Silicon samples are also used in polarization experiments since they are semimetals and special spices with different surfaces.

5.4 Polarization Experiments

To improve the performance of LIBS, it is necessary to develop new strategies to control parameters that affect the spectrum. One of which can be dealing with polarization. Taking polarization effects into account to reduce the signal to noise ratio has also been tried by Penczak et al. [57] and Liu et al. [58]. In the work of Penczak et al. [57] while dealing with aluminum, they reported that polarization decreases with increasing pulse energy. Another comment of them was they observed that continuum emission is nearly totally polarized. Similar finding of strongly polarized continuum is stated by Liu et al [58] when experiencing ultrashort ablation of silicon.



(b) Nd: YAG -532nm-pulse laser beam spot (diameter: $\sim 180\mu\text{m}$)
 @ laser beam fluences of $(0,7\text{mJ}/180\mu\text{m})$ $1,3\text{J}/\text{cm}^2$ with a
 Repetition rate (f_{rep}) of 1Hz on Si(100)

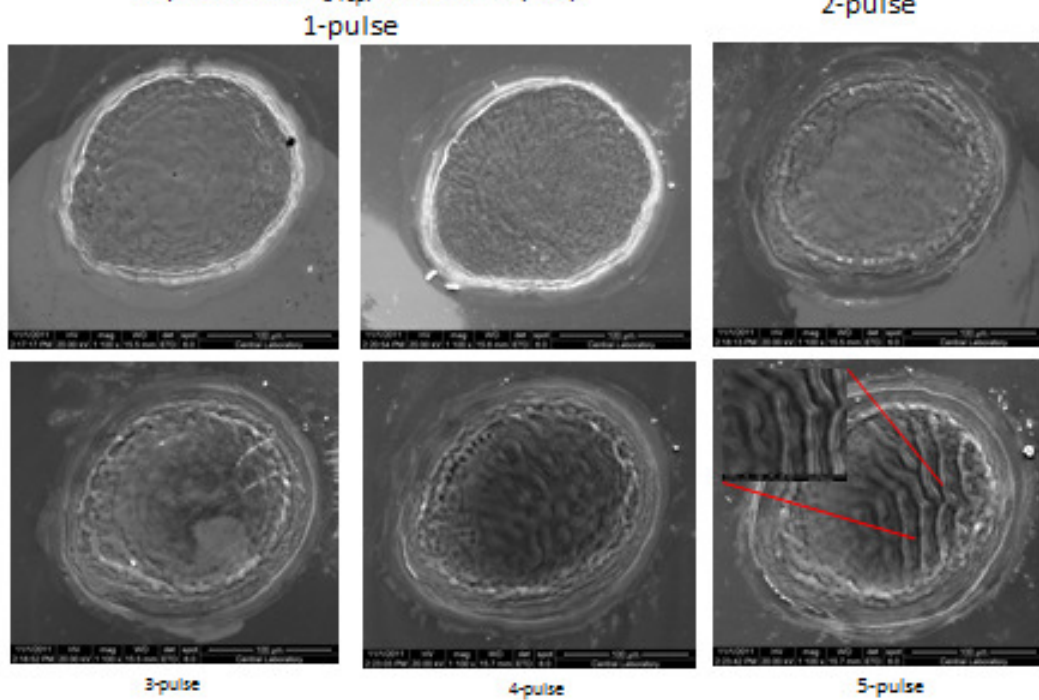


Figure 34. (a) Picture of Si (100) (b) SEM (Scanning Electron Microscope) picture of $180\mu\text{m}$ diameter crater of Si (100) taken at METU Central Laboratory

Nanosecond usage on a semimetal has not been studied as far as inspected during this study. It is therefore created a curiosity. Since usage of double pulse is an issue of different investigation which is also covered in a different section (Section 6.1) of this study and in order to keep the number of parameters and contributors small enough, for investigation of polarization dependency, only one laser with nanosecond pulse width on Si targets is used.

The 532 nm-laser sends ideally vertically polarized laser beam. In reality, it is composed of mostly V-polarized beam, however at any angle of a polarizer; the beam cannot be totally prevented. Keeping this in mind, an experimental setup is constructed by sticking to the 45 degree configuration described above. That is, as shown in Figure 35, the laser is directed with 45 degrees-angle to the normal of the sample surface and focused to a point. The notch filter which is used to eliminate the laser beam reaching to the spectrometer is placed through the normal line of the sample. The angle-adjustable polarizer and the fiber optic cable are also mounted in the same line after the notch filter. The fiber optic cable is connected to the spectrometer which records the spectra after having trigger signal controlled by a pulse generator in communication with the laser. Ultimately, the setup is prepared to detect the plasma emissions of decided angle of polarization adjusted by the polarizer.

5.5 Air Spectroscopy Experiments

LIBS, as mentioned previously, can be applied to materials of any physical state which makes it prominent among other spectroscopy techniques. In the gas state spectroscopy experiments, a higher energy laser is needed in order to generate plasma as discussed in Section 2.1. According to Cremers and

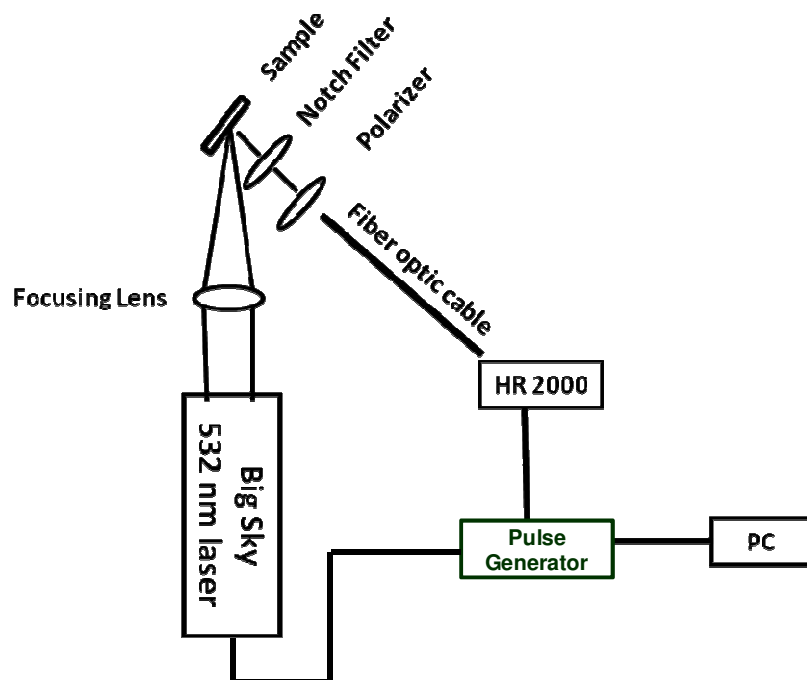


Figure 35. Polarization experimental setup

Radziemski [2], multiphoton effects are necessary for direct ionization of gases namely O_2 and N_2 . The reason is that their ionization energies are larger than photon energies of Nd:YAG laser. More specifically, ionization potential of O_2 and N_2 are 15.6 eV and 12.2 eV, respectively. However, photon energy of 1064 nm – Nd:YAG laser is 1.25 eV; even for the harmonic, 532 nm-laser, doubling of the laser energy is still much less than ionization potentials of the gases. Hence a laser with higher peak power is operated in the air plasma experiments for enabling the multiphoton processes. The laser is also an Nd:YAG laser (EKSPLA NL 301) with an energy of about 120 mJ, operating at 1064 nm. An anti reflection coated lens with high energy threshold value is used to focus the laser beam.

The HR 2000 spectrometer detected the emission lines of the air plasma via fiber optic cable. The laser could not be triggered electronically, or generate a

trigger signal which could be used as a trigger signal for the spectrometer, eventually, usage of high repetition rate is preferred so extend the life of the plasma. Since the lifetime of the plasma is not limited and the ablation is not a problem in the case of gas sample, the record is performed manually.

Another curiosity is also satisfied by measuring the air plasma under the flow of an additional gas. In this experimental setup, nitrogen gas is used to increase the elements in the area of interest. A pipe is fixed to the optic table at a height where the lens focuses the laser beam. The nitrogen gas is allowed to flow through the air plasma. While the nitrogen gas flow and the lasing are continuing the recording is done manually.

CHAPTER 6

EXPERIMENTAL RESULTS

In this chapter, first, the comparison of single pulse LIBS experimental results with different configurations of double pulse LIBS experiments are demonstrated. Then the influence of crystal surface on the intensity of the emission lines discussed through the experimental results. After that polarization dependency of the laser induced plasma is investigated. Lastly, the spectral results of the air and the air under nitrogen gas flow are compared. For most of the graphs, the emission intensities are labeled as “Relative Intensity”, since they are not absolutely measured. None of the measurements are absolute; therefore all the intensity measurements are in arbitrary units (a.u.).

6.1 Single Pulse versus Double Pulse Experiments

In minimal requirement, LIBS experiments contain a laser and a wavelength selection device. In this study, as described in Section 5.2, two different lasers are used for single and double pulse experiments. The motivation for usage of multi-pulse LIBS is to obtain intensified emission lines of samples which are not shadowed by the continuum emissions. In normal laboratory atmospheric conditions, a series of single and double pulsed experiments on different kinds of samples have been studied including various kinds of

metals, namely, Cu, Fe, Mo, Ti, W, some compounds such as CuBe, ZnSe, ZnS, GaSe and some semimetals like Si, Ge.

Previously mentioned configurations are all experienced. First two configurations, having a laser placed in the normal line of the target and the other perpendicular to this line are investigated for different samples. In Figure 36, investigation on ZnSe is graphed in which the improvement in intensity due double pulse usage is obvious. The line with "*" marking in the graph of Figure 36 is corresponding to the emission line due to double pulse LIBS experiment with a time delay of about 2 μ sec. This 2 μ sec is counted from the time when the 1064-nm laser hit sample to the time when the 532-nm laser focused to a point in the pre-plasma due to the first shot. The emission line with "o" marking is again corresponding to 2 μ sec time-delay; however it is counted from the time when 532 nm-laser focused to a point 1 mm above the surface where plasma suppose to occur in 2 μ sec time when the 1064 nm-laser hits the sample. This difference in time delays is reflected in the legend of the graph, by a "-" (minus) sign. The minus sign indicates that the 532 nm-laser is sent prior to 1064 nm-laser. For both of the configurations, the time delays about 2 μ sec give most intensified emission lines.

As seen in the graph, the intensities of the two configurations are similar. For the configuration that the sample is first hit, the peaks corresponding to Zn I lines (468.0 nm, 472.2 nm and 481.1 nm) have slightly more intensity than the configuration at which 1mm above of the surface is shot first. It is the opposite for Zn II lines. Two emission peaks of Zn II (491.2nm and 492.4 nm) are so close to each other that the resolution of HR 2000 cannot discriminate them. So the peak is a wide one and it is more intensified in first lasing of the 532 nm-laser that focused at 1mm above the sample. Since in two of the

cases, the laser which hits the sample creates the plasma, extra energy coming from the 532 nm-laser has a role on the different emission intensities. The second ionization energy is greater than the first one, obviously. In second ionization process, an electron is removed from a positively charged ion, instead of a neutral atom. Because of the electrostatic attraction between the positive ion and the electron, it is more difficult to remove an electron away from an ion than a neutral atom. That is also clear in Figure 36 that any of the single lasers are not enough to create a noticeable peak of Zn II by themselves alone. By considering this fact, second configuration at which a laser shot is focused just before the plasma is produced and just above the target seemed to generate more energy than the other configuration. Actually, it is not surprising when considering the plasma production steps in each configuration. In the first one, the laser hits the target first, it produces plasma and then the second less energetic 532 nm-laser interacts with this previously induced plasma. This less energetic laser can lead less Zn II lines in the interaction with the singly ionized ions. However, in the second case, the less energetic laser heats the atoms of the target, in other words, whether successful to ionize them or not, helps the bound electrons to gain energy. This extra energy gained by the first laser lead the higher intensity in Zn II lines. Even the intensities of the emission line corresponding to different ionization stages change slightly; overall, the temperature of the plasma is similar in any sequence of laser shots. That can be proved by using the temperature calculation of equation (16) defined in Section 3.1.5. Simply, by having the natural logarithm of the ratios of the intensities of two lines of the same ionization stage for two cases and having the ratio of these logarithms will compare the electron temperatures. In the ZnSe case, it is found very close to 1 (0.98 and 0.96 for two different trials) which is a direct implication of similar spectrums obtained even with different sequence of the laser pulses.

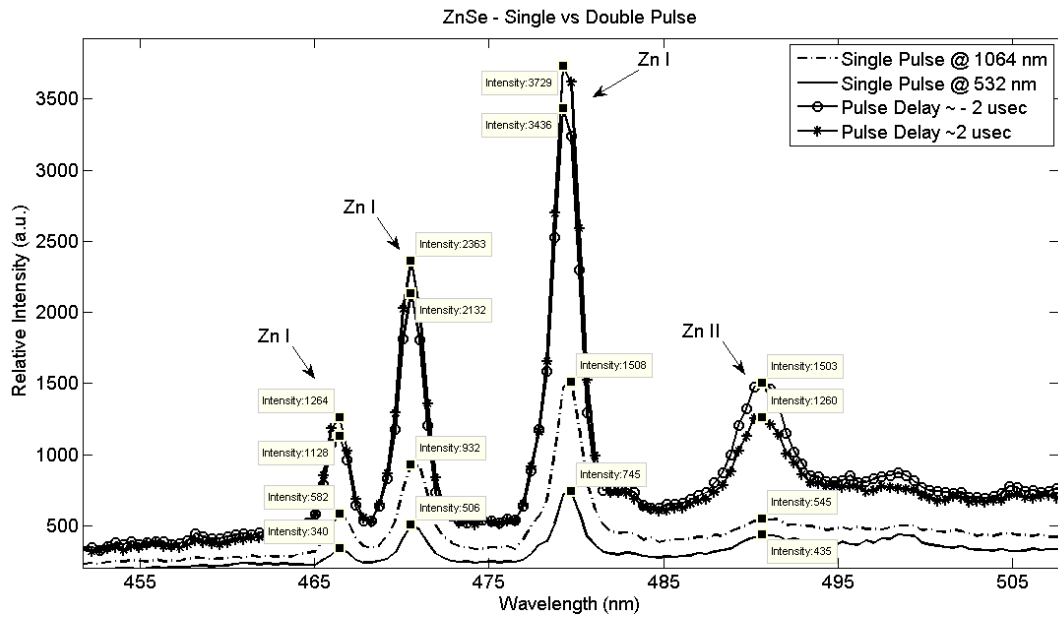


Figure 36. Experiment on ZnSe by using single pulses of 532 nm and 1064 nm laser and double pulse configurations with a time delay of approximately 2 μ sec between the two lasers, the minus sign indicates that 532 nm-laser shoots first

Spectral behaviors of the single lasers in Figure 36 also support more energy need of plasma for the formation of Zn II lines. With only one laser either with energy about 25 mJ (from 532 nm laser) or even 45 mJ (from 1064 nm laser), the wide peak covering both 491.2 nm and 492.4 nm Zn II lines is not noticeable. The actual significance is not the amount of energy of a laser of course, what influences the process is how the energy is delivered. The first laser, independent of its peak energy or focusing point, heats the target. This heating is in terms of delivering energy to bound electrons to get ready for ionization or for emission.

The enhancement by means of double pulse configurations is also needed to be emphasized here. A time delay of about 2 μ sec between the pulses results in 2 to 5 times improvement in intensity of the emission peaks and

leads to have higher values for peak to background ratios or in other words signal to noise ratios. Such an improvement can be observed in Figure 37. Different time delays changing between 1.1 and 11.5 μsec are investigated in a double pulse operation on Si (100). Any of the double pulse arrangement results in enhancement in the intensity of the characteristic emission line, but the one with about 1 μsec yields the best improvement.

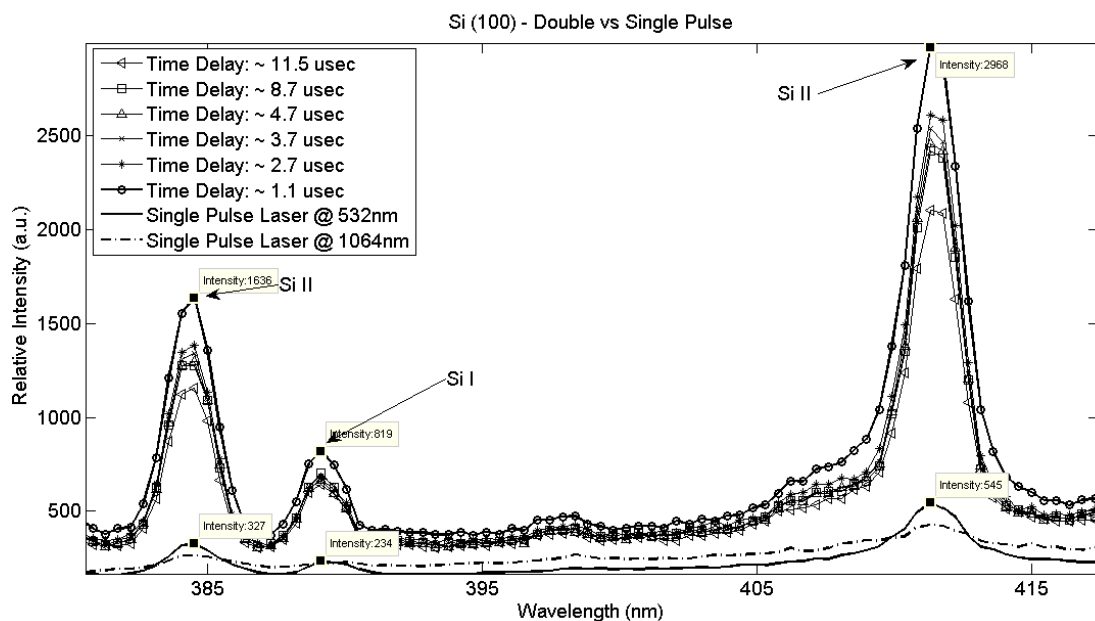


Figure 37. Experiment on Si (100) by using single pulses of 532 nm and 1064 nm laser and a double pulse configuration with different time delays of the lasers

These different time-delay laser shots could lead to wonder whether they are truly reliable or not. Such a doubt is not inappropriate, since shot to shot behavior of the lasers may change slightly. Actually with such a wonder, experiments have been repeated for a set of samples and for many times. By the usage of the experimental setups explained in this study constitute similar results for each time. That is they all achieve the most enhanced intensities with about 1-2 μsec delay times. Fortunately and of course not coincidentally, this time delay about 2 μsec is also adverted in literature [12, 36]. Although

supported by the literature, still, to guarantee no doubt, a different approach for recording is performed. In this different method, 100 laser shots and their corresponding emission spectra are recorded in an accumulation manner. The integration time is also kept high so that no data is missed before or after the second laser shot. The results of an experiment on Copper atom with accumulation 100 recordings having the integration time of 100 μ sec is graphed in Figure 38. The graph is simplified by eliminating different integration time curves in order to not to lose the significant point. The point is that, even with 100 times the plasma is produced and the resultant emission lines are accumulated, the intensities corresponding to time delay of 2 μ sec are the highest. The most probable lines of Cu I, 510.6 nm, 515.3 nm and 521.8 nm are enhanced at least three times in intensity. Even the background is also intensified because of accumulation and lack of a notch filter; the characteristic lines become much more noticeable.

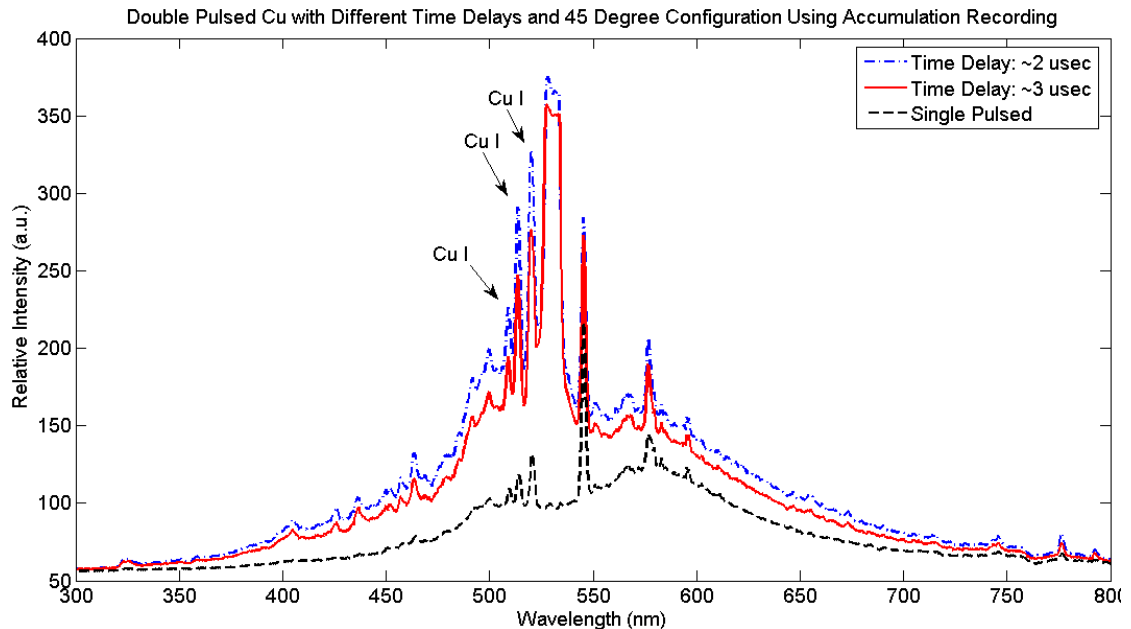


Figure 38. 45 degree configuration double pulse experiment on Cu with 100-accumulation recording with an integration time of 100ms

6.2 Different Crystal Surface

The experiments including both single and double pulses are performed to both surfaces of the Si element for many times for increasing the reliability. In Figure 39, the spectral result of a single pulse LIBS using the portable system is demonstrated. As can be interfered from the graph, the intensity of Si (100) surface is higher than that of Si (111). The similar intensity difference is seen for the double pulse experiment which is shown in Figure 40 with having a time delay of about 1 μ sec for each case. Even with a closer look, which includes taking the signal to noise ratio into account, still the Si (100) peaks have higher intensities.

Even if the same experimental conditions are used, the differences in intensity present almost always. This leads to have a look at the surface properties deeply. As calculated earlier, the dangling bond density of (100) surface is higher than that of (111) surface. Therefore the interaction within the laser spot is changing from surface to surface and this change influences the intensity. The more active or unstable the surface is the more interaction leading more intensity.

Another outcome can be about the amorphization status of Si atoms. Whether the amorphization has occurred for the Si element or not, even with more than single shot, the intensity differences imply that the dangling bond density is significantly present affecting the number of interactions and consequently the emission intensities.

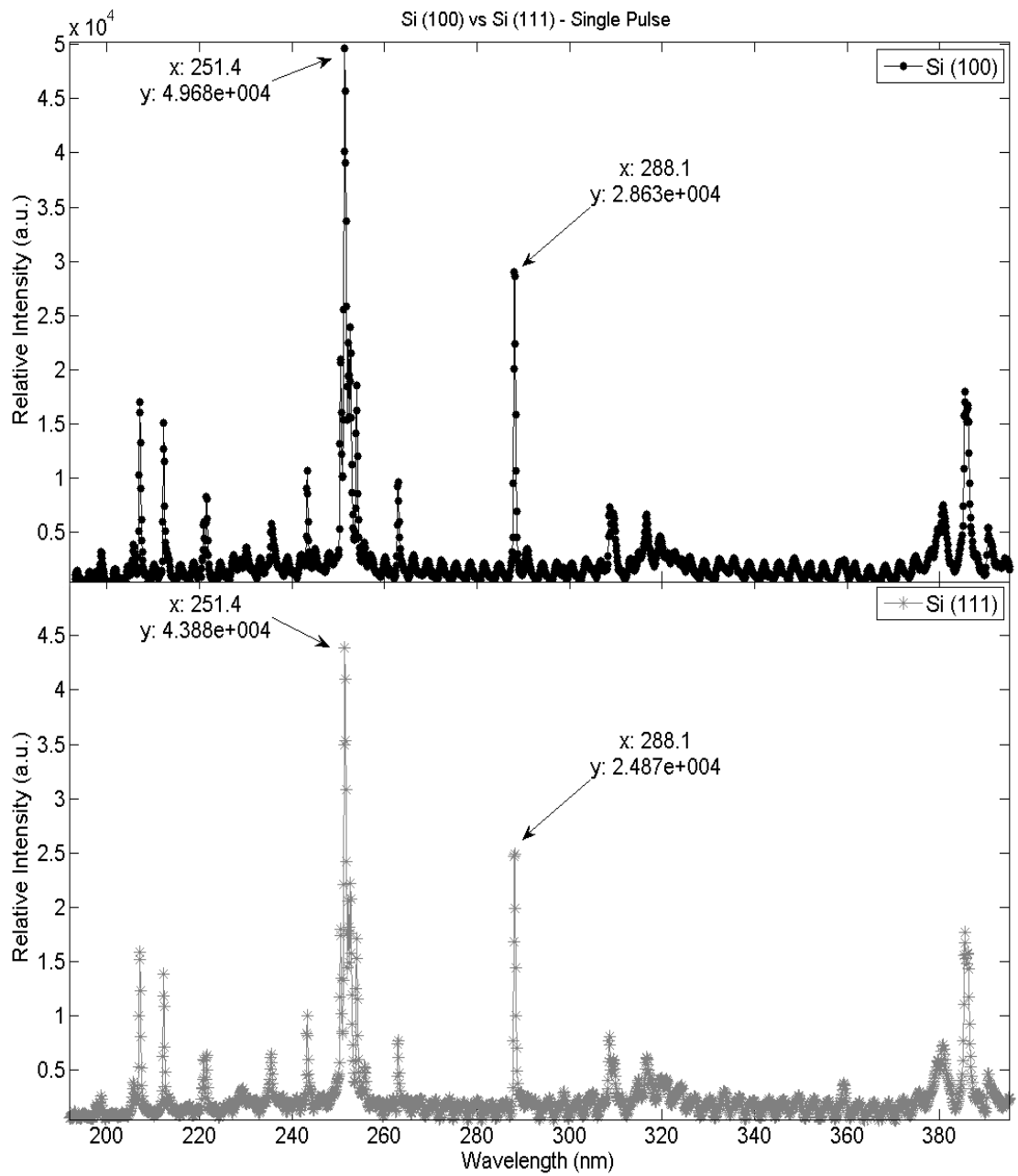


Figure 39. Single pulse spectral results for Si (100) and Si (111) by using PORTA-LIBS System of StellarNet Inc. (x being the corresponding wavelength in nm and y being the relative intensity in arbitrary unit)

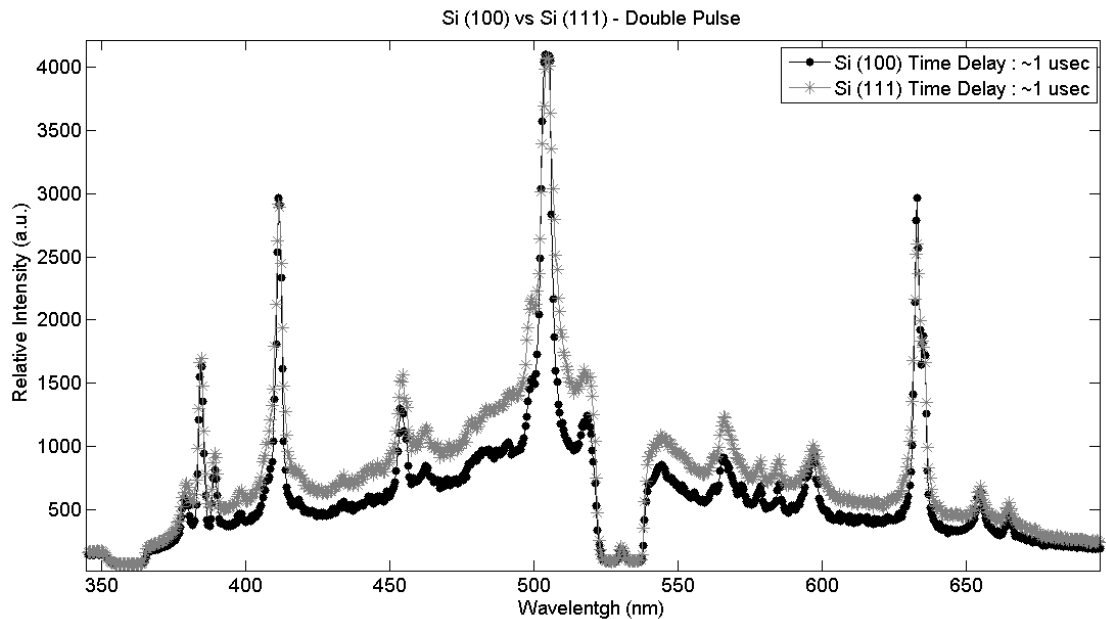


Figure 40. Double pulse spectral results for Si (100) and Si (111) with a time delay of approximately 1 μ sec between lasers

6.3 Polarization Experiments

In order to investigate the influence of polarization, an angle-adjustable polarizer is inserted between the sample and the notch filter which is set just before the fiber optic bundle of the spectrometer as mentioned before. In Figure 41, behavior of both Si (100) and Si (111) under polarization influence can be observed for different polarization angles. One of the outcome of investigation of the graph can be the behavior of the Silicon elements with different crystal surfaces are very similar for the same angle of polarization. This indicates that polarization affects the intensities of the characteristic emission lines. That may also indicate that due to the high energy transferred to the elements during the experiment, the crystal surface does not preserved, but amorphization on both element surfaces is occurred behaving similar in similar polarization conditions. Or the amorphization is not

necessarily occurring, only being the same element under polarization condition could bring such a close response.

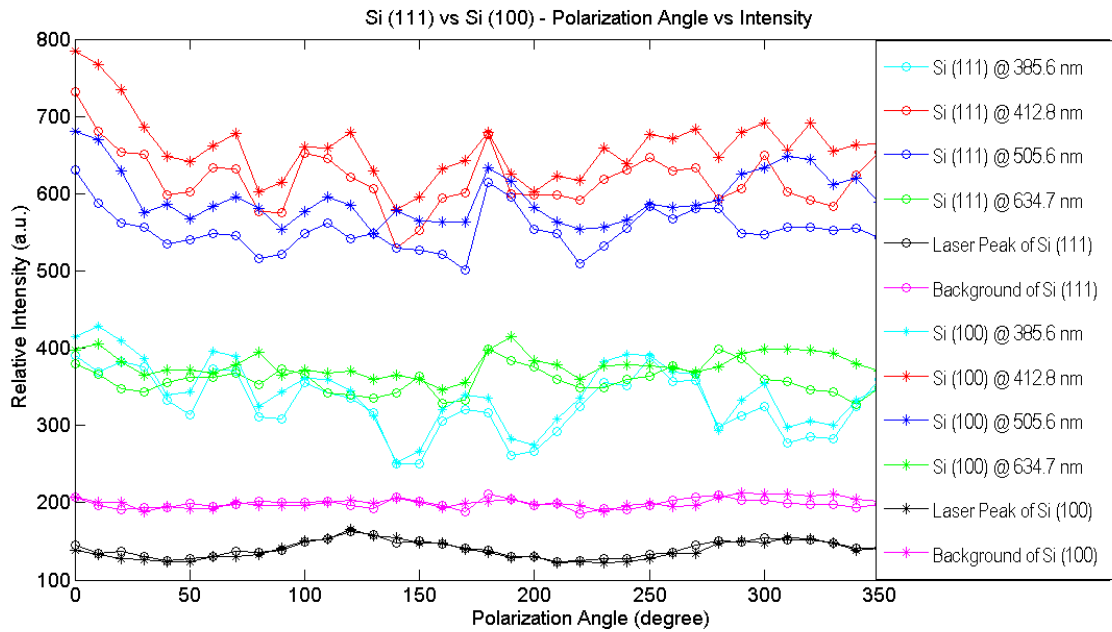


Figure 41. Polarization Angle vs Intensity graph of Si II ions for both Si (100) and Si (111)

Another result can be focused on the wavelength dependency; in shorter wavelengths, the fluctuation in the intensities with the change of the angle of polarization is much more than that of higher wavelength-emission lines which is also emphasized in a different study [58] without giving a physical explanation. Since all of the emission lines graphed in Figure 41 are due to singly ionized Si atom, the reason is not the different Coulomb force or the electrostatic field of neutral atom or singly ionized ion. However, such interference leads further investigation about the different Coulomb force or the electrostatic field that could interact and influence the polarization behavior. In this point, the transition within the singly ionized ion is investigated by means of the Grotrian Diagram. Grotrian Diagram is the energy level diagram of allowed transitions which can be useful for

visualizing the complex level structure of multi-electron atoms. These diagrams of interest can be found in the website of the National Institute of Standards and Technology [59] and they are and some more information are presented in Appendix A. The transitions in the Figure 41 are all from $3s^24x$, x being either f or d sub-shell. The transitions with more fluctuation are to $3s^23y$, y being d or p ; the less fluctuation corresponds to the transition to $3s^24z$, z being any sub-shell. In quantum physics, it is known that, “the principle quantum number determines not only the energy level of the electron, it also determines to a great extent the average distance of the electron from the nucleus” [60]. Therefore, a logical reason for fluctuation in polarization behavior in some transitions can be the distance to the nucleus, or in other words, the electrostatic field which influences the polarization rather hardly. That is, the reason of more fluctuation in intensity with a change in polarization angle can be due the more influence of electrostatic force on a transition from $n=4$ to $n=3$ is more than a transition from $n=4$ to another $n=4$ state.

Another comment can be made when comparing the laser peaks to characteristic emission lines. Those laser peaks are corresponding to the laser beam that could penetrate through the notch filter and are not entirely eliminated on purpose. One of the reasons for them to survive is to check the calibration of the spectrometers, since the laser line is fixed to its value. The second reason is to evaluate the polarization effects on the laser-matter interaction. First of all, the sinusoidal behavior of the laser peaks for both surfaces proves that polarizer works properly, since the lasers are not perfectly polarized in real world, for some angles of polarizer, the laser can pass more and for some, it will be mostly prevented. The lasers' peaks also help to choose the angles of interest, that is, an angle corresponding to highest intensity, 120 degrees, and an angle corresponding to relatively

smaller intensity, 180 degrees, are chosen to investigate. The intensities of the emission lines corresponding to these 120 degree and 180 degree at about 412 nm are close to each other. This indicates that the emission lines behave different than an ordinary laser line which means the energy gained through the laser spots are not the factors, but the polarization has some effects. For some angle of polarization, the emission lines are strong and for some weak. The background emissions corresponding to an arbitrary wavelength are also supporting this conclusion. There is no fluctuation, or in other words, there are no relatively higher or smaller intensities with changing of the angle of polarization, even if the chosen background wavelength is a short one comparable to the characteristic Si emission line at about 412 nm. Eventually, it is fair to conclude that characteristic emission lines of Si have a polarization dependency.

The polarization dependency seems to exist, however, the question of will this be correlated to the laser-matter interaction should be the next step to study deeper. For this study, the emission lines of both crystal surfaces at both 120 and 180 degrees of polarizer angle are investigated. By this investigation, the outcome about the intensity differences of different crystal-surfaces of Si which is mentioned in Section 6.2 is strengthened; Si (100) surface has more intense emission lines than that of Si (111).

In Figure 42 (a) and (b), the characteristic emission lines of Si (100) and Si (111) at about 412 nm taken by a polarizer angle of 120 degrees are shown, respectively. In the figure, for improving the accuracy the experimental results are fitted by a fit function. As can be deduced from the graph, the behavior of the curve is Lorentzian that means finding the full width at half maximum (FWHM) of the peak will lead to have an idea about the electron density of the plasma as stated in Section 3.1.4. The fit function is used to

evaluate the FWHM of the emission lines. In order to find the half maximum value, the maximum and the minimum values for the peaks should be decided. The maxima are obvious, and for minimum, the averages of the two values of piedmont at both sides are chosen as indicated in the Figure 42. After the intensity corresponding to half maximum value is found, the width, more precisely the wavelength magnitude within the peak at half maximum intensity, $\Delta\lambda$, is calculated. In order to calculate $\Delta\lambda$, the intensities that surround the half maxima at both ends are indicated. The calculation is then performed with the assumption telling that the interval between the two nearest surrounding points to the desired half maximum intensity is linear. Similar indications and calculations are also carried out for the emission lines of Si (100) and Si (111) at about 412 nm but this time taken by a polarizer angle of 180 degrees as seen in Figure 43.

One of the conclusions related to these FWHM ($\Delta\lambda$) calculations using equation (16) without caring the constants that are the same for the same emission lines of the same element is that, the $\Delta\lambda$ for 120 degree-experiment is wider than that of 180 degrees as seen in Table 2 and Table 3. The surprising part is, when the intensities corresponding to the same angle are compared, the opposite result is found, that is the intensity of emission line in the 180-degree experiment is higher than that of 120 degrees. Actually the expectation was; since the $\Delta\lambda$ is proportional to electron density, N_e , the more N_e appears to lead higher intensity. However it was not that obvious, since the intensity is not just a function of N_e , there are more factors to be taken into account. Remembering the laser lines in Figure 41, the intensity of laser line in 180-degree experiment is less compared to 120-degree one, implying that in 180 degree-experiment more interactions and dispersions take place. By these interactions, more characteristic emission have chance to occur.

Further information can be extracted from the Figure 42 and Figure 43 that is strongly related to Section 6.2. In both of the figures, the intensity and the $\Delta\lambda$ calculations show slightly higher values for the Si (100) crystal as in Table 2 and Table 3. That just supports the claim of Section 6.2; the dangling bond density exposed to the laser spot is larger in the case of Si (100), so the intensity and the $\Delta\lambda$ without constants which can be an indication of N_e are slightly higher than that of Si (111). Whether amorphization take place or not, still the claim about the influence of surface of the crystal holds.

Table 2 FWHM calculations for the graphs in Figure 42 (a) and (b)

$\Delta\lambda_{\text{Si}(100)-120} = 3.428 \text{ nm}$	$\Delta\lambda_{\text{Si}(111)-120} = 3.375 \text{ nm}$
$(\Delta\lambda_{\text{Si}(100)-120})^{3/2} = 6.347$	$(\Delta\lambda_{\text{Si}(111)-120})^{3/2} = 6.200$

When the ratio of the equation (16) is taken for the same characteristic line of the same element, the constants just cancel each other, leaving only the ratio of the N_e terms. By which, comparison of N_e is possible for different crystal surfaces. Here is a comparison for Si (100) and Si (111) on their N_e with a polarization angle of 120 degrees;

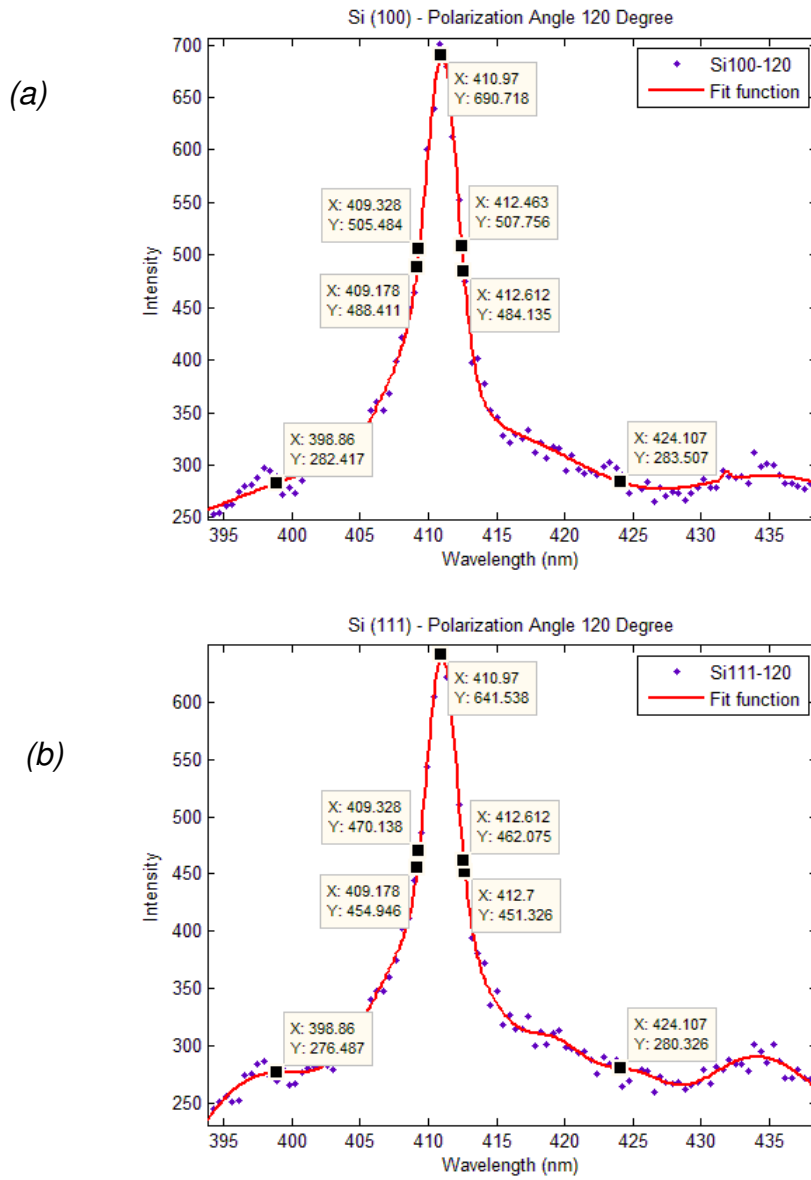


Figure 42. (a) Si (100) vs (b) Si (111) by using a polarizer at 120-degree angle (x being the corresponding wavelength in nm and y being the relative intensity in arbitrary unit)

$$R_{120} = \frac{\Delta\lambda_{\text{Si}(100)-120}^{\frac{3}{2}}}{\Delta\lambda_{\text{Si}(111)-120}^{\frac{3}{2}}} = 1.024 \quad (17)$$

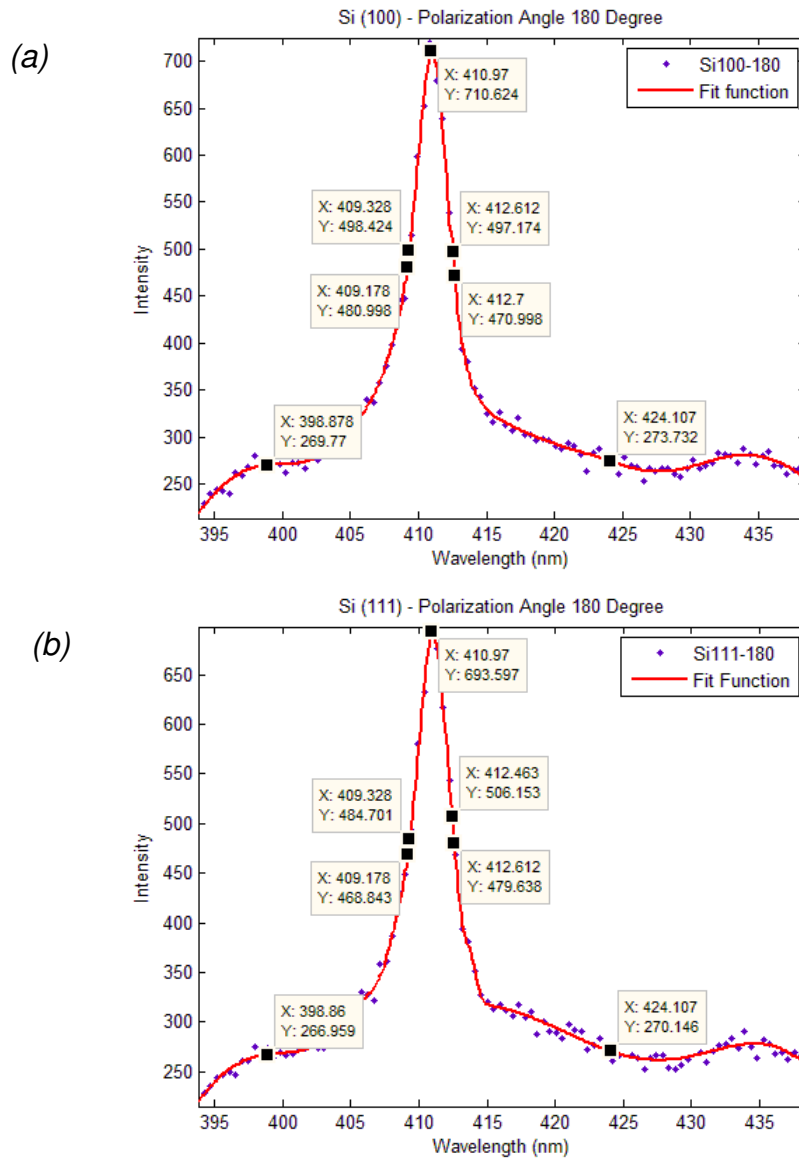


Figure 43. (a) Si (100) vs (b) Si (111) by using a polarizer at 180-degree angle (x being the corresponding wavelength in nm and y being the relative intensity in arbitrary unit)

Table 3 FWHM calculations for the graphs in Figure 43 (a) and (b)

$\Delta\lambda_{\text{Si}(100)-180} = 3.346 \text{ nm}$	$\Delta\lambda_{\text{Si}(111)-180} = 3.307 \text{ nm}$
$(\Delta\lambda_{\text{Si}(100)-180})^{3/2} = 6.121$	$(\Delta\lambda_{\text{Si}(111)-180})^{3/2} = 6.014$

The comparison for Si (100) and Si (111) on their N_e with a polarization angle of 180 degrees is;

$$R_{180} = \frac{\Delta\lambda_{\text{Si}(100)-180}^{\frac{3}{2}}}{\Delta\lambda_{\text{Si}(111)-180}^{\frac{3}{2}}} = 1.018 \quad (18)$$

The motivation to study polarization effects was the question: “if there were a polarization dependency, could this help to improve the LIBS technique?” As discussed above, plasma or more specifically, the characteristic emission lines to some extent have dependency on polarization. This dependency can be investigated deeper by comparing with an unpolarized experiment that has similar intensities with the polarized one. In Figure 44 (a) and (b), graphs of experiments on Si (100) without a polarizer and with a polarizer having an angle of 180 degrees are shown, respectively. The FWHM is calculated (Table 4) as explained above and through that N_e values are compared.

Table 4 FWHM Calculations for the graphs in Figure 44 (a) and (b)

$\Delta\lambda_{\text{Si}(100)\text{-noPOL}} = 3.562 \text{ nm}$	$\Delta\lambda_{\text{Si}(100)\text{-180}} = 3.346 \text{ nm}$
$(\Delta\lambda_{\text{Si}(100)\text{-noPOL}})^{3/2} = 6.723$	$(\Delta\lambda_{\text{Si}(100)\text{-180}})^{3/2} = 6.121$

As seen in equation (19) below, the number of electrons in the experiment without the polarizer for the similar intensities is slightly higher than N_e of the experiment with a polarizer. That is, the ratio of the electron densities, $\frac{R_{\text{noPOL}}}{180}$, is close to 1. However, the ratio of the signal to noise ratios of the two, $S/N_{\text{noPOL}/180}$, is less than 1 as indicated in the equation (20), implying that the presence of polarizer improves the signal to noise or in other words, characteristic emission to continuum ratio which was also stated in the study of Liu et al [58] and [57].

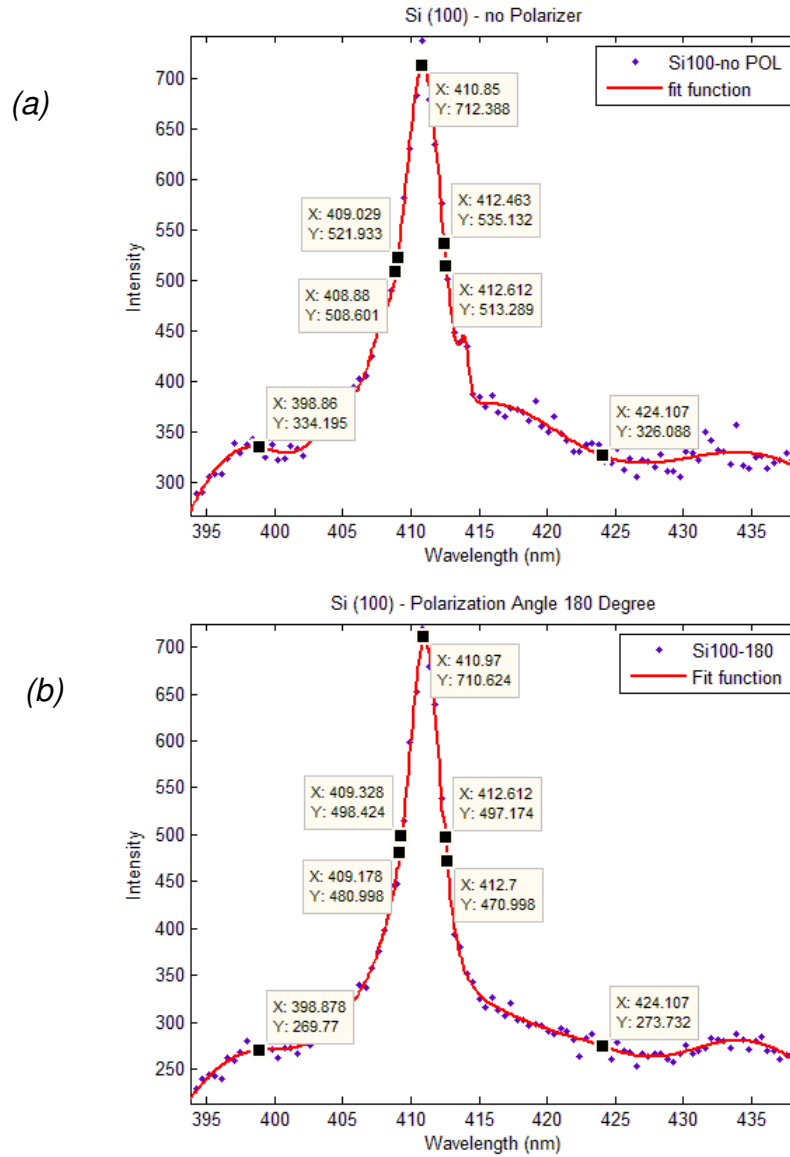


Figure 44. (a) Si (100) by using a polarizer at 180-degree angle vs (b) Si (100) without a polarizer (x being the corresponding wavelength in nm and y being the relative intensity in arbitrary unit)

$$R_{noPOL/180} = \frac{\Delta\lambda_{Si(100)-noPOL}^{\frac{3}{2}}}{\Delta\lambda_{Si(100)-180}^{\frac{3}{2}}} = 1.098 \quad (19)$$

$$S/N_{noPOL/180} = \frac{S/N_{Si(100)-noPOL}}{S/N_{Si(100)-180}} = 0.814 \quad (20)$$

Therefore usage of a polarizer could help to improve signal to noise ratio which is an important issue for both identification and searching for known element applications.

6.4 Air Spectroscopy Experiments

For air plasma production a high-peak power laser is focused to normal air in atmospheric conditions. For further analysis, flow of nitrogen gas is allowed through the surviving plasma. Spectral recording of air plasma of both cases, without and with flow of additional gas is graphed in Figure 45. The peaks labeled in the graph are belonging to elements from air, namely, oxygen and nitrogen peaks. When comparing the intensities of the peaks that correspond to air spectra with and without the flow of the additional gas, it is observed that some of the peaks get higher intensity values, where some does not. The peaks that are intensified after the gas flow are, nitrogen I emission lines at 744.2 nm, 746.8 nm, 818.4 nm, 821.6 nm and 868.0 nm. Actually, having the nitrogen lines intensified is not beyond what is expected. The more interesting result is having less intensity for oxygen I emission lines at 777.2 nm and 844.6 nm for the case with nitrogen gas flow. One of the reasons for the decrease in the intensity of the O I peaks is the lower possibility of photon interaction with the oxygen element due to excess element and ion movement within the plasma. Another reason can be the rapid expansion of the plasma because of the gas flow through it.

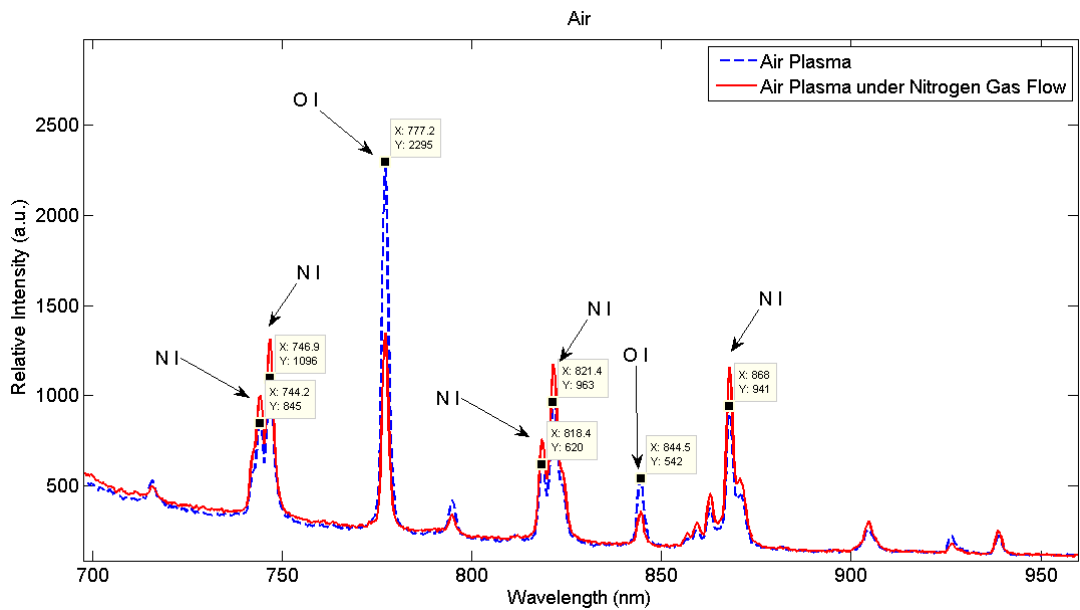


Figure 45. Air plasma vs air plasma under Nitrogen gas flow (x being the corresponding wavelength in nm and y being the relative intensity in arbitrary unit)

By means of this air plasma experiment, it is shown that LIBS is a useful spectroscopic technique for gas state samples. Even under windy or gas flow conditions, usage of a high power laser with an appropriate lens could produce plasma. These kinds of results are promising for determination needs of explosives especially in fields.

CHAPTER 7

ELEMENT IDENTIFICATION VIA SOFTWARE

For element identification, as already mentioned above, there are few significant components. One is no doubt the resolving power of the spectrometer. However, the best resolution-detector is not enough for identification since the found emission line should be compared with enormous number of emission lines. At this point, a database having the necessary emission lines and software to identify them are essentially considered.

The database of the most of the commercial softwares is based on National Institute Standards and Technology Atomic Spectra Database [61]. However, there can be an inconsistency between the NIST library and the emission lines occurring after the LIBS experiments. This inconsistency is also emphasized by Rock et al [62]. They lay stress on, for some situations; it is possible to match measured emission lines from emission lines listed in the NIST database. However, in some cases, it is not so obvious to identify an emission line by using only the NIST database. One of the reasons can be the experimental conditions used to produce the atomic spectrum database published by NIST are different from those that are used to generate LIBS spectra. In LIBS, the creation of plasma can reach temperatures on the order of 10^4 K usually at atmospheric pressures which is probably different for the NIST database collection. The second reason can be the resolution

differences. Typically, LIBS spectra are broadened or shifted by many effects like Stark collisions and Doppler Effect. In LIBS experiments, it is not possible to use the high precision in spectroscopy that is provided by the NIST database. Therefore, in LIBS measurements, line emissions from unknowns may not always be resolved and identified with a very high level of certainty. New databases using known standards and under known experimental conditions can be generated by LIBS study groups. In such a case, researches could upgrade or use the database that is generated with similar experimental conditions to theirs.

7.1 Software of the Portable LIBS System

Since the basic principle of a LIBS system is to direct a laser shot to the sample and then detect the photons due to the disturbance sourced from that shot and look for the elemental emission spectra through a database, a commercial system needs to have software. StellarNet's briefcase-LIBS system has such a software called SpectraWiz to perform UV-VIS-NIR spectral analysis of unknown samples.

The SpectraWiz software provides element identification via spectral database for qualitative measurements. However, after a set of experiments on 99.95% pure Mo, 99.95% pure Au, 99.99 % pure Fe, 99.95% pure Ti and a high purity compound, CuBe samples, the analyses give unsatisfactory results. In experiment of Mo target shown in Figure 46, the software found 23 different elements including two of three-Mo lines within its library.

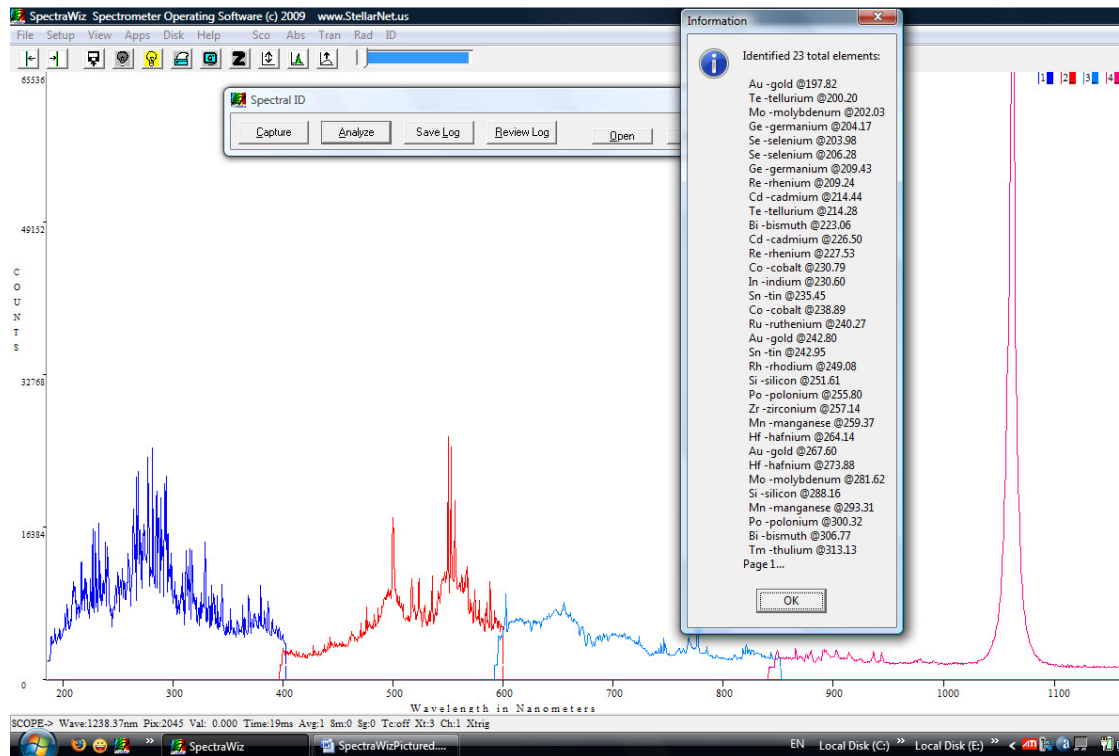


Figure 46. The experimental results obtained by commercial PORTA-LIBS to identify 99.95 % Mo element, search tolerance 0.20 nm, search threshold 15 %

In order to gather more accurate identification of the unknowns, software is designed to let user to control some of its settings. One of them is the search threshold which sets a base to peak magnitude for the library search. The user manual [63] of this system mentions that with larger values for search threshold, more elements will be reported. The other setting is letting the user to decide on the search tolerance. Search tolerance is like an error margin which is a wavelength amount around an emission line in the library. This amount is set by the user in asking the software to search for a match of identification within this set wavelength neighborhood. The manual [63] advises to set values close to the optical resolution. By changing these kinds of settings, the precision of identification is improved as seen in Figure 47 (a) for the case of Fe. There are three emission lines of Fe included in the library

and two of them are obtained indicating that they are matched with the high purity sample. However, the same setting does not work for a compound, CuBe, as seen in Figure 47 (b). Again two of the three library emission lines of Cu are found, but Be element did not show up with any of the setting combination of search tolerance and search threshold. Therefore, the other interference that the user is allowed, the library update, is tried.

```
12/18/2009 3:29:13 PM [iron1mm-1] 1 elements PL CM st=0.25
sthresh%=20.00
Fe -iron @259.94 (a)
Fe -iron @271.44
12/14/2009 9:11:22 PM [CuBe1] 1 elements PL CM st=0.25
sthresh%=20.00
Cu -copper @224.70 (b)
Cu -copper @324.75
```

Figure 47. The experimental results obtained by commercial PORTA-LIBS to identify (a) 99.99% Fe element, and (b) high purity CuBe compound, (st stands for search tolerance in nm, and sthresh for search threshold in percentage)

The original library of the system consists of 83 elements each having at most three emission lines. However, this number of elements and each element having only three emission lines seem to make the library quite poor. Considering Mo element will give an idea about how these emission lines need to be improved. Between 200-1000 nm, Mo has 1051 known emission lines, or more specifically there exists 15 persistent lines corresponding to Mo I (natural atom) and 13 persistent lines corresponding to Mo II (singly ionized ion) according to the NIST database [61].

Since the software is built such that it allows adding new elements or new emission lines of already existing elements to its library, as seen in Figure 48,

there have been 7 rows of emission lines are added including new emission lines of Be, Ti and Mo elements. Since there is a limit to add a new row and there are unrelated identifications as seen in Figure 49, such upgrade did not succeed. Consequently, neither changing any settings nor new emission line addition to the library could bring a precise result. This motivated to write a code for more accuracy and precision in element identification.

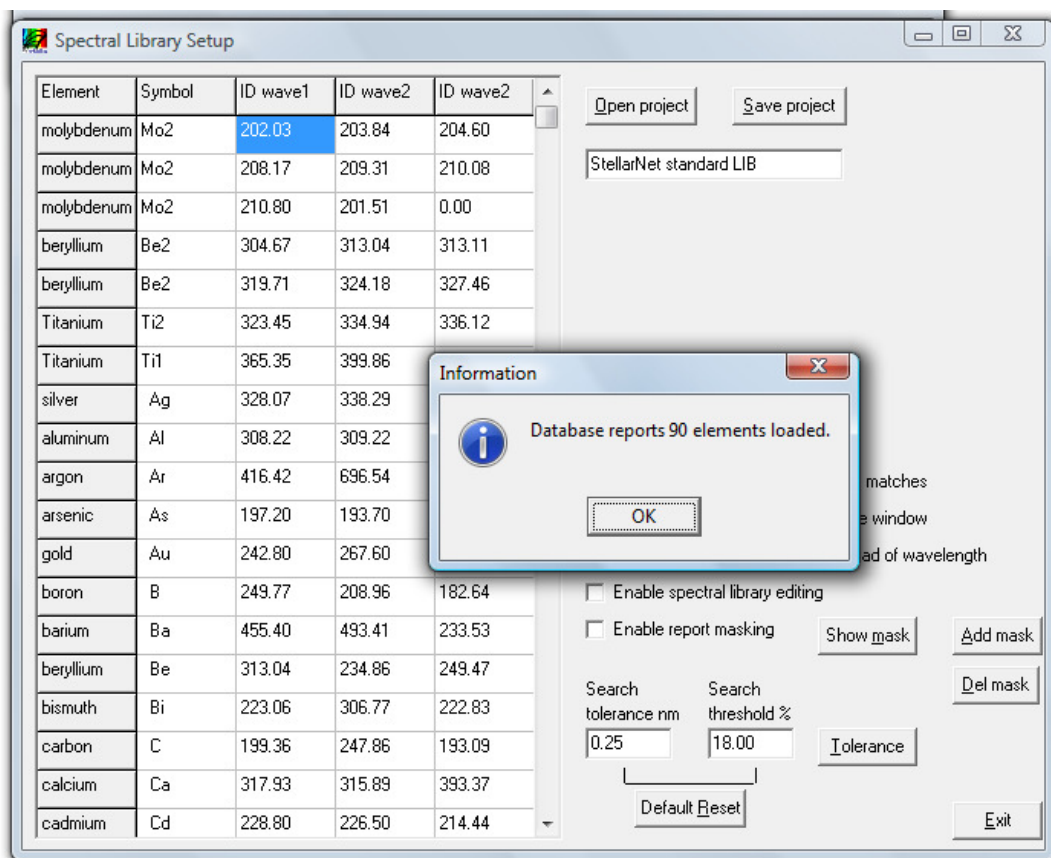


Figure 48. Library of the software with customer addition

```
12/29/2009 7:38:40 PM [CuBe with extra library added] 4
elements PL CM st=0.25 sthresh%=20.00
Mo2 -molybdenum @203.84
Mo2 -molybdenum @204.60
P -phosphorus @213.62
P -phosphorus @214.91
Cu -copper @224.70
Be -beryllium @234.86
Be -beryllium @313.04
Cu -copper @324.75
Cu -copper @327.40
```

Figure 49. The experimental results obtained by commercial PORTA-LIBS to identify CuBe with additional library

7.2 The New Code and the Database

By the motivation of the poor element identification of the commercial software, a code is developed in order to improve the accuracy of qualitative analyses. The code is constituted by using Visual Basic language (Microsoft Excel 2007) and the interface is shown in Figure 50.

First noticeable advantage of such a code is that it can be used with the outputs of any kinds of spectrometers. In this sense, the code can analyze the recordings of the HR 2000 spectrometer in addition to the spectrometers of the StellarNet Inc.

The code gives the opportunity of deciding the peaks that are going to be taken into account in identification. This is achieved by looking at their relative intensities. This property is called as “Acceptable Peak Percentage”. For this property, first the laser line is discarded. Then highest-intensity peak is determined and a certain percentage of this highest peak is chosen and

set by user as the Acceptable Peak Percentage (Figure 50). After that, the peaks that are equal or higher than this set intensity percentage are taken into account in identification procedure. The peaks having less intensity than the set value are treated as background continuum emissions without corresponding to characteristic emission lines, so they are not used for identification.

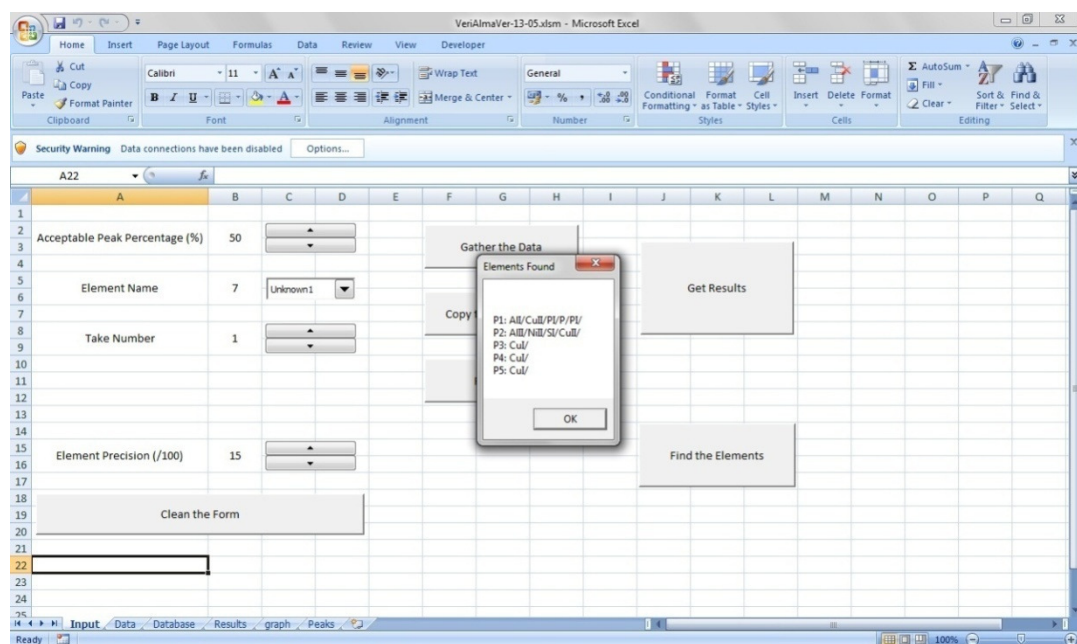


Figure 50. High purity Cu element is investigated with an element precision of 15

By means of this code, visualizing the peaks in a graph is also possible. This makes it easy to decide on a set value of the Acceptable Peak Percentage and therefore to eliminate the lower peaks that are not characteristics.

Another capability of the software is letting user to decide on the tolerance of the peak. This property is called "Element Precision". It works like the search tolerance property of the commercial software. This time, user sets the percentage of wavelength around the output peak from the sample. While

trying to match the characteristic emission lines within database to a measured peak, the wavelength neighborhood of the set value will be used. More clearly, if 20 percent is chosen for the Element Precision (Figure 50), for a measured peak at 100.00 nm, the characteristic lines between the wavelength values from 99.80 to 100.20 nm will be searched.

In the code, this mentioned database is sourced from National Institute of Standards and Technology [61] database. The emission lines that are corresponding to natural atom and singly ionized ion are selected since they are the ones that are mostly observed with the existing experimental setup. With a need of higher ionization transition lines or by building own database through standards, it can be upgraded. Moreover, for searching certain emissions, for instance, CN lines for biological or chemical treat determination, the database can be adaptively renewed.

The code works better than the commercial software and is quite well to demonstrate the composition of the samples; however, it may still show some element names other than the correct element since they lie in the close neighborhood of the mentioned elemental peak and the real peak is not narrow enough (Figure 51). Reducing the search tolerance is not a fair solution all the time, due to the resolution limits of the spectrometers. A convenient way to decide the existence of an element can be to have the indication of the same element name two or three times in the output list which can also be added to the code if only viewing and deciding manually does not seem so professional. Another smart approach is using a notification, like a star sign (*) typed next to the name of element, if the peak is the one with high probability to occur, that is a persistent line as in Figure 51. So, having a peak marked with a star sign, strongly indicates the existence of the corresponding element.

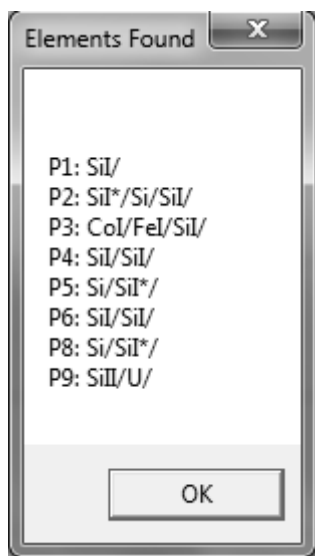


Figure 51. Results of new code

Code can also be upgraded to search for other persistent lines of the element, if it finds one, as proposed in Section 3.2, which can also ensure the precision. Asking the code to look at some ratio of certain elements can also help in searching applications like searching for biological threats among other organic compounds. By the help of this code, improvement in element identification is obtained within the resolution limits of the spectrometer. It can be claimed that it will be much more useful for searching applications. In conclusion, accuracy and precision are gained to some extent by means of the capabilities of the new code with its new database. The most promising benefit of creating a code is the ability to upgrade with the necessities encountered.

CHAPTER 8

CONCLUSIONS

This thesis had some contributions to the LIBS community in different ways. First of all, it constituted the first study on the effects of different crystal surfaces by LIBS, in which dangling bond densities were introduced and held responsible for the reasoning of the different intensity results in emission lines.

The study also tried to contribute to the emission line enhancement and accuracy in both experimental and analysis aspects. For the experimental improvement, the unconventional, orthogonal double pulse configuration with 45 degree incidence angle of opposite directions had been experienced. It had been emphasized that with such a configuration, the positioning issue, that was focusing the laser on and above the sample within the pre-pulse induced plasma formation, could be handled more easily. That yielded reproducible experiment results. It was also shown that with the configuration, increase in intensity of emission lines were observed when compared to single pulse experiments.

The next contribution involves the investigation of the polarization effect in nsec laser-pulsed LIBS of a semimetal. The experiments indicated that laser induced plasma had a polarization dependency to some extent that with

certain polarization angles, the signal to noise ratios or the emission line of interest to other lines were enhanced.

Besides the experimental approaches for more accurate and precise achievement in LIBS results, a code had been developed. This code could relate the measured emission lines to a database and could create constraints for more accurate investigation. Such constraints could be improved for the requirements of analysis. Developing a code gave the flexibility of updating the database by means of either own experimental results of standards or other spectra from experiments under similar conditions.

One of the main gains of this study was establishing a LIBS laboratory and leading a new research area to students and researchers at METU Physics Department. A dynamic laboratory, some experimental tricks, a satisfactory analysis code and potential research areas are offered for the followers by this study. By means of the experiences gained, some future works can be stated like searching for explosives by updating the database accordingly or investigations of gases and aerosols by using a vacuum chamber and high-energy lasers. Any of the two would be unique applications in Turkey for the time being. Some other research proposals can include biological investigations or elemental analysis and capability comparisons of different spectroscopic techniques which could be possible by cooperation with the Chemistry Department which has been discussed and tried for a limited time earlier.

In conclusion, by means of the different experimental approaches, some of the factors that had role in the emission intensity were discussed and besides that, the enhancement in the intensity had been observed. Furthermore, the

useful code supported the improvement in LIBS results. After all, it is believed that the new experimental approaches and code of the study presented new perspectives to improve the capabilities of LIBS systems.

REFERENCES

- [1] Il'in, A.A., Golik, S.S., Nagorny, I.G., and Bulanov, A.V., *Improving Sensitivity of Laser-Induced Breakdown Spectroscopy Using Laser Plasmas Interaction*, Thirteenth Joint International Symposium on Atmospheric and Ocean Optics/ Atmospheric Physics, Proc. of SPIE Vol. 6522, 65220Z, 2006.
- [2] Cremers, D.A., and Radziemski, L.J., *Laser-Induced Breakdown Spectroscopy*, John Wiley & Sons, England, 2006.
- [3] Radziemski, L.J., *From Laser to LIBS, The Path of Technology Development*, Spectrochimica Acta Part B, 57, 1109-1113, 2002.
- [4] Whitehouse, A.I., *Laser Induced Breakdown Spectroscopy and Its Application to the Remote Characterisation of Hazardous Materials*, Spectroscopy Europe18, 14-21, 2006.
- [5] Cremers, D.A., Ferns, M.J., and Han, C.Y., *Remote Elemental Analysis Using Laser-Induced Breakdown Spectroscopy*, SPIE 2385, 28-38, 1995.
- [6] Theriault, G.A., and Lieberman, S.H., *Remote Insitu Detection of Heavy Metal Contamination in Soils Using a Fiber Optic Laser Induced Breakdown Spectroscopy (FOLIBS) System*, SPIE 2504, 75-83, 1995.
- [7] De Lucia Jr., F.C., Gottfried, J.L., Munson, C.A., and Miziolek, A.W., *Multivariate Analysis of Standoff Laser-Induced Breakdown Spectroscopy Spectra for Classification of Explosive-Containing Residues*, Appl. Opt, Vol. 47, No. 31, G112-G121, 2008.
- [8] De Lucia Jr., F.C., Gottfried, J.L., Munson, C.A., and Miziolek, A.W., *Double Pulse Laser-Induced Breakdown Spectroscopy of Explosives: Initial*

Study Towards Improved Discrimination, Spectrochim. Acta Part B, 62, 1399–1404, 2007.

[9] F.C., Gottfried, De Lucia Jr., J.L., Munson, C.A., and Miziolek, A.W., *Standoff Detection of Chemical and Biological Threats Using Laser-Induced Breakdown Spectroscopy*, Appl. Spec., Volume 62, Number 4, 353-363, 2008.

[10] Scaffidi, J., Angel, S.M., and Cremers, D.A., *Emission Enhancement Mechanisms in Dual Pulse LIBS*, Analytical Chemistry, 25-32, 2006.

[11] Goujon, J, Giakoumaki, A., Piñon, V., Musset, O., Anglos, D., Georgiou, E., and Boquillon, J.P., *A Compact and Portable Laser-Induced Breakdown Spectroscopy Instrument for Single and Double Pulse Applications*, Spectrochim. Acta Part B 63, 1091-1096, 2008.

[12] Hohreiter, V., and Hahn, D.W., *Dual-Pulse Laser Induced Breakdown Spectroscopy: Time-Resolved Transmission and Spectral Measurements*, Spectrochim. Acta Part B 60, 968-974, 2005.

[13] Mayorov, F., *Femtosecond Imaging-Mode Laser-Induced Breakdown Spectroscopy*, PhD., Universität Kassel, 2004.

[14] Scaffidi, J., Pender, J., Pearman, W., Goode, S.R., Colston, B.W. Jr., Carter, J.C., and Angel, S.M., *Dual-Pulse Laser-Induced Breakdown Spectroscopy with Combinations of Femtosecond and Nanosecond Laser Pulses*, Appl. Opt, Vol. 42, No. 30, 6099-6106, 2003.

[15] Sorrentino, F., Carelli, G., Francesconi, F., Francesconi, M., Marsili, P., Cristoforetti, G., Legnaioli, S., Palleschi, V., and Tognoni, E., *Fast Analysis of Complex Metallic Alloys by Double-Pulse Time-Integrated Laser-Induced Breakdown Spectroscopy*, Spectrochim. Acta Part B 64, 1068-1072, 2009.

[16] Corsi, M., Cristoforetti, G., Giuffrida, M., Hidalgo, M., Legnaioli, S., Palleschi, V., Salvetti, A., Tognoni, E., and Vallebona, C., *Three-Dimensional*

Analysis of Laser Induced Plasmas in Single and Double Pulse Configuration, Spectrochim. Acta Part B 59, 723-735, 2004.

[17] Stratis, D.N., Eland, K.L., and Angel, S.M., *Effect of Pulse Delay Time on A Pre-Ablation Dual-Pulse LIBS Plasma*, Appl. Spect. 55, 1297-1303, 2001.

[18] Pasquini, C., Cortez, J., Silva, L.M.C., and Gonzaga, F.B., *Laser Induced Breakdown Spectroscopy*, J. Braz. Chem. Soc. 18, 463-512, 2007.

[19] Grönlund, R., Lundqvist, M., and Svanberg, S., *Remote Imaging Laser-Induced Breakdown Spectroscopy and Remote Cultural Heritage Ablative Cleaning*, Opt. Lett., 30, 2882-2884, 2005.

[20] Harmon, R.S., De Lucia, F.C., Munson, C.A., Miziolek, A.W., and McNesby, K.L., *Laser-Induced Breakdown Spectroscopy (LIBS) – an Emerging Field-Portable Sensor Technology for Real-Time Chemical Analysis for Military, Security and Environmental Applications*, SPIE 5994, 59940K-1-59940K-7, 2005.

[21] Pierce, W., Christian, S.M., Myers, M.J., and Myers, J.D., *Field-Testing for Environmental Pollutants Using Briefcase Sized Portable LIBS System*, Libs_2004, 3rd International Conference on Laser Induced Plasma Spectroscopy and Applications 1-14, 2004.

[22] Theriault, G.A., Mosier-Boss, P.A., and Liebermann, S.H., *Application of LIBS to In-Situ Assessment of Metal Contaminated Soils*, Part of the SPIE Conference on Advanced Sensors and Monitors for Process Industries and the Environment Boston. Massachusetts, SPIE Vol. 3535, 141-145, 1998.

[23] Cremers, D.A., Ferris, M.J., and Davies, M., *Transportable Laser-Induced Breakdown Spectroscopy (LIBS) Instrument for Field-Based Soil Analysis*, SPIE 2835, 190-200, 1996.

[24] Park, K., Cho, G., and Kwak, J., *Development of an Aerosol Focusing-Laser Induced Breakdown Spectroscopy (Aerosol Focusing-LIBS) for*

Determination of Fine and Ultrafine Metal Aerosols, *Aerosol Science and Technology*, 43:375–386, 2009.

[25] Barbini, R., Colao, F., Fantoni, R., Lazic, V., Palucci, A., Capitelli, F., and Van der Steen, H.J.L., *Laser Induced Breakdown Spectroscopy for Semi-Quantitative Elemental Analysis in Soils and Marine Sediments*, EARSeL eProceedings No. 1, 122-129, 2000.

[26] Taffe, A., Schaurich, D., Weritz, F., and Wilsch, G., *Laser-Induced Breakdown Spectroscopy (LIBS) in Civil Engineering*, ECNDT 2006 - Poster 15, 2006.

[27] Lazic, V., Palucci, A., Jovicevic, S., Poggi, C., and Buono, E., *Analysis of Explosive and Other Organic Residues by Laser Induced Breakdown Spectroscopy*, *Spectrochim. Acta Part B*, 64, 1028–1039, 2009.

[28] Harmon, R.S., DeLucia, F.C., LaPointe, A., COL Winkel, R.J. Jr., and Miziolek, A.W., *Discrimination and Identification of Plastic Landmine Casings by Single-Shot Broadband LIBS*, *Proc. of SPIE Vol. 5794*, 92-101, 2005.

[29] Harmon, R.S., DeLucia, F.C., COL Winkel, R.J. Jr., LaPointe, A., Grossman, S., McNesby, K.L., and Miziolek, A.W., *LIBS: A New Versatile, Field Deployable, Real-Time Detector System with Potential for Landmine Detection*, *Proceedings of SPIE Vol. 5089*, 1065-1077, 2003.

[30] Morel, S., Leone, N., Adam, P., and Amouroux, J., *Detection of Bacteria by Time-Resolved Laser-Induced Breakdown Spectroscopy*, *Appl. Opt.*, Vol. 42, No. 30, 6184-6191, 2003.

[31] Munson, C.A., Gottfried, J.L., Snyder, E.G., De Lucia, F.C. Jr., Gullett, B., and Miziolek, A.W., *Detection of Indoor Biological Hazards Using the Man-Portable Laser Induced Breakdown Spectrometer*, *Appl. Opt.*, Vol. 47, No. 31, G48-G57, 2008.

[32] Marquardt, B.J., Cullum, B.M., Shaw, T.J., and Angel, S.M., *Fiber-Optic Probe for Determining Heavy Metals in Solids Based on Laser-Induced Plasmas*, SPIE Vol. 3105, 203-212, 2009.

[33] Saggese, S., and Greenwell, R., *LIBS Fiber Optic Sensor for Subsurface Heavy Metals Detection*, SPIE Vol. 2836, 195-205, 2009.

[34] Izmir Institute of Technology,
<http://web.iyte.edu.tr/~serifeyalcin/index.htm>, last visit: December 2011.

[35] LATARUM, <http://latarum.kocaeli.edu.tr/int/>, last visit: December 2011.

[36] Singh, J.P., and Thakur, S.N., *Laser-Induced Breakdown Spectroscopy*, Elsevier, Amsterdam, Netherland, 2007.

[37] Kompitsas, M., Roubani-Kalantzopoulou, F., Bassiotis, I., Diamantopoulou, A., and Giannoudakos, A., *Laser Induced Plasma Spectroscopy (LIPS) as an Efficient Method for Elemental Analysis of Environmental Samples*, EARSeL eProceedings No. 1, 130-138, 2000.

[38] Eliezer, S., *Interaction of High Power Lasers with Plasmas*, Institute of Physics Publishing, Bristol and Philadelphia, 2002.

[39] Angel, S.M., Stratis, D.N., Eland, K.L., Lai, T., Berg, M.A., and Gold, D.M., *LIBS Using Dual- and Ultra-Short Laser Pulses*, Fresenius J Anal Chem, 369, 320–327, 2001.

[40] Sattmann, R., and Noll, R., *Laser-Induced Breakdown Spectroscopy of Steel Samples Using Multiple Q-Switch Nd:YAG Laser Pulses*, J. Phys. D: Appl. Phys. 28, 2181-2187, 1995.

[41] Miziolek, A.W., Pallescji, V., and Schechter, I., *Laser-Induced Breakdown Spectroscopy (LIBS) Fundamentals and Applications*, Cambridge University Press, Cambridge, New York, 2006.

- [42] Griem, H.R., *Spectral Line Broadening by Plasmas*, Academic Press, New York, 1974.
- [43] Griem, H.R., *Plasma Spectroscopy*, McGraw Hill, New York, 1964.
- [44] Thorne, A.P., *Spectrophysics, 2nd Ed.*, English Language Book Society/Chapman and Hall, London, 1988.
- [45] Muraoka, K., and Maeda, M., *Laser-Aided Diagnostics of Plasmas and Gases*, Institute of Physics Publishing, Bristol, Philadelphia, 2001.
- [46] Aragón, C., and Aguilera, J.A., Characterization of Laser Induced Plasmas by Optical Emission Spectroscopy: A Review of Experiments and Methods, *Spectrochim. Acta Part B*, 63, 893–916, 2008.
- [47] Piñon, V., Fotakis, C., Nicolas, G., and Anglos, D., *Double Pulse Laser-Induced Breakdown Spectroscopy with Femtosecond Laser Pulses*, *Spectrochim. Acta Part B*, 63, 1006–1010, 2008.
- [48] Samek, O., Kurowski, A., Kittel, S., Kukhlevsky, S., and Hergenröder, R., *Ultra-Short Laser Pulse Ablation Using Shear-Force Feedback: Femtosecond Laser Induced Breakdown Spectroscopy Feasibility Study*, *Spectrochim. Acta Part B*, 60, 1225 – 1229, 2005.
- [49] Semerok, A., and Dutouquet, C., *Ultrashort Double Pulse Laser Ablation of Metals*, *Thin Solid Films* 453 –454, 501–505, 2004.
- [50] McMillan; N., and Spooner, G., Picosecond Laser Induced Breakdown Spectroscopy (LIBS) with the Raydiance Discovery™ Platform, Raydiance, Inc.
- [51] Kittel, C., *Introduction to Solid State Physics, 7th Ed.*, John Wiley and Sons, Canada, 1996.

[52] Myers, H. P., *Introductory Solid State Physics*, 2nd Ed., CRC Press, New York, 1997.

[53] Barron, A.R., and Smith, C., *Crystal Structure*, <http://cnx.org/content/m16927/latest/>, last visited on March 2012.

[54] The Ohio State University Physics Department, http://www.physics.ohio-state.edu/~eric/teaching_files/surfacescience.course/Intro.to.crystallography.pdf, last visited on March 2012.

[55] Banerjee, R., *Absolute Coverage Measurements of Ultrathin Alkali-Metal Films on Reconstructed Silicon*, PhD., Drexel University, Philadelphia, 2001.

[56] Barron, A.R., Structures of Element and Compound Semiconductors, Connexions, <http://cnx.org/content/m23905/latest/>, last visited on March 2012.

[57] Penczak, J.S., Liu, Y., and Gordon, R.J., *Polarization Resolved Laser-Induced Breakdown Spectroscopy of Al*, J. Phys. Chem. A 113, 13310–13317, 2009.

[58] Liu, Y., Singha, S., Witt, T.E., Cheng, Y., and Gordon, R.J., *Observation of Near Total Polarization in the Ultrafast Laser Ablation of Si*, Appl. Phys. Lett. 93, 161502-161502-3, 2008.

[59] NIST Atomic Spectra Database Lines Form, http://physics.nist.gov/PhysRefData/ASD/lines_form.html, last visited on March 2012.

[60] Krane, K., *Modern Physics, 2nd Ed.*, John Wiley and Sons, New York, Chichester, 1996.

[61] National Institute of Standards and Technology, <http://www.nist.gov/index.html>, last visit: December 2011.

[62] Rock S., Marcano A., Markushin Y., Sabanayagam C., Melikechi N., *Elemental Analysis of Laser Induced Breakdown Spectroscopy Aided by an Empirical Spectral Database*, Applied Optics, Vol. 47 No.31, G99-G104, 2008.

[63] *User Documentation for PORTA-LIBS-2000*, Laser Induced Breakdown Spectroscopy Instrumentation.

APPENDIX A

GROTRIAN DIAGRAMS

Energy diagrams are the diagrams mostly used in atomic and molecular physics that involve the allowed transitions between energy levels of atoms. They are very useful for of complex structures multi-element atoms.

As in quantum physics, the first number defining the electronic state is the principle quantum number, n , indicating the shell of the electron and the letter following it, is the orbital quantum number, l , indicating the subshell where s is the $l=0$, p is the $l=1$, d is the $l=2$ and f is the $l=3$.

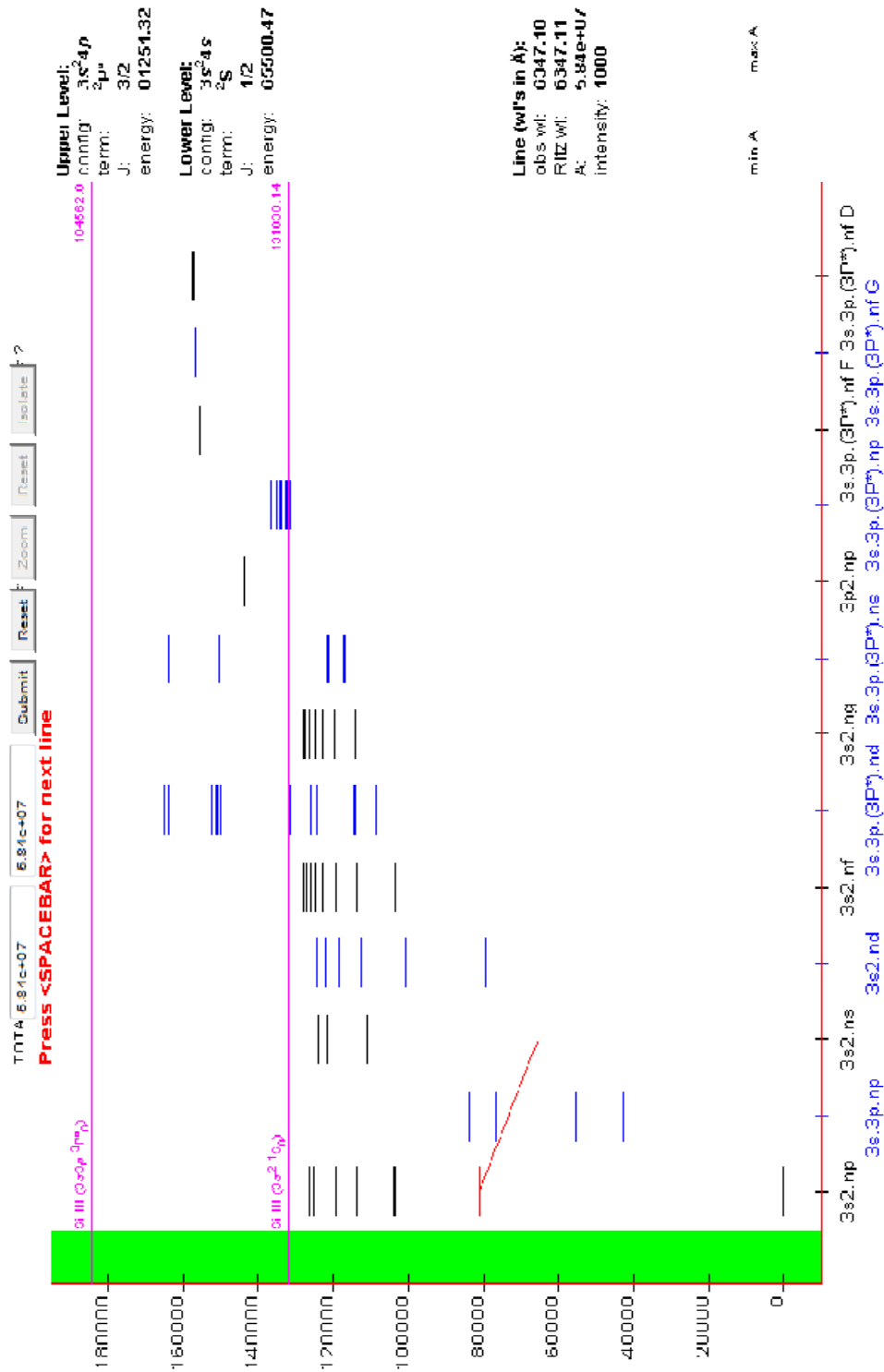


Figure 55. Grotrian Diagram for 634.7 nm Si emission line [61]

CURRICULUM VITAE

Elif YURDANUR TAŞEL

PERSONAL INFORMATION

Date and Place of Birth 03.01.1982, Ankara
Nationality Turkish (TC)
Phone +90 312 291 60 77
e-mail elif.yurdanur@iltaren.tubitak.gov.tr,
elifyurdanur@gmail.com

EDUCATION

PhD Physics Dept., METU (2006 - Present)
MS Physics Dept., METU (2004-2006)
BS Physics Dept., METU (2000-2004)
Middle and High School TED Ankara College (1994-2000)

WORK EXPERIENCE

Researcher, TÜBİTAK (The Scientific and Technological Research Council of Turkey) – BİLGEM – UEKAE – İLTAREN 2008 - Present

Research Assistant, Physics Dept., METU 2005 - 2008

Summer Practice, TAEK (Turkish Atomic Energy Authority) Dept. of Nuclear Physics 2003

SKILLS

Laboratory Skills	Laser Systems, Laser-Matter Interactions and Applications, Plasma Spectroscopy, Infrared Imaging, Opto-Electronic Design, Clean Room and Vacuum Chamber Usage Experiences
Computer Skills	C, Visual Basic, MATLAB, Zemax Optical Design Software, SolidWorks 3-D Design Software, Infrared Simulation Softwares
Languages	English (advanced), German (intermediate)

PUBLICATIONS AND CONFERENCES

“Kimyasal ve Biyolojik Tehdit ve Patlayıcıların Lazerle İrkitilmiş Bozunum Spektroskopisi ile Tespiti”, E. Yurdanur Taşel, S. Bilikmen, Manuscript waiting for response, SAVTEK 2012, Ankara, 2012

“Standoff Content Determination of Targets and Exhaust Gas of Targets Using a Laser Spectroscopic Technique”, E. Yurdanur Taşel, S. Bilikmen, Oral presentation waiting for response, ITBM&S, Ettlingen, Germany, 2012

“Investigation of Materials with Different Lattice Structure under Different Time Delays and Integration Times Using Double Pulse LIBS”, E. Yurdanur Taşel, H. Berberoğlu, S. Bilikmen, Oral presentation, 6th Euro-Mediterranean Symposium on Laser-Induced Breakdown Spectroscopy, Izmir, 2011

“Investigation of Materials Some with Different Crystal Structure Under Various Time Delays Using Double Pulse LIBS”, E. Yurdanur Taşel, H. Berberoğlu, S. Bilikmen, Manuscript waiting for response, Acta Part B, 2011

“Çeşitli Değişik Zaman Aralıklı Çift Darbe LIBS Uygulamaları – Si Elementi Farklı Örgü Yapılarının İncelenmesi”, E. Yurdanur Taşel, H. Berberoglu, B. Yedierler, S. Bilikmen, Poster presentation, Fotonik 2011, Ankara, 2011

“Design and Analysis of Ultrashort Femtosecond Laser Preamplifier and Main Amplifier”, E. Doğan, S. Bilikmen, S. İnce, E. Yurdanur, P. Yılmaz, P. Demir, Poster presentation, Frontiers in Optics, OSA, Rochester USA, 2006

“Investigation of Pre-formed Titanium Plasma for Longitudinally Pumping Ne-like Titanium X-Ray Laser”, A. Demir, E. Akman, S. Bilikmen, P. Demir, S. İnce, E. Kaçar, E. Yurdanur, Poster presentation, 10th International Conference on X-Ray Laser, Berlin, Germany, 2006